UNIVERSITÄT ZU LÜBECK

From the Lübeck Institute of Experimental Dermatology,

University of Lübeck

Director: Prof. Dr. med. Dr. rer. nat. Enno Schmidt

"Cloning of human autoantibodies and characterization of their pathophysiologic impact in IgA-mediated pemphigus"

Dissertation for Fulfillment of Requirements

for the Doctoral Degree

of the University of Lübeck

from the Department of Natural Sciences

Submitted by

Shirin Emtenani, M.Sc.

from Mashhad, Iran

Lübeck 2018

First referee: Prof. Dr. Ralf J. Ludwig

Second referee: Prof. Dr. Hauke Busch

Date of oral examination: 26.04.2019

Approved for printing: Lübeck, 06.05.2019

ABSTRACT

IgA pemphigus is an autoimmune blistering skin disease characterized by detection of tissue-bound and circulating IgA, autoantibodies (autoAbs) against epidermal cadherins, particularly desmogleins (Dsgs) or desmocollins (Dscs). Patients typically present with vesiculopustular skin eruptions, intraepidermal acantholysis, and prominent neutrophilic infiltrates, suggesting a role of neutrophils in disease induction. To facilitate dissection of pathomechanisms involved, in this dissertation antibody phage display (APD) was applied to genetically clone anti-Dsg3 monoclonal antibodies (mAbs) from an IgA pemphigus vulgaris (IgA-PV) patient, as confirmed by direct immunofluorescence (IF) microscopy and high serum anti-Dsg3 IgA reactivity. No Dsg1 or Dsc reactivity was detected. Next, three Dsg3-specific IgA mAbs were isolated here in the form of single-chain variable fragments (scFvs), genetically derived from 2 B-cell clones displaying VH3-23 and VH3-30 gene usages. As expected, these scFvs bound to Dsg3 as shown by ELISA and IF on Dsg-transfected cells. Sera from the same patient, from unrelated active IgA-PV patients, and from active IgG-PV patients led to decreased binding of our scFvs in inhibition ELISAs, indicating that they bind to similar or identical Dsg3 epitopes also bound by serum-derived polyclonal IgA/IgG autoAbs. The biological validity of mAbs was further exemplified by dose-dependent cell-sheet dissociation of cultured human keratinocytes and pathogenicity in human skin organ culture. These assays were conducted under concurrent elimination of Dsg1 by exfoliative toxin A (ETA). These findings indicate that in IgA-PV the anti-Dsg3 IgA mAbs alone are necessary but insufficient for disease induction. Additional Fc-dependent cellular mechanisms potentially involved in tissue pathology were therefore studied by an *in vitro* human skin cryosection model, using the same recombinant full anti-Dsg3 mAb in different isotypes. Incubation of cryosections with a full anti-Dsg3-IgA1 mAb and human peripheral polymorphonuclear leukocytes (PMNs) led to intraepidermal acantholysis and typical pathology, whereas the same mAb in the IgG1 format was ineffective in the same assay. I here present conclusive *in vitro* data showing that anti-Dsg3 IgA1-Fc:FcαR interaction is mediating epidermal pathogenicity in IgA pemphigus, without requiring concurrent inactivation of Dsg1 by autoAbs or ETA. Blocking the interaction of anti-desmosomal IgA and FcαR-bearing cells may be effective future treatment for this difficult-to-treat skin disorder. Shown cross-reactivity of anti-Dsg3 IgA1 and IgG1 mAbs with murine keratinocytes offers an excellent platform to extend these studies to *in vivo* models. The here presented results and potential treatments may be

translated to other diseases of the skin and mucous membrane where IgA is involved, e.g., linear IgA disease, mucous membrane pemphigoid, or IgA epidermolysis bullosa acquisita.

ZUSAMMENFASSUNG

Der IgA-Pemphigus ist eine Autoimmunerkrankung der Haut, welche sich durch den Nachweis gewebsgebundener und zirkulierender IgA-Autoantikörper gegen epidermale Adhäsionsproteine aus der Gruppe der Cadherine, insbesondere Desmogleine (Dsgs) oder Desmocolline (Dscs), auszeichnet. Patienten mit IgA-Pemphigus zeigen typischerweise an der Haut Vesikulopusteln, intraepidermale Akantholyse, und ausgeprägte Neutrophileninfiltrate, was eine mechanistische Schlüsselrolle dieser Zellpopulation in der Pathophysiologie nahelegt. Um die involvierten Mechanismen zu entschlüsseln nutzte die Promovendin in dieser Dissertationsschrift die genetische Methode des Antikörper-Phagen-Displays (APD, englisch antibody phage display) um monoklonale anti-Dsg3 Antikörper einer Patientin mit IgA-Pemphigus vulgaris (IgA-PV) zu klonieren. Die Diagnose dieser IgA-PV-Patientin wurde zuvor bestätigt mittels direkter Immunfluoreszenz und ausgeprägter anti-Dsg3-IgA-Reaktivität im Serum. Es konnte keine Reaktivität gegen Dsg1 oder die Dscs nachgewiesen werden. Mittels APD konnten hier drei monoklonale anti-Dsg3-Antikörper (als scFvs, engl. single-chain variable fragments) isoliert werden, welche genetisch von zwei B-Zell-Klonen abstammten, die das VH3-23- und VH3-30-Gen nutzten. Wie erwartet banden diese Antikörper spezifisch Dsg3, wie mittels ELISA und Immunfluoreszenz auf Dsg-transfizierten Zellen nachgewiesen. Seren der gleichen Patientin, anderer IgA-PV-Patienten, sowie solche klinisch aktiver IgG-PV-Patienten führten in einem Inhibitions-ELISA zu einer verringerten Bindung der monoklonalen scFv-Antikörper, sodass angenommen werden kann, dass letztere an ähnliche oder identische Dsg3-Epitope wie die polyklonale Serum-IgG/IgA-Autoantikörper von Pemphiguspatienten binden. Die biologische Validität erfuhr, wie in dieser Arbeit gezeigt, weitere Bestätigung durch den Nachweis einer dosisabhängige Dissoziation von Monolayern humaner Keratinozyten sowie durch eindeutige Pathogenität in einem humanen Vollhautorgankulturmodell. Diese Testverfahren wurden angewandt unter gleichzeitiger Elimination von Dsg1 durch das exfoliativ wirkende Toxin A (ETA, engl. exfoliative toxin A) von Staphylokokken. Diese Ergebnisse zeigen, dass im IgA-PV anti-Dsg3-IgA-Antikörper zwar notwendig, jedoch allein nicht ausreichend sind für die Induktion von Gewebspathologie. Fc-abhängige, zusätzliche Mechanismen wurden daher im humanen Kryohautschnittmodell untersucht, unter Nutzung der gleichen monoklonalen anti-Dsg3-Autoantikörper in verschiedenen Isotypvarianten. Inkubation der Kryohautschnitte mit

einem monoklonalen anti-Dsg3-IgA1-Autoantikörper und humanen peripheren, mehrkernigen Leukozyten führte zu intraepidermaler Akantholyse und typischer Pathologie, während der gleiche Antikörper im IgG1-Format diese Effekte nicht zeigte und sich keine Gewebspathologie nachwiesen ließ. Die Promovendin zeigt in dieser Arbeit schlüssige Daten für die Relevanz der Interaktion von anti-Dsg3-IgA1-Fc und Fcα-Rezeptor (FcαR) in der Pathophysiologie des IgA-Pemphigus, welche nicht von einer Inaktivierung von Dsg1 in der Epidermis abhängig ist. Die Blockade dieser Interaktion der Fc-Region Dsg3-bindender IgA1-Antikörper und FcαR-exprimierender Leukozyten könnte ein sehr effektives, zukünftiges Therapieprinzip für diese zum Teil sehr schwierig zu behandelnde Autoimmundermatose darstellen. Die hier ebenfalls nachgewiesene Kreuzreaktivität unserer humanen monoklonalen, rekombinanten IgA1 und IgG-Autoantikörper mit murinen Keratinozyten stellt eine exzellente Grundvoraussetzung zur weiteren Untersuchung neuer Therapieoptionen in In-Vivo-Modellen dar. Die hier gezeigten Ergebnisse lassen sich auf andere Erkrankungen der Haut und Schleimhäute übertragen, bei denen autoreaktives IgA involviert ist (z. B. lineare IgA-Dermatose, Schleimhautpemphigoid, oder IgA-Epidermolysis bullosa acquisita).

TABLE OF CONTENTS

LIST OF FIGURES

LIST OF TABLES

ABBREVIATIONS

AIBDs	Autoimmune bullous skin diseases
APD	Antibody phage display
AutoAb, AutoAbs	Autoantibody, autoantibodies
bp	Base pair(s)
BCRs	B cell receptors
BSA	Bovine serum albumin
BMZ	Basement membrane zone
cAMP	Cyclic adenosine monophosphate
CDR	Complementarity determining regions
CMV	Cytomegalovirus
DAPI	Diamidino-2-phenylindole dihydrochloride
DDW	Double distilled water
DEJ	Dermo-epidermal junction
DH	Dermatitis herpetiformis
DIF	Direct immunofluorescence
DMEM	Dulbecco's Modified Eagle's Medium
dNTP	Deoxynucleotide
DP	Desmoplakin
Dsc, Dscs	Desmocollin, desmocollins
Dsg, Dsgs	Desmoglein, desmogleins
DTD	Desmoglein terminal domain
EA	Extracellular anchor
EBA	Epidermolysis bullosa acquisita
EC	Extracellular domain
EDTA	Ethylenediaminetetraacetic acid
ELISA	Enzyme-linked immunosorbent assay
ETA	Exfoliative toxin A
Fab	Fragment antigen binding
FACS	Fluorescence-activated cell sorting
FBS	Fetal bovine serum
H&E	Hematoxylin and eosin
EGFRK	Epidermal growth factor receptor kinase
Gly	Glycine
HiB	Haemophilus influenza B
HRP	Horseradish peroxidase
HSOC	Human skin organ culture
IEN	Intraepidermal neutrophilic dermatosis
IA	Intracellular anchor
IAD	intercellular IgA dermatosis

ICF	Epidermal intercellular fluorescence
ICS	Intracellular catenin binding site
IDP	Inner dense plaque
IF	Immunofluorescence
IFT	Immunofluorescence testing
Ig	Immunoglobulin
IIF	Indirect immunofluorescence
IL	Interleukin
IMAC	Immobilized metal ion affinity chromatography
IP	Immunoprecipitation
IPTG	Isopropyl-β-D-thiogalactopyranoside
ITAM	Immunoreceptor tyrosine-based activation motif
kDa	Kilo Dalton
KIF	Keratin intermediate filaments
LAD	Linear IgA dermatosis
LB medium	Luria-Bertani medium
LC-MS/MS	Liquid chromatography high-resolution tandem MS
LD PCR	Long-distance PCR
mAb, mAbs	Monoclonal antibody, Monoclonal antibodies
ME	Monkey esophagus
MHC	Major histocompatibility complex
MIE	Major immediate-early enhancer
min	Minutes
MK2	MAPK-activated protein kinase 2
MMP	Mucous membrane pemphigoid
mTOR	Mammalian target of rapamycin
NETs	Neutrophil extracellular traps
NH IgA	Normal human IgA
NH IgG	Normal human IgG
NHS	Normal human serum
OD	Optical density
ODP	Outer dense plaque
O/N	Overnight
PBMCs	Peripheral blood mononuclear cells
PBS	Phosphate buffered saline
PCR	Polymerase chain reaction
PEG	Polyethylene glycol
PF	Pemphigus foliaceus
PFU	Plague forming units
PG	Plakoglobin
pIgR	Polymeric immunoglobulin receptor

PKP	Plakophilin
PM	Plasma membrane
PMNs	Polymorphonuclear leukocytes
PNP	Paraneoplastic pemphigus
p38MAPK	p38 mitogen-activated protein kinase
RBCs	Red blood cells
ROS	Reactive oxygen species
RT	Room temperature
PV	Pemphigus vulgaris
PVeg	Pemphigus vegetans
RUD	Repeated unit domain
SA	Splice acceptor
SB	Super broth
scFv	Single-chain variable fragment
SDS-PAGE	Sodium dodecyl sulfate polyacrylamide gel electrophoresis
Ser	Serine
SIgA	Secretory IgA
SOC	Super optimal broth
SPD	Subcorneal pustular dermatosis
ssDNA	Single-stranded DNA
TBS	Tris-buffered saline
TBS-T	TBS-Tween
TMB	3,3′,5,5′-tetramethylbenzidine
V_H	Heavy chain variable region
V_L	Light chain variable region
VH	Variable heavy chain gene
VL	Variable light chain gene

1 INTRODUCTION

1.1 Skin structure and function in human

The skin is the largest organ of the body, accounting for about 15% of the total adult body weight and a surface area of about 1.2-2.0 m^2. It exerts multiple crucial functions including the protection against external physical, chemical, and biological assailants, prevention of excess water loss from the body, and thermoregulation. It is also involved in the body's defense mechanisms, which are controlled by several types of immune cells. The skin is composed of three layers: the epidermis (outermost layer), dermis, and subcutis (consisting of fatty tissue that connects the dermis to underlying skeletal/muscular components) [1]. The epidermis is a stratified, squamous epithelium layer that is composed of many cell types, the majority (~90%) of which are keratinocytes. This layer also contains a few other distinct cell populations such as dendritic cells, Langerhans cells, melanocytes, Merkel cells, and infrequent T cells. The epidermis is commonly divided into four layers according to the keratinocyte morphology and position including the basal cell layer (stratum basale), squamous cell layer (stratum spinosum), granular cell layer (stratum granulosum), and cornified or horny cell layer (stratum corneum) (Fig. 1).

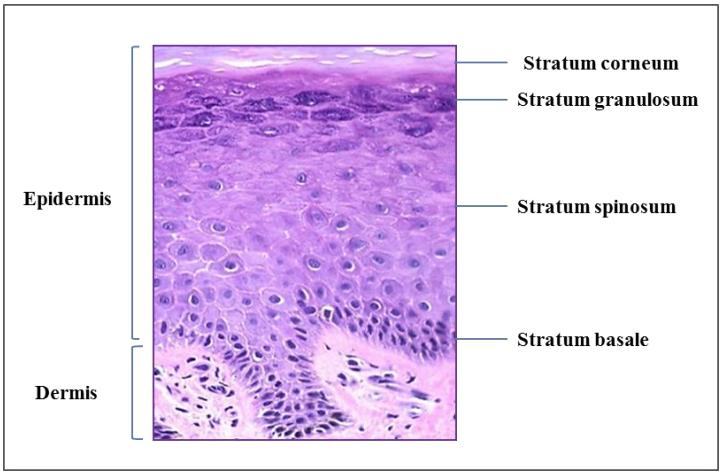

Figure 1: Structure of human skin

The skin consists of three layers: the epidermis, dermis, and subcutis (not shown). Layers of the epidermis, where the target antigens of IgA pemphigus are expressed, include stratum basale, straturm spinosum, stratum granulosum, and stratum corneum. Figure adopted and modified from [2].

The interface between the epidermis and dermis or the dermo-epidermal junction (DEJ) is formed by a porous basement membrane zone (BMZ) that allows the exchange of cells and fluid and mediating adhesion by holding the two layers together [3]. The DEJ supports the epidermis, establishes cell polarity and growth orientation, directs the organization of cytoskeleton in basal cells, provides developmental signals, and acts as a semipermeable barrier between layers. The dermis is an integrated system of fibrous, filamentous, and connective tissue that accommodates stimulus-induced entry by nerve and vascular networks. The dermis comprises the bulk of the skin and provides its elasticity and tensile strength [1, 4].

1.1.1 Desmosomes: cell-cell adhesion structures of keratinocytes

Desmosomes are junctional protein complexes that mediate intercellular adhesion and present in all stratified epithelia. The desmosome is divided into three regions: the extracellular core, outer dense plaque (ODP), and inner dense plaque (IDP) (Fig. 2A-B). The extracellular core is composed of desmosomal cadherins. These transmembrane glycoproteins provide intercellular adhesion by binding to the extracellular N-terminal of their opposing counterpart. At the intracellular level, cadherins' extremities interact with plakoglobin (PG) and plakophilin (PKP), thus forming the ODP. Besides mediating adhesion within the desmosomal protein complex, PG and PKP play a role in regulating the desmosomal assembly. PG and PKP in turn bind to desmoplakin (DP). The DP's tail, situated in the cytoplasmic IDP, directly connects to the cytoskeletal intermediate filaments. In humans, there are seven desmosomal cadherins; four desmogleins (Dsg1-4) and three desmocollins (Dsc1-3) (Fig. 2C). Dsgs and Dscs contain four extracellular cadherin homology repeats and a fifth domain termed the extracellular anchor (EA). Cadherin repeats are approximately 110 amino acids each and are separated by calcium-binding motifs. Extracellular calcium supports cadherin-mediated adhesion by allowing the cadherin extracellular domain to form a rigidified, functional conformation. The transmembrane domain of cadherins is followed by an intracellular anchor (IA) which is a binding site for PG. The Dsg cytoplasmic domain is distinguishable from that of other cadherins by its unique proline rich linker domain, a repeated unit domain (RUD) containing a variable number of a 29-amino acid motif, and a Dsg terminal domain (DTD). The desmosomal cadherins show complex developmental and differentiation patterns of expression (Fig. 2D). Dsg2 and Dsg3 are mainly distributed throughout the lower layers of the epidermis, whereas Dsg1 is expressed in the upper

layers. Dsg4 is expressed in hair follicle and heart tissue. Dsc2 and Dsc3 are present in the basal and spinous layers, whereas Dsc1 is expressed in the granular layer [5-7].

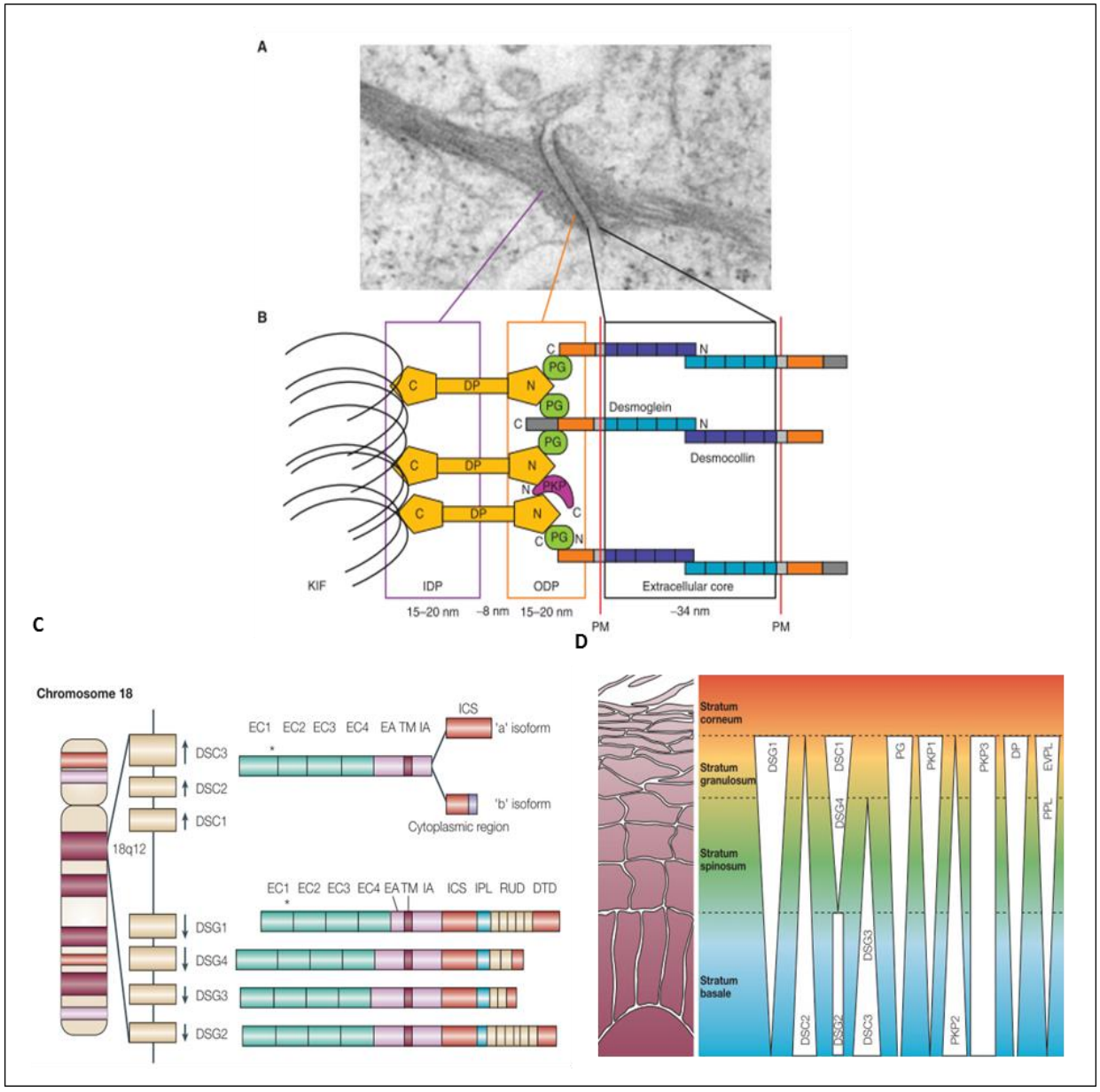

Figure 2: Schematic representation, genomic structure, and expression level of desmosomal proteins in human epidermis

(**A**) Electron micrograph of a desmosome. (**B**) Schematic representation of desmosomal proteins and relative distance from the plasma membrane (PM). (**C**) The organization of desmocollin and desmoglein genes on human chromosome 18. All cadherins contain four extracellular (EC) domains, an extracellular anchor (EA), a single transmembrane domain, an intracellular anchor (IA), and an intracellular catenin binding site (ICS). (**D**) Several desmosomal cadherin, armadillo, and plakin proteins are expressed in a differentiation-dependent manner in the mammalian epidermis. Adopted from [5, 6].

1.2 Autoimmune bullous skin diseases

Autoimmune bullous skin diseases (AIBDs) represent a group of severe, chronic, and potentially fatal skin diseases associating with autoAbs directed against desmosomal proteins (pemphigus group), hemidesmosomal proteins (pemphigoid group, e.g., epidermolysis bullosa acquisita), or transglutaminases (dermatitis herpetiformis). The appearance of blisters and erosions on the skin and/or mucous membranes, caused by loss of cell-cell or cell-matrix adhesion, is the leading clinical manifestation of AIBDs. Depending on the histological/ultrastructural location of blisters, the disease presents with either intraepidermal (intraepithelial) or subepidermal (subepithelial) blisters (Table 1). The diagnosis of AIBDs is based on the clinical presentation, histology of lesional skin, direct immunofluorescence (DIF) of perilesional skin, and indirect immunofluorescence (IIF) using monkey esophagus (ME) and salt-split human skin [8-10].

Table 1: Autoimmune blistering diseases of the skin

Disease	Split formation	Targeted skin organelle	Autoantigen(s)
Pemphigus vulgaris	Suprabasilar	Desmosome	Dsg3
Pemphigus foliaceus	Subcorneal	Desmosome	Dsg1
Paraneoplastic pemphigus (PNP)	Suprabasilar	Desmosome, Hemidesmosome	Dsg3, Dsg1, plakins, BP180, and others
IgA pemphigus	Subcorneal/intraepidermal pustules	Desmosome	Dsc1, Dsg1, and Dsg3
Bullous pemphigoid (BP)	Subepidermal	Hemidesmosome	BP180 and BP230
Herpes gestationis	Subepidermal	Hemidesmosome	BP180
Mucous membrane pemphigoid (MMP)	Subepidermal	Hemidesmosome	BP180, laminin 332
Linear IgA dermatosis (LAD)	Subepidermal	Hemidesmosome	BP180 fragments
Epidermolysis bullosa acquisita (EBA)	Subepidermal	Anchoring fibrils	Type VII collagen
Dermatitis herpetiformis (DH)	(Subepidermal)	-	Epidermal transglutaminase

1.3 Pemphigus group - diseases of intraepidermal loss of adhesion

The term pemphigus is derived from the Greek word pemphix, meaning blister. Pemphigus comprises a group of AIBDs which is clinically characterized by flaccid blisters and erosions of mucous membranes and/or skin and histologically by intraepidermal acantholysis, i.e., loss of cell-cell adhesion. In the two main subtypes, pemphigus vulgaris (PV) and pemphigus foliaceus (PF), autoAbs are directed against the desmosomal proteins Dsg3 and/or Dsg1 (Fig. 3). IgA-pemphigus is less common, but a difficult-to-treat, variant of pemphigus [11, 12]. PV frequently begins with oral lesions and progresses to skin, whereas PF only affects the skin. The blisters of PV break easily, leaving erosions and crusts. In PF, the blisters are even more fragile, therefore PF patients develop flaccid blisters and scaly, crusty skin erosions. The Nikolsky sign, i.e., mechanical induction of erosions by shearing of unaffected epidermis, is positive during the active phase of both subtypes. In PV, acantholysis of the basal cell layers leads to a suprabasilar blister. The basal keratinocytes often lose cell-cell adhesion, forming a so-called “row of tombstones” pattern. In PF, acantholysis occurs in the upper epidermis, just below the stratum corneum, within or beneath the granular layer. The immunohistological hallmark of pemphigus is the presence of cell surface-bound IgG in epidermis. Almost all classical pemphigus patients show IgG depositions in DIF testing of perilesional skin. Additionally, more than 80% of pemphigus patients have circulating autoAbs directed against keratinocyte cell surfaces. Patients with PF have only anti-Dsg1 autoAbs, whereas patients with mucosal-dominant type of PV have mostly, if not only, anti-Dsg3 autoAbs and those with mucocutaneous type of PV have anti-Dsg3/1 autoAbs. Therefore, the IF pattern alone is not sufficient to differentiate the PV and PF subtypes [9, 10, 13].

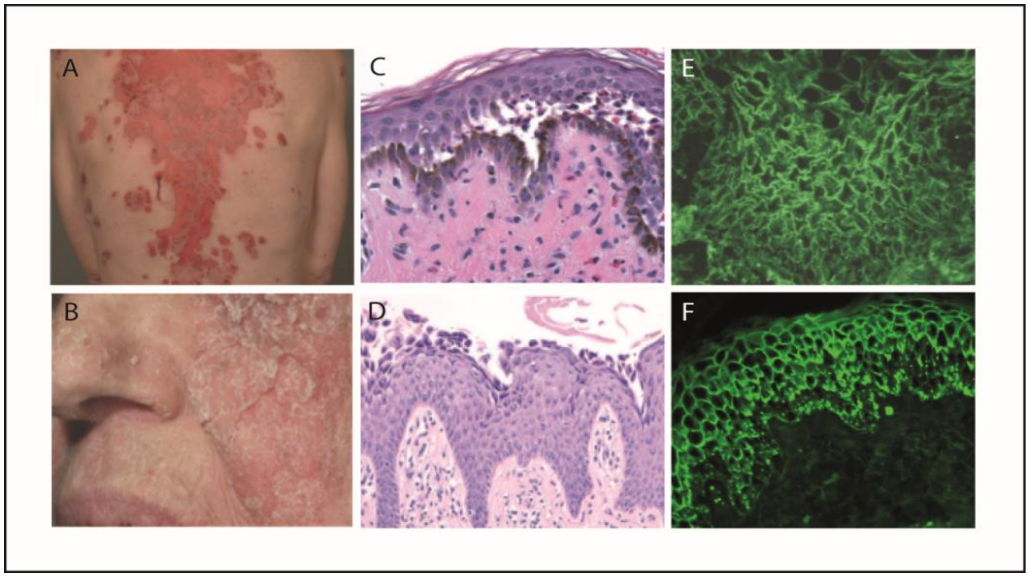

Figure 3: Clinical, histological, and immunopathological findings in pemphigus

(**A**) Clinical images of pemphigus vulgaris (PV) with large erosions and (**B**) pemphigus foliaceus (PF) with scaly crusted lesions. (**C**) Histology shows a suprabasilar blister in PV and (**D**) acantholysis at the granular layer of the epidermis in PF. (**E**) Indirect immunofluorescence (IIF) of PV on monkey esophagus (ME) and (**F**) PF on normal human skin show cell surface binding of IgG. Adopted from [13].

1.3.1 Desmoglein compensation theory

The correlation between the autoAb profile and clinical phenotype in mucosal PV, mucocutaneous PV, and PF can be pathophysiologically explained by the Dsg compensation theory [14]. This theory states that Dsg1 and Dsg3 molecules can compensate for each other when they are co-expressed in the same cell layer and the adhesive function is impaired in one of them (Fig. 4). Consistent with the compensation theory in pemphigus, exfoliative toxins produced by *Staphylococcus aureus* specifically cleave Dsg1 and cause superficial blisters in the skin but not in the oral mucosa, as the mucosa expresses high levels of Dsg3 at all layers [15].

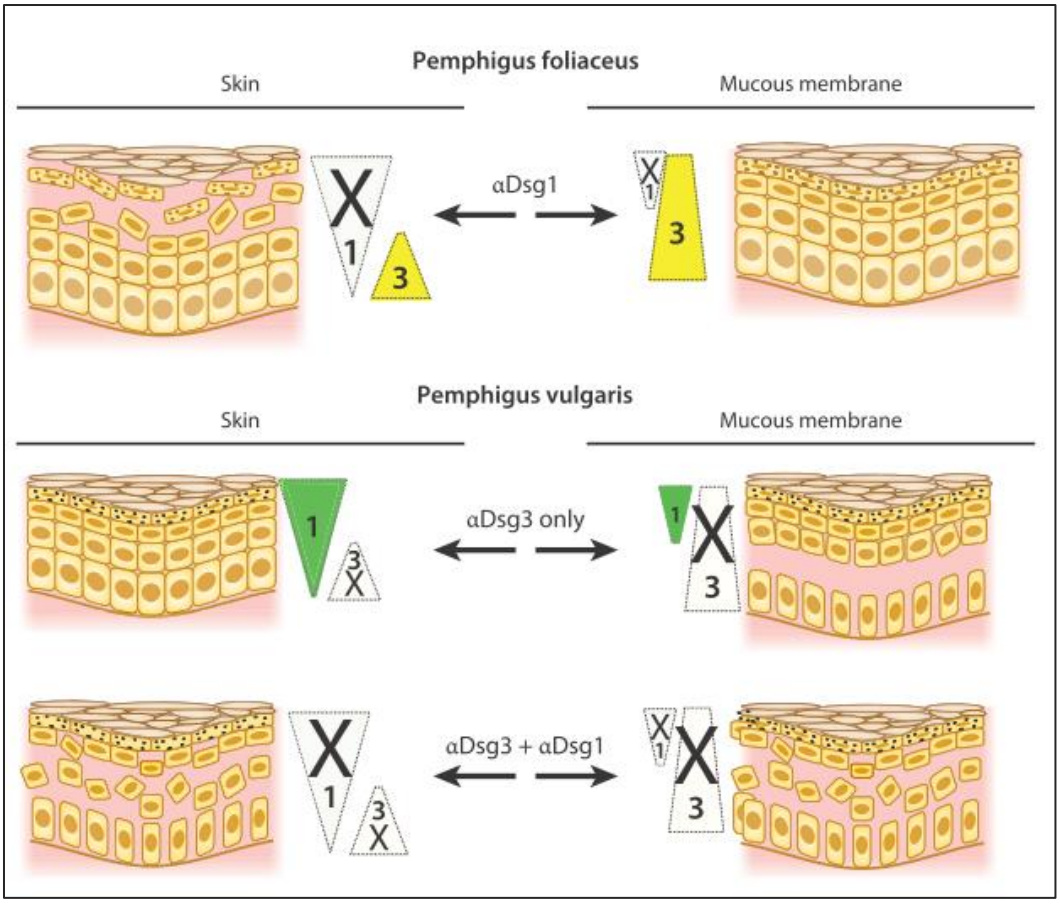

Figure 4 : Desmoglein compensation theory in pemphigus

Triangles show the normal localization of Dsg1 (green) and Dsg3 (yellow) in the skin epidermis and mucous membrane. Triangle width indicates the relative amount of Dsg presents at each cell layer. Loss of color in a triangle represents loss of function of that particular Dsg due to the presence of anti-Dsg (α-Dsg) antibodies. In any area in which Dsg1 or Dsg3 function has been inactivated and the other Dsg is not present to compensate, a blister (shown as loss of cell-cell adhesion) occurs. Adopted from [11].

1.3.2 Theories on the mechanism of acantholysis in pemphigus

Studies on experimental models of pemphigus (e.g., human cultured keratinocytes, skin biopsies of patients, and *in vivo* mouse models) suggest several molecular mechanisms by which IgG autoAbs induce epithelial acantholysis. These proposing models include: (i) the steric hindrance of desmosomal adhesion, (ii) interference with desmosomal assembly, and (iii) cell signaling (Fig. 5) [16].

The steric hindrance theory states that the anti-Dsg autoAbs directly interfere with trans- or cis-adhesive interface of Dsgs. Early support to this hypothesis was generated from induction of pemphigus by passive transfer of IgG from pemphigus patients into mice [17]. An epitope-mapping study conducted by Sekiguchi *et al.,* [18] showed that PF and PV sera are mostly bound to the N-terminal ectodomains of Dsg1/3. It was later demonstrated that a murine anti-Dsg3 mAb could induce a PV phenotype [19]. Recent research demonstrated that the bivalent F(ab′)2 and monovalent Fab′ fragments purified from PF patients' sera and the scFv mAbs cloned by antibody phage display from pemphigus patients are also able to induce acantholysis [20-23].

The Dsg non-assembly depletion theory describes how anti-Dsg autoAbs cross-link and cluster Dsgs which in turn lead to internalization of non-junctional Dsg pool and also prevention of incorporation of newly synthesized desmogleins into forming desmosomes [24, 25]. The observations made by IF and electron microscopy confirmed that the autoAb-targeted Dsgs are relocalized into clustered pattern on the skin of PV and PF patients [26]. Further evidences supporting this model are originated from *in vitro* cell culture experiments and mouse models [27-29].

Several signaling pathways have been implicated in pemphigus pathogenesis including p38MAPK (p38 mitogen activated protein kinase), Rho GTPases, cyclic adenosine monophosphate (cAMP), c-myc, epidermal growth factor receptor kinase (EGFRK), mTOR (mammalian target of rapamycin), heat shock protein 27 (HSP27), and phospholipase C or protein kinase C [30-35]. In addition, these studies suggest that signaling molecules may also be involved in the desmosomal homeostasis [36]. These suggested models are most likely not opposing one another but rather complementing observed pathologies in pemphigus.

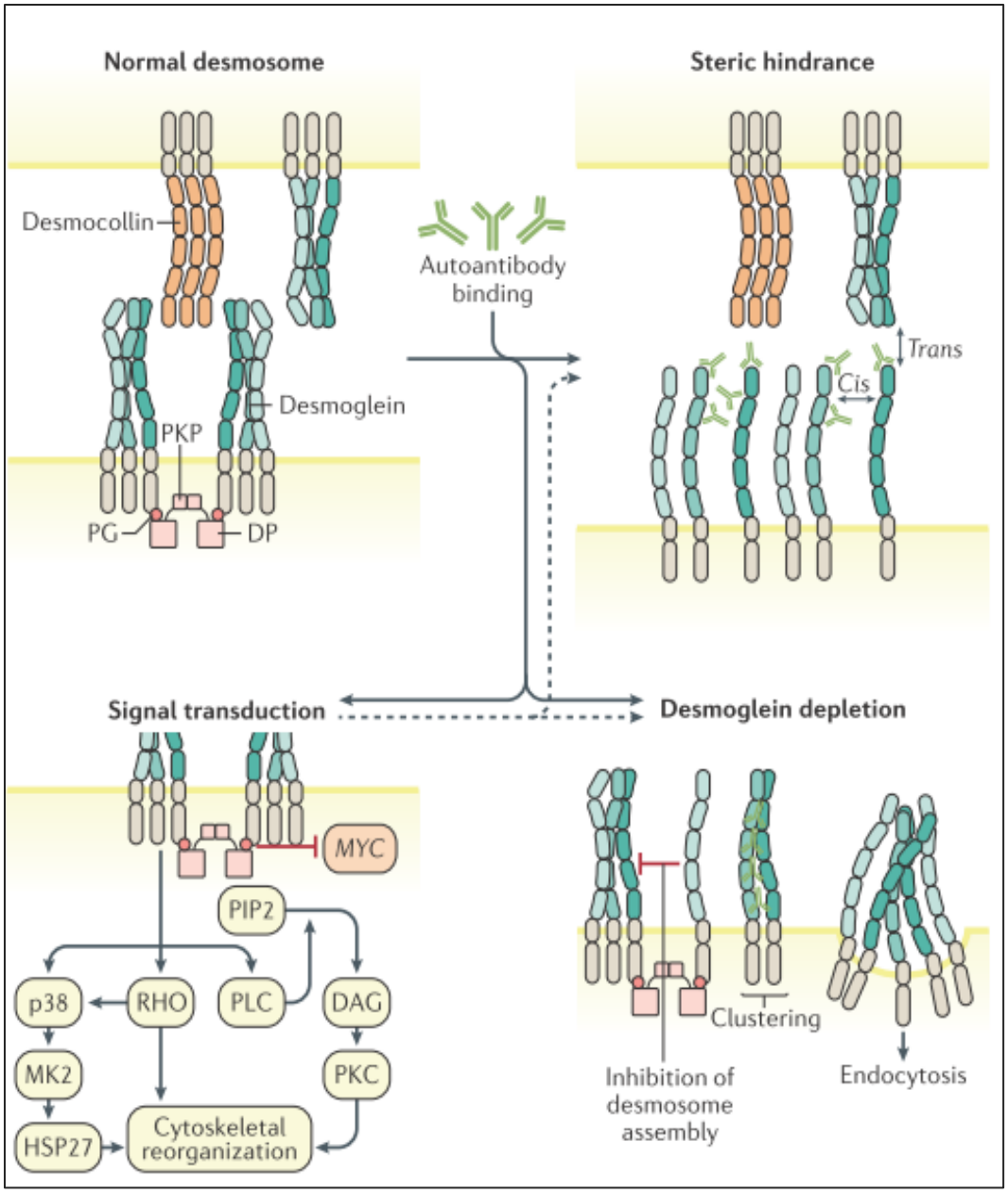

Figure 5: Mechanisms of acantholysis in pemphigus

Anti-Dsg autoAbs cause acantholysis through different mechanisms: the steric hindrance of Dsg-mediated trans- (between molecules on opposing cells) and cis- (between molecules on the same cells) adhesion, inhibition of desmosome assembly or promotion of desmosome disassembly (by clustering and/or endocytosis of Dsgs), and stimulation of signaling pathways. Adopted from [11].

1.4 Intercellular IgA dermatosis

Within the group of AIBDs, intercellular IgA dermatosis (IAD) is a heterogeneous disease entity presenting with a wide spectrum of clinical, histopathological, and immunological features. A unifying feature is tissue-bound and circulating IgA, but no, or much less so, IgG autoAbs against keratinocyte cell surface molecules, mediating cell-cell adhesion. The presence of skin-bound IgA antibodies was first reported by Varigos *et al.,* [37]. Since then, various terms have been used to describe this condition. In 1992, Wallach *et al.*, [38] named the condition as 'subcorneal pustular dermatosis and monoclonal IgA'. In their work, Wallach and colleagues reported a case with clinical phenotype of Sneddon-Wilkinson disease showing pustulo-bullous eruptions, but presenting a unique IF pattern of subcorneal IgA deposition around epidermal cells [39]. Subsequent reports emphasized the similarity of this entity to other neutrophilic dermatoses such as intraepidermal neutrophilic IgA dermatosis and intraepidermal IgA pustulosis [40]. Later case reports further stressed the immmunopathologic analogy to the pemphigus group (e.g., IgA-PF, IgA herpetiform pemphigus, and intercellular IgA vesiculopustular dermatosis) [41, 42]. IAD is classified into five subtypes including the subcorneal pustular dermatosis (SPD)-subtype, intraepidermal neutrophilic dermatosis (IEN)-subtype, IgA pemphigus vegetans (IgA-PVeg), IgA pemphigus foliaceus (IgA-PF), and IgA pemphigus vulgaris (IgA-PV) [43]. A diagnosis of the SPD-subtype was given to cases which showed clinically superficial pustules, particularly on the intertriginous areas, and histopathologically subcorneal neutrophilic pustules. Reactivity to Dscs has been documented in the SPD-subtype [44-47]. A diagnosis of the IEN-subtype was based on a clinical display of atypical pustular lesions with sunflower-like configuration and histopathologically neutrophilic pustules in the mid-epidermis. IgA antibodies against the antigens of classic pemphigus, Dsg1 and Dsg3, are detected in a small portion of the IEN cases [48]. IgA-PVeg presented with typical vegetating lesions clinically characterized by the development of papillomatous and verrucous vegetations with a predilection for intertriginous sites. The antigen of IgA-PVeg is still unknown, although one rare case showed reactivity to Dsc2 [43, 49]. IgA pemphigus is manifested clinically by fragile, fluid-filled blisters that often transform into vesiculopustular lesions and histologically present epidermal acantholysis and prominent neutrophil infiltration [8, 10]. Lesions tend to occur on the trunk and proximal extremities with flexural predilection and can be intensely pruritic. While involvement of

mucosal membrane is generally rare, isolated cases with more pronounced, refractory mucositis may clinically mimic the paraneoplastic pemphigus (PNP). IgA pemphigus is rare autoimmune blistering disorder, although it is probably underdiagnosed. It has been reported in those aged 1 month to 92 years [50]. The sex distribution reveals a male-to-female ratio as 1:1.33 [51]. Diagnosis of IgA-PV and IgA-PF is made based on the detection of anti-Dsg IgA antibodies by ELISA and immunoblotting. Regardless of clinical and histopathological diagnoses used for other IAD subtypes, cases with positive ELISA results for Dsg1-IgA and Dsg3-IgA are classified as IgA-PF and IgA-PV, respectively [52]. Treatment of IgA pemphigus is performed based on the disease pathomechanism and anecdotal reports [53]. IgA pemphigus responds to a variety of anti-inflammatory, often specifically anti-neutrophilic agents. Traditionally, dapsone has represented as drug of first choice due to its ability to inhibit neutrophil infiltration. Although many patients respond to treatments within a few weeks, responses may be either insufficient, transient or even absent. Retinoids, either alone or in combination with dapsone, are considered as the second-line therapy. Rituximab, an anti-CD20 mAb, is recommended when the conventional immunosuppressive drugs are ineffective, contraindicated or have unacceptable side effects. Previous studies in pemphigoid diseases demonstrated that rituximab was effective in recalcitrant IgG-dominant but not in IgA-dominant pemphigoid cases. Hence, it is concluded that the complete remission of this condition is difficult to achieve and maintenance therapy is usually required [43, 51, 54-56].

1.4.1 Pathophysiology of IgA pemphigus

IgA pemphigus is characterized by deposits of IgA autoAbs in the skin as well as dense inflammatory infiltrates, mainly dominated by neutrophils. In contrast to IgG, little is known about the pathogenic effects of IgA-subtype autoAbs. Although their molecular targets are well-studied, the potential of IgA autoAbs to induce tissue damage and the pathogenic relevance of their interaction with granulocytes have not yet been investigated. The few current hypotheses on the pathomechanisms of IgA pemphigus suggest that the tissue damage occurs due to weakening of the cell-cell adhesion molecules, as seen in the case of IgG pemphigus. In contrast to classical IgG pemphigus, complement deposition has not been demonstrated in most cases of IgA pemphigus indicating that pathophysiology may be complement independent [57]. The regulatory role of helper T cells or their products on IgA antibody production has been

demonstrated. *In vivo* studies showed that interleukin-(IL)-5 produced by Th2 CD4+ T cells increased IgA class switching [58]. An impaired mucosal IgA response was also demonstrated in γ/δ TCR-deficient mice [59]. A positive correlation between the levels of circulating IL-8 and IgA antibodies was also described in the IgA-mediated skin conditions [60]. Most importantly, IgA autoAbs can activate the IgA-Fc receptor FcαRI (CD89) expressed on cells of the myeloid lineage such as neutrophils. Cross-linking of FcαRI by IgA immune complexes initiates complement-independent inflammatory responses such as phagocytosis, antigen presentation, and release of inflammatory cytokines, reactive oxygen species (ROS), neutrophil extracellular traps (NETs), and proteases, which ultimately result in tissue damage [61, 62]. In support to this concept, a study conducted by van der Steen *et al.*, suggests that the neutrophil migration and activation via FcαRI is responsible for tissue damage in linear IgA dermatosis (LAD) [63]. Further research is required to better understand the exact pathophysiology of IgA autoAbs and the potential contribution of neutrophil accumulation in tissue pathology in the understudied IgA pemphigus.

1.5 General concepts on immunoglobulins

Given the critical role of the antibody response in AIBDs, here I briefly present an overview of the antibody structure and its functional properties. Antibodies or immunoglobulins (Igs) are key mediators of the humoral immune response and are produced by B lymphocytes as a response to foreign antigens. An antibody monomer is composed of two identical light chains and two identical heavy chains, which are assembled via a series of covalent and non-covalent interactions into globular structures, hence the term immunoglobulin (Fig. 6). The variable heavy (V_H) and light (V_L) chains are present in the Fab (fragment antigen binding) region that interacts with antigen. The variable region consists of conserved framework regions and hypervariable or complementarity determining regions (CDR) in between. The CDR3 loop is a region of the antibody heavy chain that has the greatest impact on the antigen specificity. The constant region of the heavy chain, the Fc region or Fc tail, is composed of several globular subunits homologues to one another and also to the constant region of the light chain. The Fc-portion determines the antibody isotype and interacts with Fc receptors on immune cells [64, 65]. The genetic complexity of the antibody repertoire in an individual's B cells, prior exposure to the antigen, is

generated by the combinatorial assembly of variable (V), diversity (D), and joining (J) gene segments, CDR3 diversity, and unique pairing of the heavy and light chains. Developing B cells generate the heavy chain by assembling the germ line arrays of V, D, and J gene segments with an IgM type constant region. The heavy chain is then combined with a subsequently rearranged light chain, made from a V and J segment in conjunction with a constant light (CL) gene. Light chains are of two types, kappa (Igκ) or lambda (Igλ), while heavy chains are of five isotypes (IgM, IgD, IgG, IgA, and IgE). An overview of the basic features of antibody classes is given in Table 2 [66].

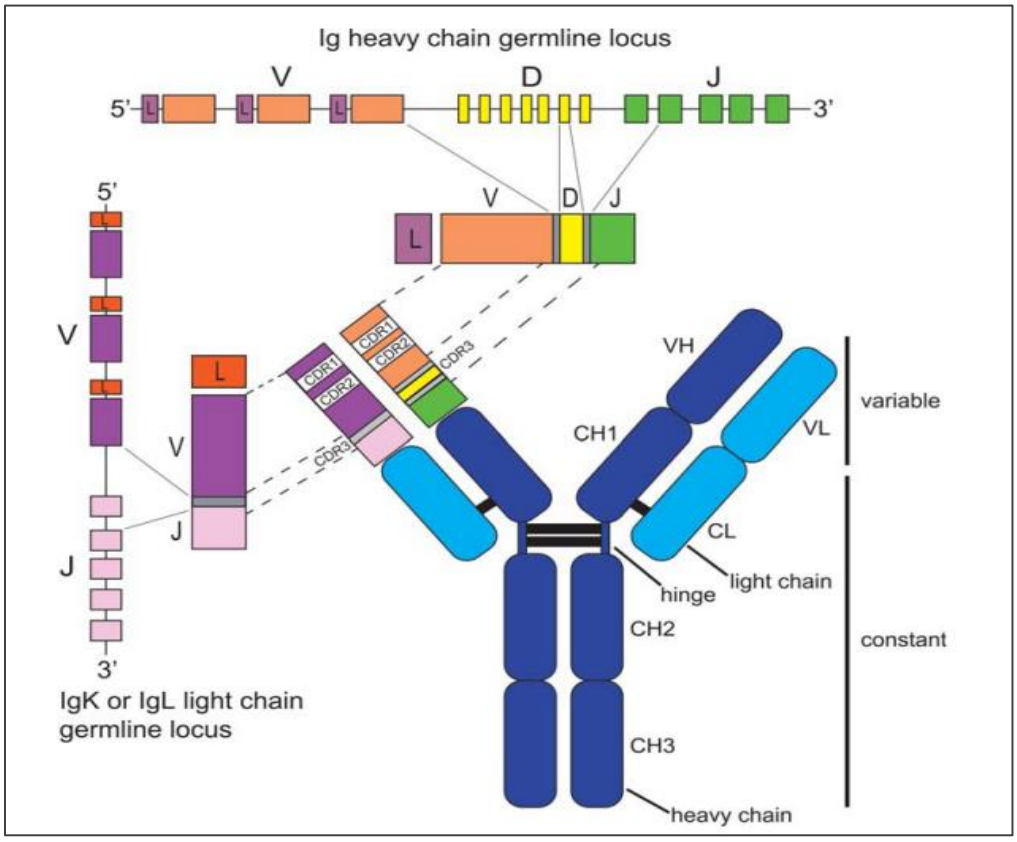

Figure 6: Antibody structure and genetic encoding

The germ line genomic DNA configuration of the immunoglobulin heavy chain locus is depicted at the top of the figure. A germ line kappa or lambda light chain locus is shown on the left-hand side. The antibody constant regions (domains CH1, CH2, and CH3 for the heavy chain and CL for the light chain) are encoded by downstream exons that are joined to the rearranged V(D)J gene by mRNA splicing. Disulfide bridges joining protein chains in the full antibody structure are shown with black line segments. Adopted from [64].

Table 2: The five classes of human antibody and their functions

Immunoglobulin	IgA	IgD	IgE	IgG	IgM
Heavy chain class	α	δ	E	γ	μ
Heavy chain subclass	α_1 α_2	δ_1 δ_2	-	γ_1 γ_2 γ_3 γ_4	-
Light chain type	κ and λ	κ and λ	κ and λ	κ and λ	κ and λ
Molecular weight (kDa)	160	180	200	150	900
Valence	2 or 4	2	2	2	10
Add. polypeptides	JC* and SC**	-	-	-	JC
Complement activation	-	-	-	+***	+++
Plasma half-life (d)	6	3	2	23 7 for IgG4	5-10
% Total Ig	13	0.2	0.005	80	6
Serum conc. (mg/mL)	1.8	0.03	0.00005	10	1.2
Maternofetal transfer	-	-	-	+++	-
Antibacterial activity	++	-	-	+++	+++
Antiviral capacity	+++	-	-	+++	+
Allergic reaction	-	-	++	-	-
Antitoxin activity	+	-	-	+++	-
Agglutination capacity	++	-	-	+	+++
Biological function	sIgA in mucosa	B cell development	Allergy, parasites	Secondary response	Primary response

*JC: joining chain, **SC: secretory component, ***: depending on IgG subclasses (IgG_1 >> IgG_4)

Mature B cells circulate through blood and secondary lymphoid organs. B cell activation is triggered by binding the B cell receptor to an antigen. Consequently, the B cell starts proliferating and differentiates into an antibody producing plasma cell. Antibodies produced after first exposure to the antigen have low affinity and are of IgM type. IgM forms a pentameric structure, which makes it particularly effective in complement activation [67]. Following activation, the B cells undergo somatic hypermutation towards higher affinity and isotype switching from IgM to IgG isotype. Thus, in a second immune response high-affinity IgG antibodies are produced. IgG is the principal isotype in the blood and extracellular fluid and can efficiently opsonize pathogens for engulfment by phagocytes and complement activation [65]. On the contrary, very sparsely present IgE antibodies are bound avidly by Fcε receptors on mast cells found beneath the skin and mucosa or along the blood vessels in connective tissues. IgE plays a role in parasitic infections and in allergy by binding to allergens and triggering histamine release [68]. The function of IgD is unclear because it is not known to participate in the major antibody effector mechanisms [69].

1.5.1 Immunoglobulin A

Immunoglobulin A (IgA) represents the most prominent antibody class at mucosal surfaces and the second prevalent antibody class in human serum. Two subclasses of IgA are described, IgA1 and IgA2, based on differences in the hinge region of the heavy chains which is displayed as a 13-amino acid deletion in the IgA2 hinge region (Fig. 7). Consequently, the IgA1 hinge region contains six 3-5 O-linked carbohydrate moieties that IgA2 lack [70]. However, both subclasses show high levels of N-glycosylation (6-7% for IgA1 and 8-10% for IgA2) [71]. IgA1, but not IgA2, is sensitive to IgA1-specific proteases produced by bacterial pathogens. Both subclasses of IgA are mainly produced as monomers in serum and as dimers in mucosal tissues, though their distribution is not equal throughout the body. In serum, the predominant subclass of IgA is IgA1 (>85%), while IgA2 expression in the upper airways (10%), salvia, small intestine or large intestine (30-40%), and female genital tract (>50%) varies between these tissues. IgA possess an additional 18-amino acid C-terminal sequence which allows the formation of polymeric molecules. Furthermore, incorporation of a third protein, termed joining chain (JC), enhances the IgA dimerization and enables transcytosis via the polymeric immunoglobulin receptor (pIgR) into the mucosal tissues to form secretory IgA (SIgA) [72].

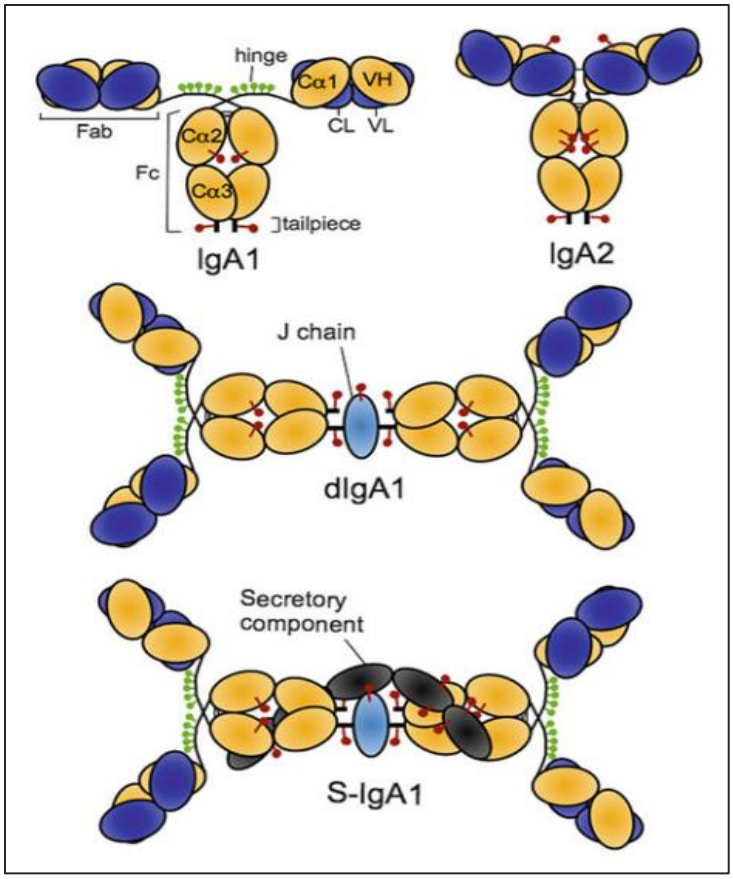

Figure 7: Structure of the IgA molecule

Schematic representation of the monomeric forms of human IgA1 and IgA2 as well as the dimeric (dIgA1) and secretory (SIgA1) forms of IgA1. Heavy chains are shown in gold and light chains in dark blue. Joining (J) chain is shown in light blue and secretory component in dark grey. O-linked sugars on the IgA1 hinge are shown in green, while N-linked oligosaccharides are shown in red. Adopted from [70].

1.5.2 Human IgA Fc receptor (FcαRI)

Several receptors have been identified for IgA such as Fcα/μ, asialoglycoprotein-transferring, SC- or M-cell receptors [73]. IgA receptors bind at the IgA Fab region, Fc-tail, carbohydrate side chains or via the accessory components JC or SC [74-76]. FcαRI, a member of the Fc receptor immunoglobulin superfamily, is expressed on cells of the myeloid lineage that include neutrophils, eosinophils, monocytes, and macrophages. FcαRI is composed of two extracellular domains (EC1 and EC2), a transmembrane region, and a cytoplasmic tail (Fig. 8). The binding site for FcαRI lies at the interface of Cα2 and Cα3 domains of IgA molecule. The interaction site on FcαRI resides in its EC1 domain.

FcαRI signaling requires crosslinking with FcRγ via their respective transmembrane regions (TMs), since FcαRI lacks the immunoreceptor tyrosine-based activation motif (ITAM). ITAM signaling pathway results in the activation of immune cells and induction of proinflammatory functions like phagocytosis, degranulation, oxidative burst, release of cytokines and inflammatory mediators, antigen presentation, and neutrophil migration [77-79].

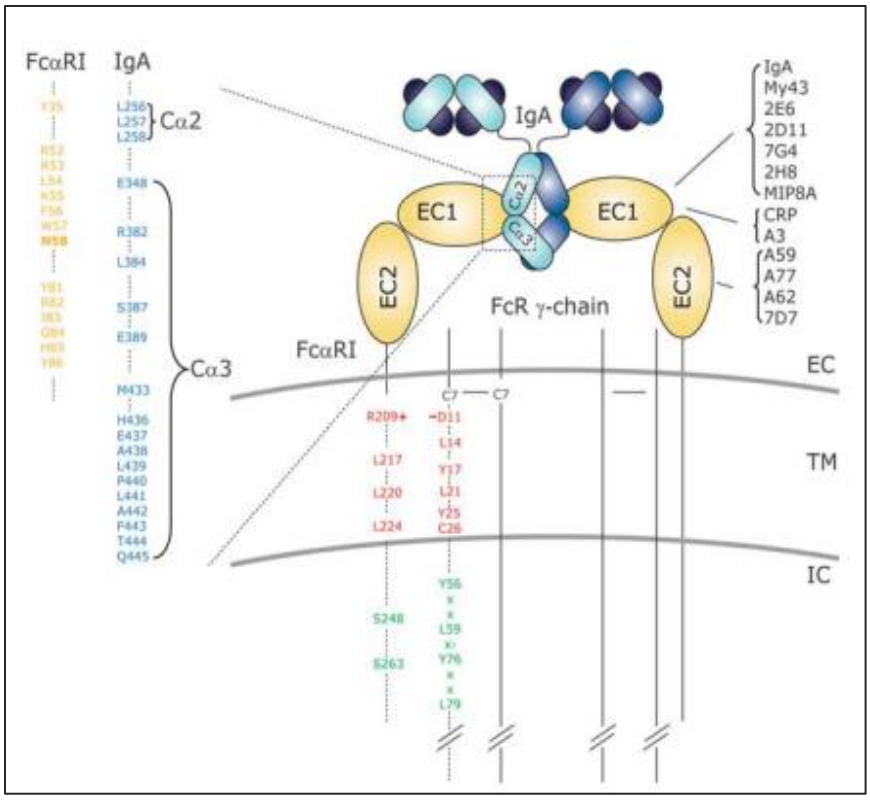

Figure 8: Schematic representation of FcαRI-FcRγ chain complex, binding IgA in 2:1 stoichiometry

Two FcαRI bind each IgA-Fc region at the Cα2 and Cα3 junction via extracellular 1 (EC1). Amino acids involved in ligand-receptor binding are depicted in yellow for FcαRI-EC1 and in blue for Cα2 and Cα3. Amino acids of the transmembrane regions (TMs) in FcαRI-FcRγ chain homo-dimer are depicted in red, whereas amino acids involved in signaling are shown in green. Adopted from [78].

1.6 Antibody phage display technology

Characterization of specific autoAbs will provide significant information on the pathogenesis of disease and may facilitate the design of targeted therapies. To investigate the underlying pathomechanisms involved in IgA-mediated pemphigus, the well-established antibody phage display (APD) method was used here. Phage display is a powerful methodology that allows selection of a particular phenotype (e.g., ligand-specific to a desired antigen) from repertoires of proteins displayed on the surface of filamentous bacteriophage. The methodology was first introduced by Smith in 1985, as a method to display specific binding peptides on the surface of the non-lytic filamentous bacteriophage fd [80]. Since then, different molecules (e.g., small peptides or antibodies) have been displayed on phage coat proteins, greatly expanding the applications of technology in diverse areas such as generation of therapeutic recombinant antibodies, studying protein-ligand interactions, drug discovery, and targeted therapy [81-85]. Production of human mAbs for research and clinical use is closely related to the development of APD technology. The key feature that enables the identification and isolation of favored candidates from antibody libraries is the linkage between the antibody variant to the coding genetic information [85]. Different antibody fragments are used in APD technology: scFv (single chain fragment variable), Fv (fragment variable), Fab (fragment antigen binding) and their derivatives, antibodies with one V-gene domain, bispecific or bivalent antibodies, and other oligomers (Fig. 9) [83, 86].

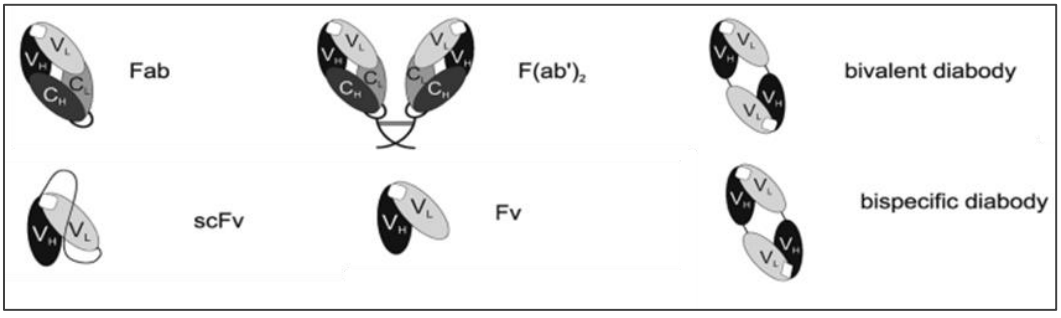

Figure 9: Schematic presentation of antibody fragments

Fab (fragment antigen binding), F(ab') 2 fragments of antibodies, bivalent antibody, scFv (single chain fragment variable), Fv (fragment variable), and bispecific antibody. Adopted and modified from [83].

The most frequently used form of recombinant antibody is scFv, due to its simple structure and low molecular mass (Fig. 10). In addition, scFvs retain the entire antibody-binding site and usually bind to the antigen with an affinity comparable to that of the parental antibody [87]. To construct a human scFv library, RNA obtained from the chosen cell source is reverse-transcribed into cDNA, which is used for PCR of the V_H and V_L chains of the encoded antibodies. PCR products, representing the antibody repertoire, are assembled into a single scFv gene using a DNA linker fragment. The assembled fragment is inserted into a phage display vector (e.g., pComb3X) that is engineered to display scFv fragments as fusion to the pIII minor capsid protein of a filamentous bacteriophage of *Escherichia coli.* The recombinant phagemid is then introduced into competent *E. coli* cells. Phagemid-containing bacterial cells are grown and then infected with a helper phage (e.g., M13VCS or KO7), a process known as "phage rescue". Diverse phage libraries are produced from ~10^8 independent *E. coli* transformants.

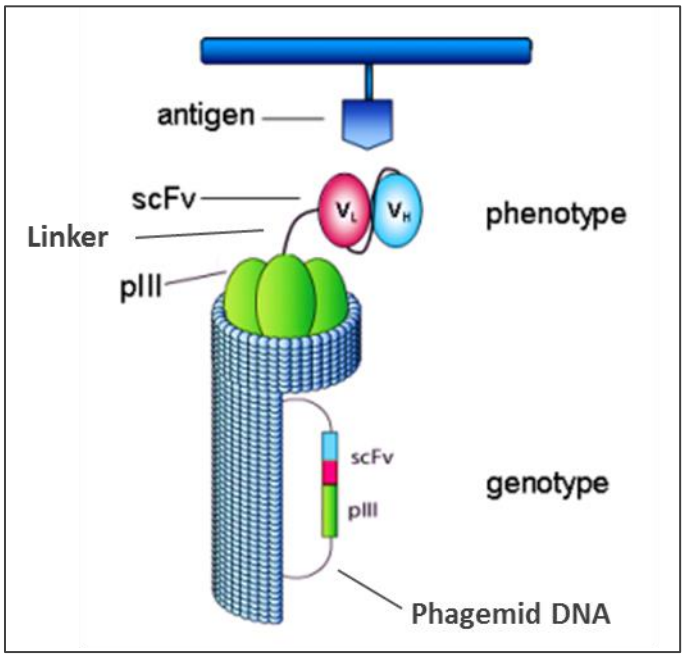

Figure 10: Phage displaying a binding scFv antibody

Schematic representation of a phage bound to an immobilized antigen via the scFv antibody displayed on its surface. The interior of phage harbors the phagemid vector in which the gene for displayed protein is fused to 3' end of the filamentous phage gene pIII coat protein. Abbreviations: scFv, single chain variable fragment; V_H, variable heavy chain; V_L, variable light chain. Figure adopted and modified from [88].

An antibody library is screened for phage binding to a target antigen through its expressed surface mAb by a technique called bio-panning (Fig. 11). Cyclic panning allows for "pulling out" potentially very rare and highly specific, antigen-binding clones. During each round of phage binding, specific binders are selected out from the polyclonal pool by washing away non-binders and selectively eluting the binding phage clones. Elution and reamplification in *E. coli* are performed in every round of panning. Highly specific antigen-bound phages are eluted off either through pH change or protease digestion. The resultant (polyclonal) phage library (i.e., a mixture of all the phages that bind to the antigen chosen) would be sufficiently enriched so that the individual clones can be isolated, tested by monoclonal phage ELISA, sequenced, and finally expressed as soluble scFv in *E. coli*. These mAbs are then purified by metal chelation (e.g., through polyhistidine tag) or affinity purification (e.g., through a HA tag) [89, 90].

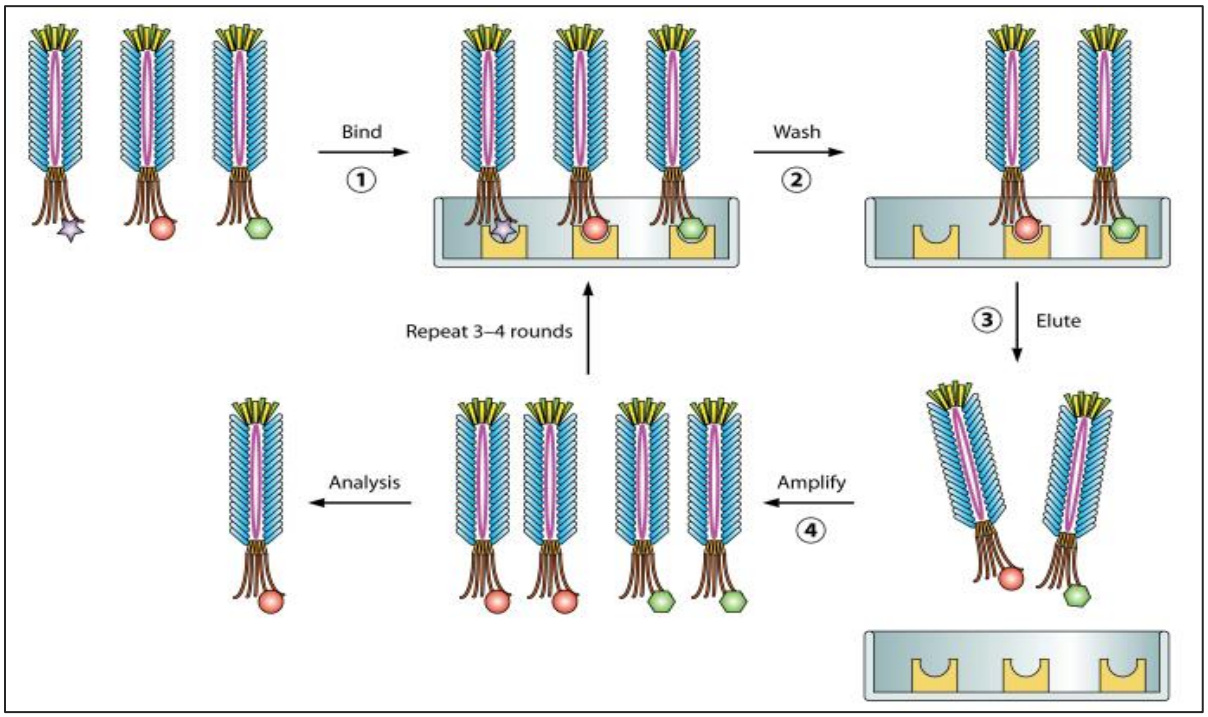

Figure 11: Biopanning of a phage display library to select phage binding to an immobilized target

Biopanning procedure involves four principal steps for phage selection. (**1**) The target is presented to the phage-displayed library allowing the binding (**2**) After incubation, unbound phages are washed. (**3**) The specific phages containing binders to the target can be released after elution. (**4**) To reamplify the eluted phages *E. coli* infection is performed. More than one selection round is needed to permit enrichment of high-affinity clones. Figure adopted from [89].

1.7 Aims of the present study

The main objective of the present study is to gain precise insights into the pathogenesis of IgA pemphigus. The exact mechanism of antibody pathogenicity is difficult to be characterized using serum-derived polyclonal autoAbs. Until recently, little was known about the pathomechanisms leading to tissue pathology in this IgA-mediated skin disease. Moreover, no disease model or antigen-specific IgA monoclonal has been described for this condition so far. Accordingly, the treatment of IgA autoimmune skin disorders is empiric, with the therapeutic modalities being more or less identical for all subtypes. To facilitate dissection of pathomechanisms involved, the high-throughput technique antibody phage display was used to clone, select, and characterize antigen-specific mAbs from circulating IgA^+ B-cell repertoires of our IgA pemphigus patient. Detailed characterization of these mAbs will lead to a better understanding of the disease pathogenesis and help in developing more targeted therapeutic approaches against this sometimes highly treatment-resistant disorder.

2 MATERIALS and METHODS

2.1 Materials

A complete list of all materials used in this study can be found in Appendix.

2.2 Methods Part I: Characterization of polyclonal serum autoAbs

2.2.1 Ethical approval

All experiments were conducted in accordance with the Declaration of Helsinki Principles. Approval for studies using human biological materials was obtained from the Institutional Review Board of the University of Luebeck (reference numbers: 12-178, 15-051) and written informed consent was received from the patients and healthy blood donors.

2.2.2 Recruitments and characteristics of patients included

Serum sample and peripheral blood mononuclear cells (PBMCs) were obtained from a 58 year-old female patient with IgA pemphigus. The patient had active disease and was off systemic therapies at the time of blood draw. Diagnosis of IgA-PV was established by typical clinical presentation (e.g., vesiculopustular lesions on the skin and mucous membranes), histology, and immunological findings. A control cohort comprising sera from IgA pemphigus patients and age- and sex- matched healthy individuals was included.

2.2.3 Immunofluorescence microscopy

Immunofluorescence (IF) assays are an important tool for diagnosing autoimmune blistering diseases, since they detect *in vivo* bound autoAbs. There are two main subtypes: direct immunofluorescence (DIF), which is performed on perilesional skin or mucous membranes to detect tissue-bound autoAbs; and indirect immunofluorescence (IIF), which identifies patient's circulating autoAbs on normal human skin or monkey esophagus (ME) substrates [91].

2.2.3.1 Direct immunofluorescence microscopy

To detect tissue-bound antibodies in patient's skin, DIF microscopy was performed. In brief, skin cryosections (6 μm) were prepared from perilesional skin biopsies using a cryostat. Sections were air-dried for 10 min at room temperature (RT), fixed in cold acetone (10 min at -20˚C), and washed 3 times (for 5 min) in 1x TBS washing buffer, pH 7.4 (supplemented with Tween 20 and 1 mM $CaCl_2$) before staining. These pre-fixed cryosections were then separately incubated with goat anti-human IgA-FITC (dilution, 1:100; SouthernBiotech) and F(ab)2 anti-human IgG FITC (dilution, 1:100; Bio-Rad) secondary antibodies for 60 min at RT. All antibodies were diluted in blocking buffer (1% BSA in TBS washing buffer). Subsequently, slides were washed as above and mounted with diamidino-2-phenylindole dihydrochloride (DAPI) Fluoromount-G® (Ready to use, SouthernBiotech). Slides were stored at -20˚C until visualization using a BZ-9000E series Keyence microscope.

2.2.3.2 Indirect immunofluorescence microscopy

The presence of circulating serum antibodies was tested by IIF staining. Specimen of human skin was acquired from dermatologic surgery procedures using Institutional Review Board-reviewed protocols and cryosectioned onto glass slides. The BIOCHIP-mosaics, coated with ME and Dsg1/Dsg3 extracellular domains were purchased from EUROIMMUN. Using the TITERPLANE technique, a BIOCHIP mosaic allows the simultaneous detection of autoAbs against the most frequent target antigens facilitating the diagnosis of bullous skin diseases. According to the TITERPLANE technique, serum sample or labeled antibody is applied to the reaction fields of a reagent tray. BIOCHIP slides are then placed into the recesses of the reagent tray, where all come into contact with the fluids and the individual reactions commence simultaneously. Briefly, slides were blocked for 30 min at RT. Blocked slides were incubated with serum diluted in blocking buffer (dilution; 1:10, 1:20, 1:50, 1:100, 1:200, and 1:400) at RT for 60 min. Slides were washed as above and incubated with the secondary antibody diluted in blocking buffer for 60 min at RT. The following secondary antibodies were applied: FITC-labeled anti-human IgA (ready to use, EUROIMMUN), goat anti-human IgA-FITC, and F(ab)2 anti-human IgG FITC. Following extensive wash, slides were mounted with DAPI fluoromount

G. Normal human serum (NHS) was used as negative control. IIF images were finally evaluated as strong (++), moderately strong (+), and negative (-) by two observers.

2.2.4 Hematoxylin and eosin (H&E) staining

H&E staining is a standard diagnosis method used in histology. The complex of hematoxylin and aluminum salts acts as a positively charged, basic dye which can react with negatively charged, basophilic cell components such as nucleus resulting in a blue stain. Nuclear staining is followed by counterstaining with an aqueous eosin solution. Anionic dye eosin acts as an acidic dye; therefore reacts with positively charged, acidophilic components in tissues coloring them in red/pink. For histopathology analysis, skin biopsies were fixed in 4% formalin solution and embedded in paraffin blocks. Paraffin sections (6 µm) were cut on microtome and stained for H&E according to standard protocols used in the routine histopathology laboratory at the Department of Dermatology, Luebeck. All sections were visualized using a BZ-9000E series Keyence microscope.

2.2.5 Enzyme-linked immunosorbent assay (ELISA)

Availability of cDNA clones for pemphigus antigens has helped to produce recombinant proteins which represent epitopes of the native antigens including conformational ones. Using the recombinant antigens (rDsg1 and rDsg3), sensitive and highly specific ELISA systems (e.g., MBL and EUROIMMUN) have been developed for serological diagnosis of pemphigus [92].

2.2.5.1 Detection of circulating autoAbs

Since commercial ELISAs for human anti-Dsg-IgA are lacking, I developed a modified protocol for detection of serum IgA against Dsg1/3. In details, serial dilutions of serum were prepared in conjugate diluent and incubated with Dsg1/3-coated microtiter wells (MESACUP-2 Desmoglein Test Dsg1 and Dsg3 Kits, MBL, Japan) for 60 min at RT. Sera from other IgA pemphigus patients and healthy donors were used as controls. After washing three times, wells were incubated with 100 µL of HRP-conjugated anti-human IgA1 (B3506B4; dilution, 1:1,000; SouthernBiotech) and IgA2 (A9604D2; dilution, 1:4,000; SouthernBiotech) secondary antibodies for 60 min at RT. Development was performed using 3,3′,5,5′-tetramethylbenzidine (TMB)

substrate solution. The reaction was terminated by addition of 100 µL/well stop solution. The colorimetric measurement was performed at a wavelength of 450 nm using an Infinite M200 PRO ELISA reader. Serum IgG reactivity against Dsg substrates was detected using Dsg1/3 (IgG) ELISA tests (EUROIMMUN and MBL), following the manufacturers' instructions.

2.2.5.2 Ethylenediaminetetraacetic acid (EDTA)-pretreated ELISA

EDTA-pretreated ELISA was performed as previously reported [22]. To modify calcium-dependent conformational epitopes on Dsg, ELISA wells (MBL) were treated with EDTA (0.005, 0.05, 0.5, and 5 mM) for 30 min at RT. After washing four times with wash buffer that contained EDTA of the same final concentration used for wells' pretreatment, the conventional Dsg1/3 IgA1 ELISA protocol was carried out. Sera were diluted in dilution buffer supplemented with the corresponding EDTA concentrations. The reference well (EDTA-untreated) had no EDTA and the control well contained 10 mM calcium.

2.2.6 Affinity purification of serum IgA

Serum IgA was purified using Peptide M agarose (InvivoGen Europe). Peptide M is a 50-residue synthetic peptide derived from *streptococcal* M protein which binds human monomeric and dimeric of IgA1 and IgA2 subclasses with high affinity. In brief, serum was diluted 1:3 in 1x TBS-calcium and incubated with 100 µL of Peptide M agarose for 60 min at RT. After excessive washing, IgA antibodies were eluted with 0.1 M glycine-HCl, pH 2.5 and immediately neutralized with 1 M Tris-HCl, pH 8.0. Eluates were dialyzed against TBS and concentrated at 4°C using Amicon Ultra-15 centrifugal filter (cut-off: 30 kDa). Original serum, eluates of total IgA affinity purification, and pass-through were analyzed by total IgA ELISA (Bethyl Laboratories), according to the manufacturer's instruction. As secondary antibodies, HRP-conjugated anti-human IgA and IgG-Fc antibodies (dilution, 1:10,000; Bethyl Laboratories) were applied.

Moreover, specific ELISA testing and IFT on Dsg-transfected HEK cells (EUROIMMUN) were performed for both IgA and IgG isotypes by adjusting the affinity purified IgA antibodies to the respective input serum concentrations.

2.2.7 Immunoblot assay

The entire ectodomain of human Dsg (Dsg1/3(ec)-His) was produced in recombinant HEK293 cells by EUROIMMUN. Dsg1/3(ec)-His proteins were purified from the culture supernatants with immobilized metal ion affinity chromatography (IMAC) using TALON Superflow (GE Healthcare). After imidazole elution, buffer exchange of elutes was carried out against TBS-calcium buffer. The purified proteins were incubated with 1/5 sample volume of 4x Laemmli sample buffer (Bio-Rad) plus β-mercaptoethanol at 95°C for 3 min. Samples were separated by sodium dodecylsulfate-polyacrylamide gel electrophoresis (SDS-PAGE) using 4-15% Mini-PROTEAN® TGX™ Precast Gels (Bio-Rad). Spectra Multicolor BR Protein Ladder (Thermo Fisher Scientific) was used as a size marker. Electrophoresis was performed using 1x Tris/Glycine/SDS running buffer (Bio-Rad). Proteins were transferred to a 0.45 µm nitrocellulose membrane (Bio-Rad) by electroblotting (100 V, 60 min, and 4°C). Thereafter, the membrane was stained for 10-30 sec in Ponceau S staining solution. This is a rapid and reversible staining method used to evaluate blotting efficiency and protein content. The membrane was destained in TBS-Tween (TBS-T) and blocked with 5% skim milk powder in TBS-T for 60 min at RT. The blocked membrane was then incubated with primary antibody at 4°C on an orbital shaker O/N. Between each step, the membrane was washed 3 times for 10 min with TBS-T. The washing step was followed by 60 min incubation with HRP-conjugated secondary antibody (Table 3). All antibodies were diluted in blocking buffer. The membrane was finally developed with ECL western blotting detection reagent (Amersham Biosciences Corp.) and exposed to X-ray film to visualize the immunoreactive proteins.

Table 3: Antibodies used in immunoblot analysis

Antibody	Dilution	Clone	Supplier
Rabbit anti-human IgA-HRP	1:1,000	Polyclonal	Dako
Goat anti-mouse IgG-HRP	1:1,000	Polyclonal	Dako
6x-His Tag Monoclonal Antibody	1:1,000	Clone 4E3D10H2/E3	Thermo Fisher Scientific

2.2.8 Pathogenicity assays

2.2.8.1 *In vitro* keratinocyte dissociation assay

Keratinocyte dissociation assay was performed as previously described [22, 93]. HaCaT cells, the spontaneously immortalized human keratinocyte cell line, were grown in Dulbecco's Modified Eagle's Medium (DMEM, Sigma-Aldrich). Medium was supplemented with 10% FBS Gold Plus (Bio&SELL) and penicillin-streptomycin (10,000 U/mL). Confluent cells, seeded on 12-well plates, were incubated with sera or antibodies for 24 hours. At the final 2 hours of incubation, 0.5 µg/mL exfoliative toxin A (ETA, Toxin Technology, Inc.) was added to specifically cleave Dsg1. After rinsing twice with DPBS, cells were treated with dispase (2.4 U/mL, Sigma-Aldrich) until the cell sheets were released as a uniform monolayer from the wells (20-30 min). Dispase disrupts cell-matrix interactions without affecting the cell-cell adhesion. The released cell sheets were gently exposed to mechanical shear stress by pipetting five times with a 1-mL pipette. Gentle pipetting results in fragmentation of epidermal cell sheet if the added antibody is pathogenic. The fragments were fixed in 10% formalin and stained with crystal violet. The dissociation assay was quantified by counting the number of fragments manually.

2.2.8.2 Human skin organ culture (HSOC) model

In the HSOC model, blister formation is induced by injection of antibodies into the dermis of freshly obtained human skin [94]. All steps were performed under sterile conditions routinely applied for cell culture experiments. Specimens obtained from left-over of skin surgery (within 60 min) were trimmed of fat and cut into 5×5 mm sections. Interaepidermal injection (final volume of 50 µL) was performed using insulin syringes. Injected skin was gently placed on the insert of a Trans-well culture plate (Corning) containing Defined Keratinocyte-serum free medium (Thermo Fisher scientific) plus 1.2 mM calcium in the outer compartment. To investigate the effect of incubation period on histological features of cultured skin, a time course experiment was firstly performed. PBS-injected skins were incubated in a humidified incubator with 5% CO_2 at 37˚C at different time points (6, 12, 24, 36, and 48 hours). Injected skins were harvested and sectioned into half; one half was frozen in Tissue-Tek O.C.T compound for DIF and the other half was fixed in 10% formalin solution for H&E histology. Titration of injected ETA was performed to obtain the highest dose that does not lead to pathology (subclinical dose).

2.3 Methods Part II: Construction of an IgA1 antibody phage display library

Selective cloning of the IgA1 antibody repertoire from PBMC-cDNA of the representative IgA-PV patient was conducted to isolate antigen-specific mAbs by selection on the antigen of interest (e.g., Dsg3). An overview of APD technique is depicted in Figure 12 [90].

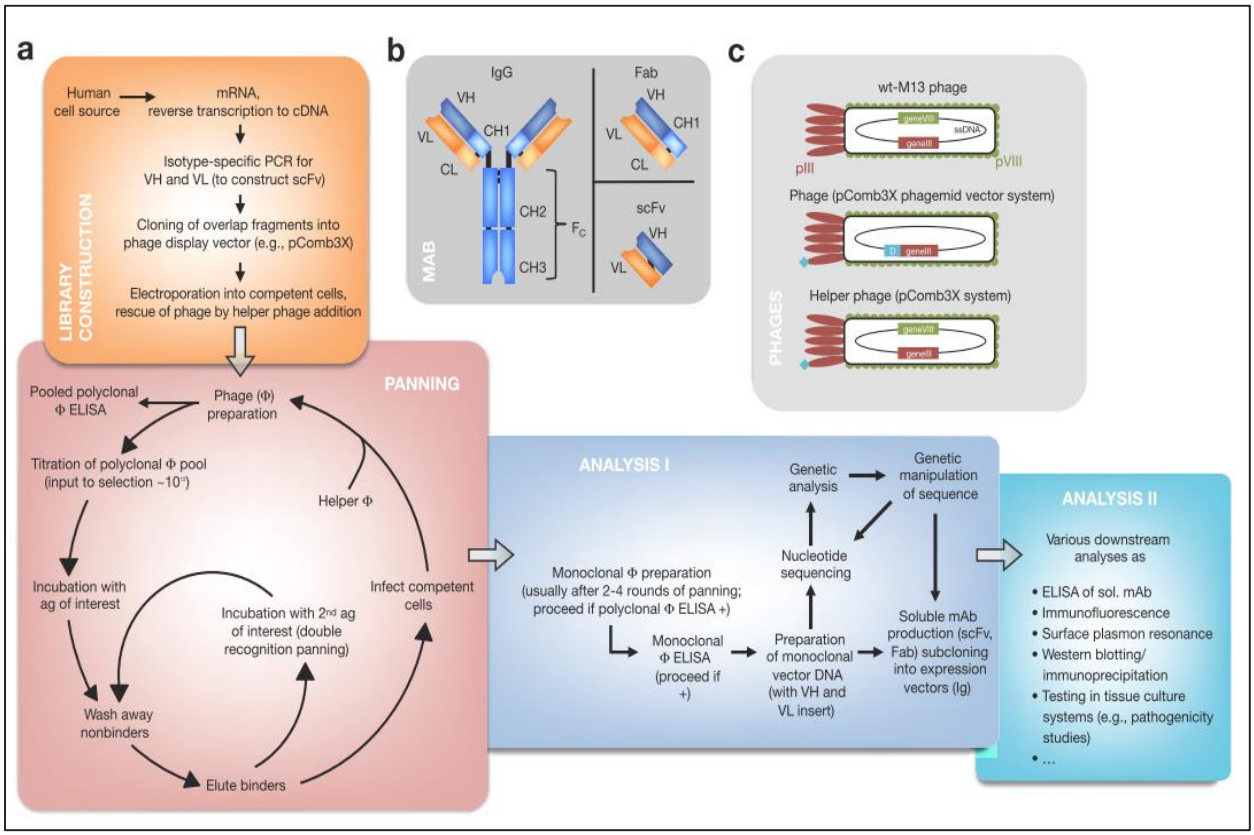

Figure 12: Antibody phage display technique

(**A**) Diagram showing how APD is performed. (**B**) Schematic representation of immunoglobulin (Ig), scFv, and Fab structures. (**C**) Phage display systems are derived from wild-type bacteriophage of *E. coli*. Monovalency of the displayed ensures selection for high-affinity mAbs in phagemid vector-based systems (here, pComb3x). Abbreviations: scFv, single chain variable fragment; Fab, fragment antigen binding; V_H, variable heavy chain; V_L, variable light chain; C_H/C_L, constant heavy/light chains. Adopted from [90].

2.3.1 Peripheral blood collection

Peripheral blood (~ 50 mL) was collected in EDTA tubes (Sarstedt) and then transferred to 50 mL conical tubes (Falcon) each containing 15 mL RPMI-1640 medium (Lonza Cologne GmbH). PBMCs were isolated using a standard Ficoll-Paque^{TM} Plus density gradient method [95]. PBMCs are blood cells which mainly consist of lymphocytes (T cells, B cells, and NK cells), macrophages, and dendritic cells. For the procedure, 15 mL EDTA blood: RPMI-1640 was layered over 10 mL Ficoll-Paque™ (GE Healthcare) and centrifuged (35 min, RT, and 500 g). Deceleration was done without brake. After centrifugation, blood was separated into a top layer of plasma, middle white layer of PBMCs, and lower fraction of polymorphonuclear cells and erythrocytes, which were removed during the centrifugation due to their higher density (Fig. 13). Diluted EDTA-plasma was first collected and saved at -20°C. Afterwards, the PBMC layer was carefully harvested and transferred to a new conical tube. The tube was filled with 40 mL RPMI-1640 and centrifuged at 500 g for 10 min at RT. This washing step was repeated twice. To remove any residual red blood cells (RBCs), the pellet was suspended in 1 mL lysis buffer for 30 seconds after which 25 volumes of HBSS buffer were added. Cells were then centrifuged (10 min, 4°C, 400 g). The cell pellet was resuspended in 1 mL RLT buffer containing 10 uL of β-mercaptoethanol and saved at -80°C.

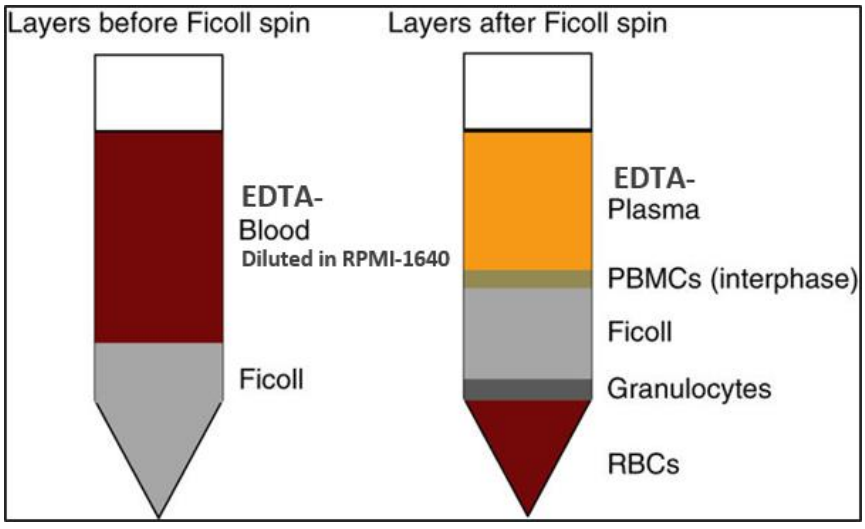

Figure 13: Schematic of Ficoll-Paque Plus separation of human peripheral blood

After blood has been layered onto the Ficoll and centrifuged without brake, blood components are separated into layers. Adopted and modified from [96].

2.3.2 RNA extraction and quantification

Total RNA was extracted from 5×10^7 PBMCs using RNeasy Midi Kit (QIAGEN). Briefly, one volume of 70% ethanol (molecular biology grade) was added to the lysate and mixed thoroughly. The lysate was applied onto the column and centrifuged for 5 min at 3-5×10^3 g. The pass-through was discarded and 4 mL buffer RW1 was added to the column. The column was centrifuged for 5 min at 3-5×10^3 g. In the next step, 2.5 mL buffer RPE was applied to the column followed by 2 min centrifugation at 3-5×10^3 g. To elute RNA, column was transferred to a new tube and 250 µL of UltraPure™ DNase⁄RNase-Free Distilled Water was pipetted onto the RNeasy silica-gel membrane. After 1 min incubation at RT, the column was centrifuged (2 min, 3-5×10^3 g). RNA concentration was measured using Nano-Drop 2000c. Isolated RNA was saved in 2.5 volume of 100% ethanol and 1/10 volume of 3 M sodium acetate at -80°C until used.

2.3.2.1 Ethanol precipitation of RNA

This procedure is used to change the RNA solvent, remove contaminants (e.g., phenol/chloroform), and concentrate RNA. The RNA tube was centrifuged at full speed for 45 min at 4°C. Immediately after aspirating the ethanol/sodium acetate, 600 µL of 70% ethanol was added to the tube and centrifuged for 30 min at 4°C to remove the excess contaminants, especially the inhibitory salts and chelaters. The supernatant was gently aspired. The pellet was air-dried for 5-10 min at RT and resuspended in nuclease-free water.

2.3.3 SMARTer PCR cDNA synthesis

All commonly used cDNA synthesis methods rely on the ability of reverse transcriptase to transcribe mRNA into single-stranded DNA (ssDNA) in the first-strand reaction. However, because the enzyme cannot always transcribe the entire mRNA sequence, the 5’ ends of genes tend to be underrepresented in cDNA populations. Using the proprietary SMARTer method, reverse transcriptase is able to preferentially enrich for full-length cDNAs. When the SMARTScribe reverse transcriptase reaches the 5’ end of mRNA, it adds a few additional nucleotides to the 3’ end of cDNA by its terminal transferase activity. The few added SMARTer oligonucleotide base-pairs with the non-template nucleotide stretch, creating an extended template. SMARTScribe enzyme then switches templates and continues replicating to the other

end of the oligonucleotide. The resulting full-length cDNA contains the complete 5' end of mRNA and sequences complementary to the SMARTer oligonucleotide (Fig. 14).

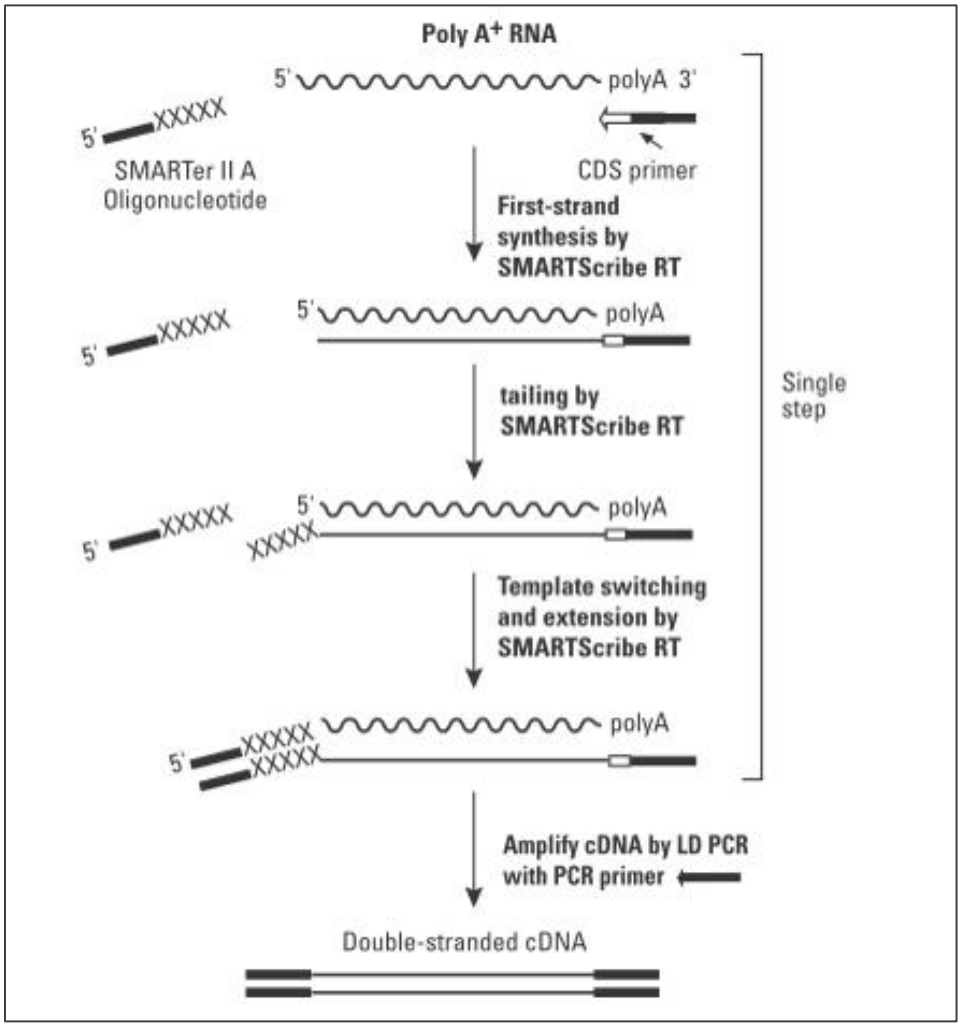

Figure 14: Flowchart of SMARTer™ cDNA synthesis

The SMARTer II A Oligonucleotide, 3' SMART CDS Primer II A, and 5' PCR Primer II A all contain a stretch of identical sequence. Graphic obtained from the SMARTer™ PCR cDNA Synthesis Kit User Manual.

2.3.3.1 First-strand cDNA synthesis using SMARTer™ PCR cDNA synthesis kit

For each sample, RNA, 3'SMART CDS Primer II A, and nuclease-free water (4.5 µL/reaction) were combined in 0.2 mL tubes (Table 4). The tubes were incubated at 72°C in a T100 thermal cycler (Bio-Rad) for 3 min, then at 42°C for 2 min. The remaining reagents were added to each tube, as outlined in Table 4. The tubes were further incubated at 42°C for 60 min. The reaction was terminated at 70°C for 10 min. The resulting first-strand reaction product was diluted in 40 µL of TE buffer.

Table 4: Reaction mix for first-strand cDNA synthesis

Reaction component	Volume (µL)	Final concentration/amount
RNA	1-3.5	5-10 µg
3'SMART CDS Primer II A	1	12 µM
5x First-Strand Buffer	2	1x
DTT	0.25	100 mM
dNTP Mix	1	10 mM
SMARTer II A Oligonucleotide	1	12 µM
RNase Inhibitor	0.25	10 U
SMARTScribe Reverse Transcriptase	1	100 U
Total volume	10 µL	---

2.3.3.2 Double-stranded cDNA amplification by long-distance PCR (LD PCR) using Advantage® 2 PCR kit

PCR master mix was prepared for each reaction by combing the following reagents (Table 5):

Table 5: Reaction mix for double-stranded cDNA amplification

Reaction component	Volume (µL)	Final concentration/amount
Nuclease-free water	74	---
10x Advantage 2 PCR Buffer	10	1x
dNTP Mix	2	10 mM
5' PCR Primer II A	2	12 µM
50x Advantage 2 Polymerase Mix	2	5x
Diluted first-strand cDNA	10	---
Total volume	100 µL	---

Thermal cycling for cDNA amplification was conducted using the following program (Table 6):

Table 6: PCR program for double-stranded cDNA amplification

Cycle step	Temperature (°C)	Time	No. of cycles
Initial denaturation	95	1’	1
Denaturation	95	15”	
Annealing	65	30”	15-30
Extension	68	3’	
Final extension	72	5’	1

Each reaction tube was subjected to 15 cycles of PCR and then the program was paused. Subsequently, 30 µL of each tube was transferred to a second tube labeled as “Optimization”. The “Experimental” tubes were stored at 4°C. Using the Tester PCR (Optimization) tube, the optimal number of PCR cycles was determined. For this procedure, 5 µL from each 15 cycle PCR reaction tube was transferred to a clean tube (for agarose gel analysis). The Optimization tubes were returned to the thermal cycler and three additional cycles (for a total of 18) were run with the remaining 25 µL of PCR mixture. Another 5 µL was transferred from 18 cycle PCR reaction tube to a new clean tube. Then, three additional cycles were run with the remaining PCR mixture (20 µL). This procedure was performed for a total of 27 cycles. Each 5 µL aliquot of PCR reaction was electrophoresed alongside a 1 kb DNA ladder on a 1.2% agarose gel. According to the results, the optimal number of cycles required for each sample was finally determined. The Experimental PCR tubes were retrieved from 4°C, returned to the thermal cycler, and subjected to additional cycles, if necessary, until it reached the optimal number determined before. When the cycling was completed, 5 µL of each PCR product was analyzed on gel (Fig. 15).

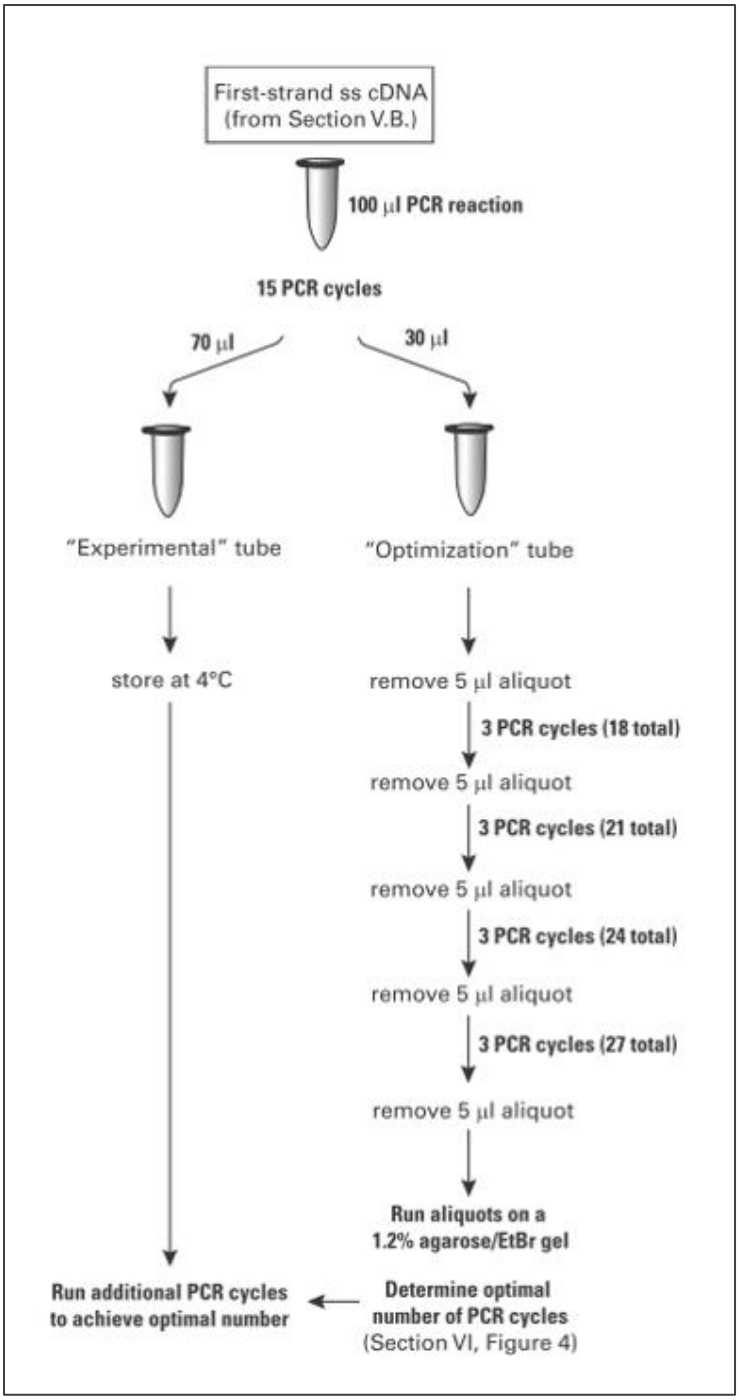

Figure 15: Optimizing PCR parameters for SMARTer cDNA synthesis

Graphic obtained from the SMARTer™ PCR cDNA Synthesis Kit User Manual.

2.3.3.3 Analysis of double-stranded cDNA amplification results

In general, double-stranded cDNA synthesized from total RNA with SMARTer cDNA synthesis/amplification should appear as a moderately strong smear at 0.5-5 kb with some distinct bands on a 1.2% agarose gel. For the best results, PCR cycling parameters need to be optimized for each specific experiment. Choosing the optimal number of PCR cycles ensures that the double-stranded cDNA will remain in the exponential phase of amplification. When the yield of PCR products stops increasing with more cycles, the reaction has reached its plateau. Overcycled cDNA can result in a less representative and biased template for downstream experiments. Undercycling results in a lower yield of cDNA. The optimal number of cycles is one cycle fewer than the one is needed to reach the plateau.

2.3.4 PCR amplification and assembly of light- and heavy-chain coding sequences

To generate the scFv fragments, two PCR steps are generally required; a primary PCR which separately amplifies the antibody variable light (V_L) and heavy (V_H) chains and a secondary overlap PCR which randomly combines the V_H and V_L products via a common linker sequence to form a full-length scFv fragment (Fig. 16). The first round products have a size of about 350-400 base pairs (bp). In the second round of PCR, the purified V_H and V_L products are fused by overlap extension PCR using forward and reverse extension primers. The resulting product is about 750-800 bp and referred to as a scFv PCR fragment. It has the *Sfi1* restriction sites, on the 5' and 3' ends, that are used for directional cloning into the pComb3X vector [97, 98].

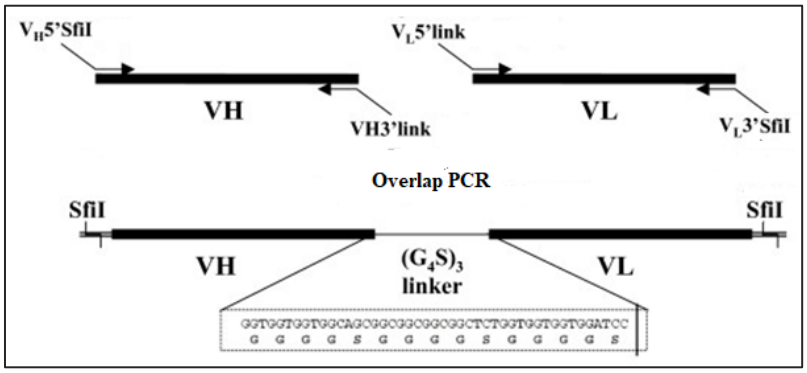

Figure 16: scFv generation by overlap extension PCR [98]

An antibody in the scFv format consists of V_H and V_L chains joined together by a flexible short (GGSSRSS) or long (GGSSRSSSSGGGGSGGGG) peptide linker. A linker is used for the stabilization of V_L-V_H chains and proper antigen binding site formation without the loss of antibody affinity. The linker can either connect the N-terminus of the V_H with the C-terminus of the V_L or vice versa. The scFvs with short peptide linkers tend to form dimers, called bivalent diabodies, whereas scFvs with long peptide linkers tend to be monomers. Apart from the length of the linkers, their amino acid composition also plays an important role. Linker must have a hydrophilic sequence to avoid intercalation of the peptide within or between the variable domains throughout the protein folding. The most commonly used designs of linkers have sequences comprising the stretches of glycine (Gly or G) and serine (Ser or S) residues for flexibility and/or together with the charged residues such as glutamate and lysine interspersed to enhance the solubility [99].

2.3.4.1 First round of V_H PCR

Using the double-stranded cDNA as template, 6 V_H fragments covering most, if not, the entire V_H repertoire of the individual studied, were amplified (Tables 7 and 8):

Table 7: Reaction mix for IgA1-specific V_H gene amplification

Component	Volume (µL)	Final concentration/amount
Double-stranded cDNA	1	---
10x PCR Buffer	10	1x
V_H forward primer	3	20 µM
Reverse primer (IgA1_hinge)	3	20 µM
dNTPs	0.8	25 µM
Taq/anti-Taq DNA polymerase	1	
Nuclease-free water	to a final volume of 100 µL	

Table 8: PCR program for V_H gene amplification

Cycle step	Temperature (°C)	Time	No. of cycles
Initial denaturation	94	5’	1
Denaturation	94	15”	
Annealing	56	25”	35
Extension	72	90”	
Final extension	72	10’	1

The first-round PCR, using IgA1-hinge reverse primer, ensures the specific amplification of just the IgA1 isotype. Each reaction was evaluated by loading 5-10 µL on a 2% agarose gel along with a 100 bp DNA ladder. A ~550 bp product for the amplified V_H-C_H hinge is expected. PCR clean-up was performed using a PureLink™ PCR Purification Kit (Invitrogen) to remove primers, dNTPs, enzymes, short spurious PCR products, and salts from PCR products.

2.3.4.2 Second round of V_H PCR

In the second round of PCR, the purified first-round V_H products were used as templates for a PCR performed as depicted in Tables 9 and 10:

Table 9: Reaction mix for second round of PCR

Component	Volume (µL)	Final concentration/amount
PCR-purified V_H products	1	
10x PCR Buffer	10	1x
HSCV-FL sense primer	3	20 µM
Reverse primer (HSCA-B_rev)	3	20 µM
dNTPs	0.8	25 µM
Taq/anti-Taq DNA polymerase	7.5	
Nuclease-free water	to a final volume of 100 µL	

Table 10: PCR program for second round of V_H PCR

Cycle step	Temperature (°C)	Time	No. of cycles
Initial denaturation	94	5’	1
Denaturation	94	15”	
Annealing	56	15”	25
Extension	72	2’	
Final extension	72	10’	1

PCR products were evaluated on a 2% agarose gel, pooled separately, and ethanol precipitated (together with glycogen and 3 M sodium acetate). To purify the second-round V_H DNA products suited for overlap PCR, pooled samples were loaded on a precast 3% TAE Mini Ready Agarose™ Precast Gel (Bio-Rad). The correct-size products were excised using a clean razor blade and purified by a QIAEX II Gel Extraction Kit (QIAGEN). In brief, gel slices containing the DNA fragment of interest were placed into a tube and weighted. Three volumes buffer QX1 were added to 1 volume of gel. After addition of QIAEX II, the tube was incubated for 10 min at 50°C to solubilize the agarose and bind the DNA. To keep the QIAEX II in suspension, the tube

was mixed every 2 min. The tube was centrifuged and the supernatant was discarded. The pellet was washed with Buffer QX1 and rinsed twice with Buffer PE. Finally, the pellet was air-dried and suspended in 20 µL of nuclease-free water. After 5 min incubation at RT, the tube was centrifuged for 30 seconds and the supernatant (purified DNA) was collected and gel-quantified.

2.3.4.3 Single PCR reaction for amplification of V_κ and V_λ genes

Since the variable light chains are the same for each isotype/subclass of antibodies, only a single PCR reaction was needed to amplify the V_L fragments. Using 16 V_κ and 18 V_λ sets of primers, PCR products of ~350 bp are expected. PCR products were separately pooled and ethanol precipitated. The precipitated products were gel-quantified, then purified from 3% TAE Mini ReadyAgarose™ precast gels, and gel-quantified again.

2.3.4.4 Overlap extension PCRs

Overlap extension PCRs yielding scFv-coding amplicons were performed with equal ratios of gel-purified and gel-quantified V_H and V_L (V_κ and V_λ) fragments, as illustrated in Tables 11-12.

Table 11: Reaction mix for overlap extension PCR

Component	Volume (µL)	Final concentration/amount
Gel-purified and gel-quantified V_H products	---	100 ng
Gel-purified and gel-quantified V_κ or V_λ products	---	100 ng
10x PCR Buffer	10	1x
RSC-F forward primer	3	20 µM
RSC-B reverse primer	3	20 µM
dNTPs	0.8	25 µM
Taq/anti-Taq DNA polymerase	1	
Nuclease-free water	to a final volume of 100 µL	

Table 12: PCR program for overlap extension PCR

Cycle step	Temperature (°C)	Time	No. of cycles
Initial denaturation	94	5’	1
Denaturation	94	15”	25
Annealing	56	15”	
Extension	72	2’	
Final extension	72	10’	1

The V_H/V_κ and V_H/V_λ PCR products were ethanol precipitated for subsequent gel-quantification.

2.3.5 Restriction-digest of the overlap PCR product and pComb3X vector

Cloning of scFv gene fragments for display on the surface of phage requires a phagemid vector that allows expression of scFv fused to the gene III product. The phage display vector, pComb3X, allows a uniform cloning strategy that utilizes a single restriction endonuclease, *Sfi*I (Fig. 17). It contains the amber codon, inserted between the 3' *Sfi*I restriction site and the 5' end of gene III, which allows soluble protein expression in nonsuppressor strains of bacteria without first excising the gene III fragment. The vector also contains two peptide tags, the hemagglutinin (HA) tag for immune detection and the six histidine tag (6His or H6) for protein purification. This vector is used for expression of both Fab and scFv fragments. The pComb3X vector expresses β-lactamase; therefore requires Ampicillin or Carbenicillin for selection. Containing the lacZ promoter, the pComb3X requires isopropyl-β-D-thiogalactopyranoside (IPTG) for protein expression. Overlap PCR introduced *Sfi*I sites which allows the scFv cloning into the pComb3X vector [97].

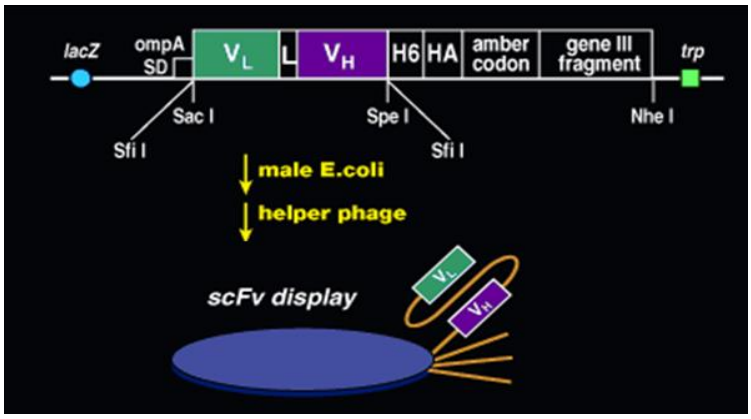

Figure 17: Map of pComb3X vector for display the scFv or Fab gene products on the phage surface
Figure adopted from www.scripps.edu.

Digest reactions of overlap product and vector contained the following reagents (Table 13). The digestion tubes were incubated for 5 hours at 50°C, cleaned up with phenol-chloroform extraction, and then ethanol precipitated. The corresponding DNA bands for *Sfi*I-digested scFv

(~800 bp), stuffer fragment (~1600 bp), and *Sfi*I-digested pComb3X vector (~3400 bp) were purified from gel, ethanol precipitated, and gel-quantified each.

Table 13: Digestion of scFv and pComb3X vector

Component	Final concentration (scFv or V_H:V_L)	Final concentration (vector)
Template	1 µg	1 µg
*Sfi*I (40 U/mL)	36 Units of *Sfi*I	6 Units of *Sfi*I
10x buffer M	2 µL	2 µL
Nuclease-free water	to a final volume of 20 µL	to a final volume of 20 µL

2.3.6 Ligation of overlap PCR products into the pComb3X vector

The *Sfi*I-cut, gel-purified and gel-quantified scFvs were ligated into the *Sfi*I-cut, gel-purified and gel-quantified pComb3X vector via the corresponding sites. The amount of vector DNA and insert DNA used in the ligation reaction varies depending on their size and concentration. Commonly, a 1:3 molar ratio of vector: insert is used in cloning. To calculate the ng of insert to include in the ligation reaction, the following equation was used:

(ng of vector × kb size of insert) / kb size of vector × molar ratio of insert/vector = ng of insert

Ligation was first performed as follows (Table 14):

Table 14: Ligation of *Sfi*I-digested scFv into the pComb3X

Component	Final concentration/amount (vector:insert ratio 1:3)
pComb3X (~3400 bp)	1.4 µg
V_H-V_λ or V_H-V_κ insert (~800 bp)	700 ng
5x T4 DNA Ligase buffer	40 µL
T4 DNA Ligase (1 U/µL)	10 µL
Nuclease-free water	to a final volume of 200 µL

The ligation reaction was incubated for 18 hours at 20°C and heat inactivated for 10 min at 70°C. To check the ligation, 10 µL of ligation was loaded on a 1% agarose gel for 90 min. DNA was purified, ethanol precipitated, and gel-quantified.

2.3.7 Preparation of VCSM13 interference resistant helper phage

The pComb3X phagemid contains an f1 origin of replication from a filamentous bacteriophage. For completing the infection process, phagemid needs a helper phage (e.g., VCSM13) to provide the genes required for phage replication and assembly [84]. To prepare the helper phage, 100 µL of XL-1 Blue electroporation-competent cells was grown out to OD600=0.3 at 300 rpm and 37˚C in 100 mL SB/100 µL Tetracycline (stock at 10 mg/mL in 70% EtOH). Then, 1 vial of VCSM13 interference-resistant helper phage (Agilent) was added to the cells and incubated at 37˚C for 15 min without shaking. The culture was further incubated at 37˚C and 300 rpm for 2 hours, then supplemented with 280 µL Kanamycin (stock at 25 mg/mL in ddH_2O) and cultured O/N at 30˚C and 300 rpm. On the next day, the incubation was continued at 37˚C and 300 rpm until afternoon and then the culture was distributed into 4x 50 mL Falcon tubes. Afterwards, the tubes were centrifuged for 10 min at 9,400 g and 4˚C. The supernatant was transferred to 4x high speed centrifuge tubes and incubated in a 65˚C water bath for 15 min. Finally, the tubes were centrifuged for 10 min at 10,000 rpm and 4˚C. The supernatant was transferred in equal aliquots into 3-4x 50 mL Falcon tubes and saved at 4˚C. Subsequently, a titration of the supernatant was performed (helper phage titers should be between $1\text{-}10\times10^{11}$ pfu/mL) and the required volumes for 1×10^{12} and 2.5×10^{11} pfu were calculated (which is the required volume for phage library construction). The plaque forming unit (PFU, infectious phage particles/mL) was calculated using the following formula:

PFU/mL = number of colonies / (dilution factor × total volume of culture)

2.3.8 Electroporation of V_H/V_L-vector ligations into electrocompetent *E. coli*

In detail, electrocompetent XL-1 blue *E. coli* cells (Agilent) were thawed for 1 min. Then, 5 µL of the final ligation products from APD cloning was added into one tube of XL1-blue *E. coli* competent cells. DNA/XL1-cells were mixed by gentle pipetting. DNA/XL1-cells were transferred to a pre-chilled 2 mm cuvette (Bio-Rad) without making air bubbles. The electroporation was performed using a Micro-Pulser (Bio-Rad) device which was set on “Ec2” and “bacteria” program. The cuvette was flushed immediately after electroporation with 1 mL of pre-warmed SOC medium. This step was repeated two more times. The final 3 mL mixture was

transferred to a 50 mL Falcon tube. The tube was placed in a shaking incubator for 60 min at 250 rpm and 37°C. The electroporation was conducted twice for each V_H-V_κ and V_H-V_λ libraries. Afterwards, 10 mL of SB/Carbenicillin (C)/Tetracycline (T) (45 mL/11.7 µL/58.5 µL) was added to each tube. The 13 mL cultures were incubated at 37˚C and 300 rpm for 60 min. Next, 50 µL of each V_H-V_κ and V_H-V_λ culture was used for cfu titration. Different dilutions (1:10, 1:100, and 1:1000) of each culture were prepared and plated onto LB/Carbenicillin plates. Each tube with the transformed culture was supplemented with 3.9 µL of Carbenicillin stock and incubated at 37°C and 300 rpm for 60 min. The κ1+κ2 and λ1+λ2 were combined in one 50 mL falcon tube. Then, 10^{12} helper phage was added to each 26 mL of combined culture and incubated for 15 min at RT without shaking. Each 26 mL culture was added to 100 mL SB/C/T (100 mL/50 µL/100 µL) and incubated at 37˚C and 300 rpm for 2 hours. Each 126.72 mL of culture was supplemented with 355 µL Kanamycine (final concentration = 70 µg/mL) and incubated O/N at 30˚C and 300 rpm. On the next morning, the plates were sealed with parafilm and saved at 4°C until counting the colonies and calculation of cfus.

In the next step, P0 phage harvest from above electroporations was performed. Firstly, 126 mL of each κ and λ cultures was transferred to 3x 50 mL tubes and centrifuged for 15 min at 4˚C and 6,000 g. The cell pellets were saved at -20˚C. The supernatants were transferred to 4x high speed centrifuge tubes and centrifuged for 15 min at 4˚C and 15,000 g. The supernatants were transferred to large centrifuge tubes. Then, ¼ volumes 5x PEG was added each tube and incubated on ice with shaking for 30 min. After incubation, the tubes were centrifuged for 30 min at 4˚C and 15,000 g. The supernatants were carefully aspirated without touching the phage pellets. The tube was incubated on ice while phage pellets face up for 10 min. Subsequently, the remaining supernatants were aspirated. Each large tube was supplemented with 2 mL of 1% BSA/TBS and phage pellets were resuspended by shaking on bench top for 30 min. Solved phage was transferred to Eppendorf tubes and centrifuged for 5 min at RT and 13,400 rpm. The supernatant was transferred to new Eppendorf tubes and saved at 4˚C indefinitely.

2.3.9 Library panning of pooled V_H/V_κ and V_H/V_λ phages on immobilized antigens

"Panning" consists of several rounds of phage binding to an antigen immobilized on a solid support (e.g., ELISA well), a defined number of washing steps, elution by trypsinization or low pH, and reamplification of phage in *E. coli*. During each round, specific binding phage clones are selected and reamplified. These clones predominate after 2-4 rounds. The input of each round is usually in the range of 10^{12} to 10^{13} phages and the output is about 10^5 to 10^8 phages, depending on the number of washing steps and the degree of enrichment occurring at any given round. A 10- to 100-fold increase in output phage after 3-4 rounds is typical.

Selections of phage particles displaying specific scFv fragments were performed on Dsg3-ELISA plates (EUROIMMUN). Wells were firstly blocked at RT for 60 min by adding 380 µl of 3% milk (in 1x TBS/1 mM $CaCl_2$). Blocking buffer was then discarded. To prepare the P0 phage, 400 µL of a 1:1 mixture of P0 λ/kappa phage was combined with 171.4 µL of 10% milk (in 1x TBS/1 mM $CaCl_2$) for a final concentration of 3% milk with P0 phage. After adding 100 µL of freshly prepared P0 phage to each well, the plate was sealed and blocked for 2 hour at RT. The unbound phages were discarded from the wells and the wells were washed 3 times with 2x 188 µL sterile filtered 1x TBS/0.1% Tween 20/1 mM $CaCl_2$. Next, 100 µL of the blocked P0 phage was added to each well for panning. The wells covered and incubated at RT for 2 hours. Following incubation, the phage was discarded and the wells were filled with 2x 188 µL 1x TBS/0.1% Tween 20/1 mM $CaCl_2$. The washing buffer was gently pipetted up and down for 5 times. After 5 min, the washing buffer was discarded and the washing process was repeated 5 times for the first panning. Subsequently, 100 µL of 76 mM citric acid (pH 2.2) was added to each well for elution and the wells were incubated with elution buffer at RT for 10 min. The elution buffer was pipetted up and down 10x vigorously. The elution was transferred to a 50 mL Falcon tube with 36 µL of 2 M unbuffered TRIS base. Next, 10 mL of XL1-cells with OD=1.0 was added to eluted and neutralized phage and incubated at RT for 15 min. After incubation, the culture was poured into a 125 mL Erlenmeyer flask. In the next step, 10 mL of prewarmed SB/C/T (15 mL/6 µL/15 µL) was added to a Falcon which has been used for culture and transferred to the Erlenmeyer flask. To titer the elution, 100 µL of 20 mL total volume was removed and incubated at 37˚C and 300 rpm. After 60 min incubation, 6 µL of Carbenicillin was added to the culture and incubated at 37˚C and 300 rpm for 60 min. Then, 10^{12} helper phage was

added and incubated at RT for 15 min. The total culture volume of about 21 mL was transferred to 100 mL SB/C/T (100 mL SB/50 µL C/100 µL T) in 500 mL Erlenmeyer flask and incubated at 37˚C and 300 rpm for 2 hours. The culture was finally supplemented with 341 µL of Kanamycine (final concentration of 70 µg/mL) and incubated at 30˚C and 300 rpm O/N. Accordingly, P2-P4 panning steps were conducted in which the washing process was repeated 10 times.

2.3.10 Polyclonal M13 phage ELISA

To monitor the selection process, binding of polyclonal antigen-specific phage pools obtained from rounds 2-4 (P2-P4) of panning was tested in parallel with the unselected APD library (P0). If specific binders were enriched during the panning procedure, a positive signal is obtained when testing the phage pools. The Dsg1/3-ELISA plates (EUROIMMUN) were used for anti-M13-phage ELISA. Briefly, 1:1,000 and 1:5,000 dilutions of phages were prepared in 3% milk/TBS. Dsg3 and Dsg1 ELISA wells were blocked by adding 380 µL of 3% milk-TBS for 60 min at 37°C. Then, 100 µL of phage dilutions was added to each well and incubated for 2 hours at RT. Phage was dumped out and the wells were washed with 0.1% Tween 20/TBS/1 mM $CaCl_2$ for 6 times (2x 185 µL). Subsequently, 100 µL of freshly prepared HRP-conjugated anti-M13 antibody (dilution, 1:5,000; GE Healthcare) was added to each well and incubated for 60 min at RT. The wells were washed 6 times, supplemented with 100 µL of ABTS peroxidase substrate solution (ready to use; Roche), and incubated at RT (protected from light). The absorbance at 405-490 nm was measured after 30, 45, 60, and 90 min. ELISA signal should increase during the course of panning, but signal from the control should remain low throughout the panning. An increasing signal form the control might indicate non-specific “sticky” clones or plastic binders.

2.3.11 Selection of monoclonals and screening by M13 phage ELISA

In details, 2x 40 mL of SB, 20 µL of Carbenicillin, and 40 µL of Tetracycline were mixed in a 50 mL Falcon tube. The medium was distributed to 4x 50 mL Falcon tubes with 10 mL each. A single, isolated bacterial colony was picked up from a P2 output titer plate. Each single colony was separately placed into one of the aliquots of 10 mL SB/C/T and was grown O/N at 37˚C and 225 rpm. In the next day, 500 µL of O/N culture was added to a cryovial tube containing 500 µL

of 30 % Glycerol (sterile filtered, in ddH_2O) and stored at -80˚C. Then, 3 mL of each culture was transferred to a 15 mL Falcon and centrifuged at 4,000 g and 4˚C for 15 min. The supernatants were aspirated off and the cell pellets were placed into separate plastic bags and saved at -20˚C for DNA preparation. In the next step, 125 mL Erlenmeyer flasks containing 33 mL SB/16.5 µL C/33 µL T were prepared and each supplemented with 330 µL of respective O/N culture in each (resulting in a 1:100 dilution). The flasks were placed in an incubator at 37˚C and 300 rpm until OD = 0.3. Afterwards, 2.5×10^{11} helper phage was added to each flask and incubated without shaking for 15 min at 37˚C. Incubation was continued at 37˚C and 300 rpm for 2 hours. The culture (32 mL) was supplemented with 92 µL of Kanamycine to flasks and incubated at 30˚C and 300 rpm O/N. The culture from the 125 mL flasks were transferred to 50 mL Falcon tubes and centrifuged at 6,000 g and 4˚C for 15 min. The supernatant was transferred to high speed centrifuge tubes and centrifuged at 15,000 g and 4˚C for 15 min. The cell pellet was discarded and the supernatant from each tube was transferred to new high speed centrifuge tube. Next, ¼ volume (6.25 mL) of 5x PEG was added to each tube, mixed well by inverting and allowed to rock on ice for 30 min. Then, the tubes were centrifuged at 15,000 g and 4˚C for 36 min (no brake). The supernatant was discarded with sterile, baked glass Pasteur pipettes and vacuum and the tubes were placed on ice at an angle for 10 min. All remaining supernatant was discarded and the pellet was resuspended in 500 µL of 1 % BSA/TBS. The tubes were incubated at angle (pellets down) for 30-60 min at RT. Using a 2 mL pipet, the suspension was transferred to 2 mL Eppendorf tube. The tubes were centrifuged at RT and 13,400 rpm in bench top centrifuge for 5 min. The supernatant was transferred to new 2 mL Eppendorf tube and stored at 4˚C until monoclonal anti-M13 phage ELISA.

To perform the monoclonal anti-M13 phage ELISA, 1:1,000 dilution of phages were firstly prepared in 3% milk/TBS. The Dsg3 and Dsg1 ELISA wells were blocked with 380 µL 3% milk/TBS for 60 min. The blocking buffer was discarded from ELISA wells. The wells were washed with 0.1% Tween 20/1x TBS/1 mM $CaCl_2$ for 3 times (2x 185 µL). Then, 100 µL of phage dilutions was added to each well and incubated at RT for 2 hours. After incubation, the phage was dumped out and the wells were washed with 0.1% Tween 20/1x TBS/1 mM $CaCl_2$ for 6 times. Next, 100 µL of freshly prepared 1:5,000 diluted anti-M13-HRP was added to each well (10 mL 1x TBS/1% BSA/1 mM $CaCl_2$ + 2 µL anti-M13-HRP). Following 60 min incubation at

RT, the liquids were dumped out and the wells were washed with 0.1% Tween 20/1x TBS/1 mM $CaCl_2$ for 6 times. Each well was supplemented with 100 µL freshly prepared ABTS. The wells were incubated at RT and protected from light. The OD was measured at 15 min, 30 min, 45 min, 60 min, 75 min, and 90 min at λ=405-490 nm.

2.3.12 Sequence analysis of monoclonal phage colonies

The *E. coli* cell pellet of each monoclonal was subjected to plasmid DNA purification (QIAGEN). The coding sequences for variable heavy (V_H) and light (V_L) chains were identified by Sanger sequencing using pComb3X specific primers (ompseq/dpseq). The nucleotide sequences were compared with the germline sequences using vbase2 sequence directory (http://www.vbase2.org) and IMGT/V-QUEST.

2.3.13 Liquid chromatography high-resolution tandem MS (LC-MS/MS)

2.3.13.1 Sample preparation for LC-MS/MS

The analytic approach is summarized in Figure 18. Dsg3-conjugated matrix (EUROIMMUN) was used to selectively capture the antigen-specific antibodies. About 500 µL of patient's serum was diluted with 1 mL TBS-calcium and then incubated with 500 µL of Dsg3-conjugated matrix by end-to-end rotation (40 min at RT). The pass-through was collected following centrifugation. After extensive washing of the matrix, two different elution procedures were applied. The Dsg3-specific IgA (bound fraction) was eluted with acidic pH (0.1 M Glycine buffer, pH 2.2) and immediately neutralized with 1 M Tris buffer, pH 8.5. As second elution method, the matrix was incubated with Laemmli sample buffer at 90°C for 3 min. Affinity purification was repeated as six separate experiments each confirmed by ELISA. The pass-through of the matrix was further purified by Peptide M agarose and termed as "unbound" fraction. Similar amounts of bound and unbound fractions were subjected to SDS-PAGE after staining the gel with SimplyBlue SafeStain (Invitrogen), bands corresponding to antibody heavy chains were cut out, reduced, and alkylated. After trypsin-digestion O/N, the digested peptides were desalted and analyzed by LC-MS/MS [100-102].

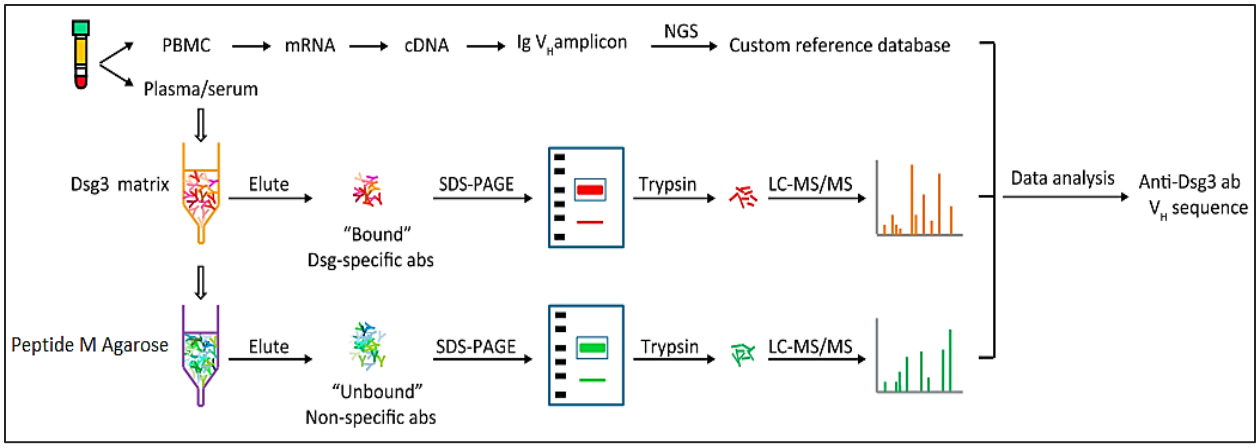

Figure 18: Proteomic platform to identify the circulating anti-Dsg3 autoAbs

The heavy chains of IgA antibodies in the bound and unbound fractions were analyzed by LC-MS/MS. Resultant spectra were searched against a custom database of all V_H sequences from the same patient to identify antibody peptides. Informative peptides match variable heavy chain (V_H)-CDR3 (H-CDR3) amino acid sequences that define the antibody clonotypes. Figure adopted from [101].

2.3.13.2 LC-MS/MS measurements and proteomics data analysis

LC-MS/MS analysis was performed as one run by the Wistar Proteomics Facility (Philadelphia, PA) using a Q Exactive Plus mass spectrometer (Thermo Scientific) coupled with a Nano-ACQUITY UPLC system (Waters). The tryptic peptides were separated by RP-HPLC on a BEH C18 nanocapillary analytical column (75 µm i.d. x 25 cm, 1.7 µm particle size; Waters). Chromatography was developed using a binary gradient of solvent A (0.1% formic acid in water) and solvent B (0.1% formic acid in acetonitrile). Peptides were eluted at 200 nL/min for 5-30% B over 75 min, 30-80% B over 5 min, and constant 80% B for 10 min before returning to 5% B over 1 min. A 30-min blank gradient was run between sample injections to minimize carryover. Eluted peptides were analyzed by the mass spectrometer set to repetitively scan m/z from 400 to 2,000. Full LC-MS/MS scan was collected at 70,000 resolution followed by data-dependent MS/MS scans at 17,500 resolution on the 20 most abundant ions exceeding a minimum threshold of 10,000. To identify antibody peptides, resultant MS/MS spectra were analyzed using MaxQuant 1.5.2.8 software. Bound and unbound LC-MS/MS experiment was searched using MaxQuant's 'Match Between Runs' option. Ultimately, a set of universal MS spectrum match filters were applied to the representative PSMs such as an unambiguous one-peptide-one-CDR3

relationship and other MaxQuant specific criteria (PEP % 0.01, score R70, mass error PPM % 1.5) [100-102].

2.3.14 Expression and purification of scFv antibodies

2.3.14.1 Transformation of TOP10F' cells with pComb3X plasmid

Soluble His-tagged scFv antibodies were expressed in TOP10F' non-suppressor strains of *E. coli*. In brief, 5 µL of the monoclonal plasmid, purified from a positive clone identified through phage ELISA and characterized genetically by sequencing, was directly added to a 50 µL vial of TOP10F' one shot cells (Invitrogen). The cells and plasmid were mixed by gently tapping the tube and incubated on ice for 15 min. The vial was incubated for 30 seconds in a 42˚C water bath and then quickly placed on ice. The vial was supplemented with 250 µL of prewarmed SOC medium and placed at an angle of about 30˚ in a 37˚C shaker incubator at 250 rpm for 60 min. Then, 50 µL of 1:10 and 1:1,000 dilutions was plated on LB/Carbenicillin plates O/N at 37˚C. The plates were saved at 4˚C until needed.

2.3.14.2 Soluble expression of scFv antibody in *E. coli*

Briefly, 25 mL of SB/Carbenicillin containing 500 µL of 1 M $MgCl_2$ were inoculated with one single colony from the freshly prepared plate. The starter culture was incubated O/N in a 30°C shaker (250 rpm). To make the large culture, the starter culture was diluted 1 to 100 in SB/Carbenicillin supplemented with $MgCl_2$ and then incubated at 37°C and 250 rpm until OD600=0.8-1.0. The induction was performed by adding 1 M IPTG (final concentration of 1 mM) followed by O/N incubation at 30°C. The culture was harvested in 500 mL centrifuge bottles (30 min, 4°C, and 8,000 g). The supernatant was carefully transferred to clean centrifuge bottles. The pellet was completely suspended in 1x FastBreak cell lysis reagent (Promega) supplemented with DNase I. The bottle was incubated for 60 min at RT on a shaking platform. The cellular debris was removed by centrifugation (15 min, 4°C, and 15,000 g) and the cell lysate was transferred to a clean tube. To optimize the scFv expression, 25 mL cultures were incubated with different amounts of $MgCl_2$ or at various time points (8, 10, 12, 14, and 16 hours) after IPTG induction. Furthermore, the antibody expression was monitored in the culture

supernatant and in the periplasmic extract. Large-scale antibody production was performed according to the optimized protocol.

2.3.14.3 Purification of scFv antibody by IMAC using Ni-NTA resin

Using the phagemid vector pComb3X, the His-tag is incorporated at the C-terminal of scFv antibody. Proteins that express six histidine residues can be purified using a resin that contains immobilized Ni^{2+} or Co^{2+} ions. The antibody fragments elute with imidazole buffer, which competes for binding to the ions. TALON Superflow resin (GE) was equilibrated by washing 750 µL of beads with 50P/300N buffer three times. The lysate was incubated with pre-washed TALON beads for 60 min at RT. The mixture was loaded onto a gravity column (Bio-Rad) and the resin was allowed to settle. The pass-through was collected and reapplied onto the equilibrated column 2-3 times. The column was washed with 50P/300N buffer (three times, 10 mL each). Elution was conducted ten times using 1 mL of 300 mM imidazole/50P/300N buffer. The eluates were dialyzed against PBS and concentrated using Amicon Ultra-15 centrifugal filter (cutoff: 3 kDa). Protein concentration was determined by SDS-PAGE using BSA as a standard.

2.3.15 Dsg1/3 scFv ELISA

Binding of HA-tagged monovalent scFv antibodies to Dsg substrates was measured using the Dsg1/3-ELISA plates (EUROIMMUN). Each scFv mAb was diluted in sample diluent and incubated on wells for 60 min at RT. After washing, wells were developed with HRP-conjugated anti-HA antibody (dilution, 1:1,000; Roche) for 60 min at RT. To test the calcium sensitivity of scFvs, the EDTA-pretreated anti-HA-ELISA was performed.

2.3.16 IIF staining for scFv mAbs

IIF staining was performed on ME, normal human skin, and mouse skin [22]. Slides were blocked at RT for 30 min. Blocked slides were incubated with different dilutions of scFv at RT for 60 min. After washing, slides were incubated with rat anti-HA antibody (3F10 clone; dilution, 1:100; Sigma-Aldrich) for 60 min at RT. Finally, binding was detected through staining with an Alexa Fluor® 594 goat anti-rat IgG (dilution, 1:200; Invitrogen) for 30 min at RT. Following three times washing, slides were mounted with DAPI fluoromount G.

2.3.17 Immunoblotting analysis

Protein sample (Dsg3(ec)-His) was separated by SDS-PAGE and transferred to a nitrocellulose membrane. After blocking with 5% milk powder in TBS-T for 60 min, the membrane was incubated O/N at 4°C with diluted scFv antibodies (2 µg/mL). The membrane was washed three times with TBS-T between each intermediate steps. Probing of transferred scFvs was carried out using HRP-conjugated anti-HA antibody (dilution, 1:1,000; Invitrogen) for 60 min at RT. The membrane was finally developed with ECL reagent.

2.3.18 Inhibition ELISA

To determine whether the patient's serum antibodies bind to similar or identical epitopes on Dsg3 as our scFv mAbs, inhibition ELISA assay was performed [22]. Briefly, the anti-Dsg3 scFvs were used at dilutions that result in OD_{540nm}=1.0-1.2 in anti-HA ELISA (in the absence of blocking serum). The scFvs were incubated together with sera on the ELISA plate for 30 min at RT on platform shaking. Binding was analyzed by ELISA, as previously described.

2.3.19 Haemophilus influenza Type B (HiB) ELISA

Since the VH3-23 predominance was also observed in the HiB-reactive antibodies [103, 104], the cross-reactivity of our mAbs against HiB capsular polysaccharide was investigated. Using HiB ELISA kit (IBL International), different dilutions of scFv3-6 (1 µg/µL) or the patient's serum were incubated on ELISA wells for 60 min at RT. ELISA was then carried out according to the standard protocol.

2.4 Cloning and expression of recombinant IgA1 mAbs

2.4.1 Conversion of human anti-Dsg3 scFv into full-length IgA1 antibody

As outlined in Figure 19, I designed a full-length human IgA1 expression cassette based on the backbone of scFv3-6 variable domains. The 3-6 V_H and V_L sequences were ligated into a leader sequence (HAVT20) for secretion and a splice donor sequence (SD) for fusion with constant domains. The variable cassettes were followed by the corresponding constant domains: human

IgA1 heavy chain and lambda light chain. The full-length constructs were chemically synthesized at GeneArt Gene Synthesis (Thermo Fisher Scientific). The cloning vectors were digested with *EcoR*I and *Hind*III restriction enzymes and the representative constructs further subcloned into the pEE 6.4 and pEE 14.4 mammalian expression vectors (Lonza Group, Basel, Switzerland). The expected sequence arrangement in the final constructs was confirmed by automated Sanger sequencing.

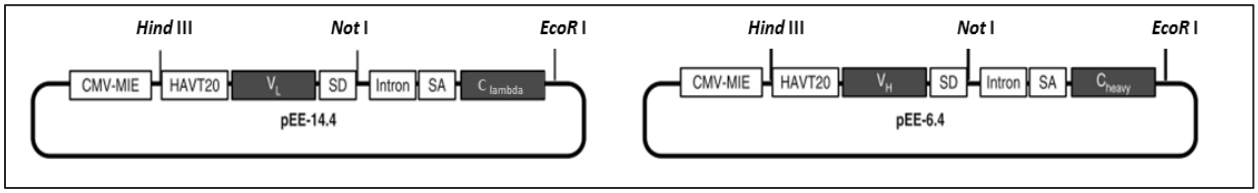

Figure 19: Conversion of anti-Dsg3 scFv3-6 into full-length IgA1 mAb

Variable chain cassettes from scFv3-6 were separately ligated into a HAVT20 leader sequence (HAVT20), a splice donor sequence (SD), and the relevant constant domain (human IgA1 (C_{Heavy}) and light chain (C_{Lambda})). All constructs were cloned into the pEE 14.4 (light chain) and pEE 6.4 (heavy chain) expression vectors. Abbreviation: CMV-MIE, cytomegalovirus (CMV) major immediate-early (MIE) enhancer; SA, splice acceptor; Intron, intronic sequence containing *Not*I restriction site. Figure adopted and modified from [105].

2.4.2 Production of IgA1 mAb by transient transfection of HEK293 cells

Human embryonic kidney cells (HEK293) were co-transfected with plasmid DNA of pEE14.4_3-6VL/λ, pEE6.4_3-6VH/IgA1, and pAdVAntage (Promega) using FuGENE® HD Transfection Reagent (Promega). FuGENE® HD is a novel, nonliposomal formulation used in mammalian cell transfection with high efficiency and low toxicity. Co-transfection of mammalian cells with pAdVAntage vector enhances the transient protein expression by increasing the translation initiation. In brief, 1-1.5×10^4 HEK293 cells were seeded in each well of a 24-well tissue culture plate one day before transfection. The transfection was performed when the cells reached approximately 60-80% confluent. Plasmid DNA (500 ng) was added to appropriate amount of FuGENE® HD in a DNA LoBind tube. After 15 min incubation at RT, the FuGENE® HD:DNA mixture was added to each well and mixed gently. The culture supernatant was collected after 48 hours, centrifuged at 3,000 rpm for 10 min to remove cell debris, and

tested by total IgA ELISA and anti-Dsg3-IgA1 ELISA. No IgA antibody expression was detected by ELISA.

To determine whether the heavy chain or light chain or both are causing problem in full antibody production, mixed cloning of 3-6 constructs with mismatched heavy and light chains of a control antibody (i.e., αDVH/VL) was performed, according to the standard protocol. The culture supernatants were tested by total IgA and anti-Dsg3-IgA1 ELISAs. The 3-6VH+αDVL combination demonstrated high level of antibody expression by total IgA ELISA. However, further analysis by anti-Dsg3 IgA1 ELISA and IFT on Dsg3-transfected HEK293 cells (EUROIMMUN) showed no binding specificity against Dsg3 of this chimeric construct. As an alternative strategy, a previously reported and sequenced anti-Dsg3 IgG clone named F779 was used. F779 IgG was isolated from a PV patient by heterohybridoma [106-108].

2.4.3 Expression and characterization of the recombinant F779 anti-Dsg3 mAbs

The F779 IgG1 and IgA1 mAbs were recombinantly produced in HEK293 cells by EUROIMMUN. The cultures of transfected cells were harvested and analyzed by SDS-PAGE analysis. Binding specificity of F779 IgA1 mAb was first confirmed by anti-Dsg3 IgA1 ELISA and IIF on human skin, ME, and Dsg3-transfected HEK293 cells following the standard protocols. F779 IgG1 mAbs was also tested by ELISA and IIF. To further characterize F779 IgA1, immunoprecipitation (IP) combined with western blotting was performed. In details, 70-100 µL of slurry of Peptide M agarose was transferred into a protein LoBind tube and equilibrated with TBST-calcium buffer. The antibody was added to the tube and incubated for 60 min at RT by gently mixing on a suitable shaker. The tube was centrifuged at 1,000-3,000 g for 2 min 4°C and the supernatant was discarded. After washing the antibody-bead conjugate for three times, the antigen (Dsg3-ectodomain) was added to the tube. The antigen-bead/antibody mixture was incubated for 60 min at RT under rotary agitation. At the end of the incubation, the tube was centrifuged and the supernatant was discarded. The washing steps were performed three times to remove non-specific binding. In each washing step, the bead was mixed gently with wash buffer and centrifuged at 1,000-3,000 g and 4°C for 2 min. The antibody-antigen complex was eluted by boiling the beads in Laemmli sample buffer for 3 min at 95°C. The eluate was then subjected to SDS-PAGE and immunoblotted with anti-Dsg3/1 PX4-3 scFv and anti-HA-HRP antibody. For

inhibition ELISA assay, different dilutions of F779 IgA1 mAbs (dilution: 1:10, 1:50, 1:100, 1:200, and 1:400) were pre-incubated with 3-6 mAb for 30 min at RT. Anti-HA-ELISA was subsequently conducted as described in paragraph 2.3.14. Furthermore, cross-reactivity of F779 IgA1 and IgG1 mAbs to murine skin was analyzed by IF microscopy, according to the standard protocol. As secondary antibodies, goat anti-human IgA-FITC (dilution, 1:100; SouthernBiotech) and F(ab)2 anti-human IgG FITC (dilution, 1:100; Bio-Rad) were used.

2.4.3.1 *In vitro* cryosection assay

To address the role of Fc-dependent cellular mechanisms in pathogenesis of IgA pemphigus, an *in vitro* cryosection assay of human skin was conducted. This *in vitro* model was originally described by Gammon *et al.,* [109] and modified by Sitaru *et al.,* [110] to study the dermal-epidermal separation in autoAb-induced skin diseases. Briefly, human leukocytes were prepared by dextran sedimentation of freshly collected, heparinized blood from healthy donors. Following dextran (Carl Roth) sedimentation for 30 min at RT, the leukocyte-rich supernatant was collected and centrifuged for 12 min at 1200 rpm and RT. Cells were washed with 10 mL RPMI-1640 for 12 min at 1200 rpm and 4ºC. After centrifugation, hypotonic red blood cell lysis was applied for 30 seconds using 10 mL 0.2% NaCl followed by addition of 10 mL 1.6% NaCl. Cells were finally washed in RPMI-1640 for 7 min at 1200 rpm and 4ºC. Concurrently, cryosections of human skin were pre-incubated with F779 IgA1 for 60 min at 37ºC. The IgG1 isotype variant of the F779 mAb and negative controls (normal human IgA (NH IgA) and normal human IgG (NH IgG)) were included. After washing the sections with PBS twice, chambers were prepared. Slide containing the pre-incubated tissue was covered with a second slide, to which transparent adhesive tape has been placed. Taping both slides together formed a gap of 0.3 mm between adjacent slides into which about 1×10^6 cells were injected. Chambers were incubated in a humidified air incubator containing 5% CO_2 for 3 hours at 37°C. Subsequently, chambers were disassembled and sections were extensively washed in PBS to remove the excess unbound cells. The slides were air-dried, fixed in formalin, and stained with H&E. Experiments were repeated three times using different healthy blood donors.

2.4.4 Analysis of binding F779 IgA1 to human polymorphonuclear leukocytes (PMNs)

2.4.4.1 Polymorphprep™ isolation of human PMNs

To isolate polymorphonuclear leukocytes (PMNs), peripheral blood from healthy individuals was collected in EDTA-containing tubes. In a 50 mL Falcon tube, 9 mL of whole blood was layered over 9 mL of Polymorphprep™ (Axis-Shield). Tubes were centrifuged for 35 min at 500 g and RT without brake. After removing the plasma and PBMCs (upper band of cells), the lower band (PMNs) was collected. The PMN suspension was supplemented with 5 mL of half medium (RPMI-1640 diluted 1:1 with ddH_2O). The tube was filled up with RPMI-1640 and centrifuged at 400 g for 10 min at RT. To remove any residual erythrocyte contamination, the cell pellet was lysed using 3 mL lysis buffer. The tube was filled up with RPMI-1640 and cells were harvested by centrifugation at 400 g for 10 min. The cells were further washed with RPMI-1640, resuspended in 1 mL of CL medium, and counted using a Neubauer chamber.

2.4.4.2 Fluorescence-activated cell sorting (FACS) analysis

Soluble immune complexes of F779 IgA1-PMN were formed by incubating the isolated human PMNs (1×10^4 cells) with 5 µg of mAb at 37°C for 60 min. Cells were subsequently harvested by centrifugation (1200 rpm, 7 min), washed twice with DPBS, and labeled by incubation for 20 min at 4˚C with the following mAbs (all diluted in DPBS): Fixable Viability Stain 450 (FVS450, dilution; 1:500, BD Bioscience), APC-conjugated anti-human CD66b antibody (5 µg, BioLegend), and FITC-conjugated anti-human IgA antibody (1 µg; SouthernBiotech). The labeled cells were washed with DPBS and fixed with 100 µL of fixation buffer for 20 min at RT. After centrifugation, the fixed, labeled cells were resuspended in 200 µL of FACS buffer and filtrated. Flow cytometry was performed using MACSQuant Analyzer 10 (Miltenyi Biotec). Data analysis employed MACSQuantify software.

3 RESULTS

3.1 Part I: Selection and preclinical characterization of IgA pemphigus patients

3.1.1 Patient selection

The study cohort included 15 patients newly diagnosed with IgA pemphigus based on the clinical features, typical histology, and DIF findings. The immunological profile of these patients is presented in Table 15. To construct a phage display library, a severely affected patient with long-standing IgA-PV disease was selected (Patient #1). In all experiments, sera from healthy individuals were used as negative controls.

Table 15: Summary of IgA pemphigus sera used in this study

≠ Serum	Diagnosis	Source	ELISA/Dsg3	ELISA/Dsg1	IIF, ICF pattern	Sample
1	**IgA-PV**	**DE***	**++**	**-**	**++, ICF pattern**	**Serum/cells**
2	IgA-PF	DE	-	++	++, ICF pattern	Serum/cells
3	IgA-PV	PL**	++	-	++, ICF pattern	Serum
4	IgA-PV	NL***	+	-	+, ICF pattern	Serum
5	IgA-PV	NL	++	-	++, ICF pattern	Serum
6	IgA-PF	NL	-	+	+, ICF pattern	Serum
7	IgA-PV	JAP****	+	-	(+), No clear ICF	Serum
8	IgA-PV	JAP	+	-	+, ICF pattern	Serum
9	IgA-PV	JAP	++	-	++, ICF pattern	Serum
10	IgA-P + BP180-MMP	JAP	-	-	+, ICF pattern	Serum
11	IEN-IgA-P	JAP	-	+	++, ICF pattern	Serum
12	IgA-PF	JAP	-	+	+, ICF pattern	Serum
13	IgA-PF	JAP	-	+	+, ICF pattern	Serum
14	IgA-PV	JAP	++	-	++, ICF pattern	Serum
15	IgA-PV	DE	+	-	+, ICF pattern	Serum/cells

Abbreviations: *Germany, **Poland, *** the Netherlands, **** Japan, IIF: indirect immunofluorescence, ICF: Epidermal intercellular fluorescence, IgA-P: IgA pemphigus, MMP: Mucous membrane pemphigoid, IEN: Intraepidermal neutrophilic dermatosis.

3.1.2 Clinical and histopathological features of the selected patient

A 58 year-old female patient was admitted to our clinic, with a history of vesicolupustular skin eruptions and erosions on the scalp, and orally at the hard palate and the gums (Fig. 20A-C). Histological examination of skin biopsy revealed intraepidermal acantholysis with prominent neutrophilic infiltrates (Fig. 20D). Histology was consistent with the IEN-subtype of IAD. Nikolsky's sign was negative. No neoplastic diseases were found upon screening. Patient treatment with less than 15-20 mg/day oral prednisolone was not effective. Dapsone (100 mg/day), substituted for dexamethasone pulse therapy, also failed to produce much improvement. In the case of recurrent changes in oral mucosa, acitretin p.o. (up to 50 mg/day) was additionally prescribed, with little effect. Rituximab administered did not result in complete remission.

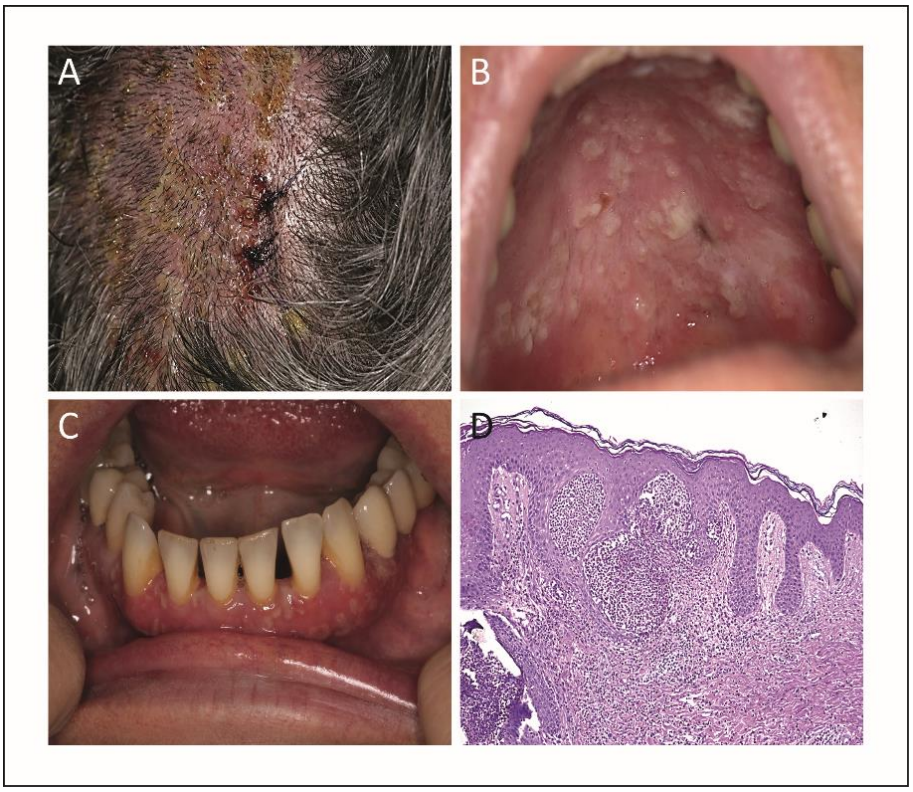

Figure 20: Clinical and histological findings in our IgA pemphigus patient

Clinical appearance of the representative IgA pemphigus patient: (**A**) vesiculopustular lesions on the scalp, (**B**) hard plate, and (**C**) gums. (**D**) Histology of perilesional skin; stained section of a corresponding skin biopsy lesion showed intraepidermal neutrophilic infiltrate and acantholytic keratinocytes. Figures are provided by the Department of Dermatology, University of Luebeck.

3.1.3 Immunopathology and diagnosis

DIF testing on a perilesional skin biopsy demonstrated intercellular IgA deposition on cell surfaces of epidermal keratinocytes (Fig. 21A). No IgG deposition (Fig. 21B) or C3 complement fixation (not shown) was detected. The presence of circulating IgA antibodies was detected by IIF microscopy on normal human skin and ME (Fig. 21C-D). No circulating IgG antibody was found in the same tests (Fig. 21E). Testing by IFT on Dsg-transfected HEK cells detected Dsg3 as the target autoantigen of IgA autoAbs (Fig. 21F). No Dsg1 (Fig. 21G) or Dsc (not shown) reactivity was identified by IFT. An IgA-PF control serum showed binding to ME and Dsg1-transfected HEK cells (Fig. 21H-L).

The patients' sera were tested by Dsg1/3-IgA1/2 ELISAs. The IgA-PV patient showed exclusive serum IgA1 reactivity against Dsg3, whereas no binding to Dsg1 was detected. Moreover, no IgA2 reactivity was identified (Fig. 22A). The IgA-PF serum with known anti-Dsg1 reactivity was used as a control (Fig. 22B). No IgG reactivity was detected against Dsgs for either sera tested (Fig, 22C-D). Taken together, the IgA-PV patient's serum exhibited Dsg3, but not Dsg1, reactivity as confirmed by ELISA and IFT on Dsg-transfected HEK cells. Hence, the representative patient was diagnosed with IEN-subtype by histology and IgA-PV based on the serological data.

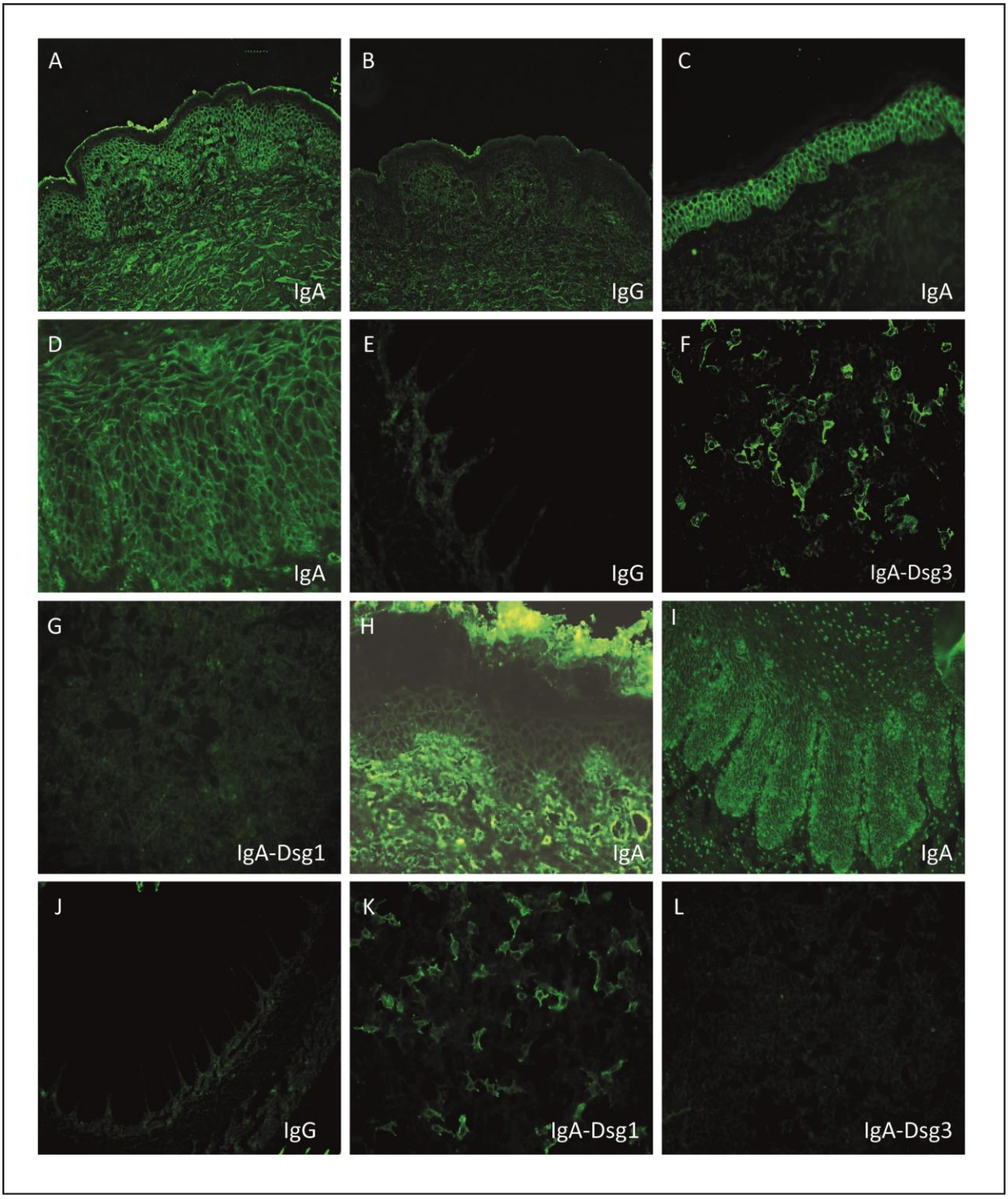

Figure 21: Immunopathological findings in the IgA pemphigus patients

(**A**) DIF analysis of perilesional skin showed IgA but (**B**) no IgG depositions on the epidermis. (**C**) IIF confirmed IgA binding on the epidermal cell surfaces of ME and (**D**) normal human skin. (**E**) No IgG deposition was detected on normal human skin. (**F**) IgA stained Dsg3- (**G**) but not Dsg1-transfected cells. (**H-L**) IgA-PF serum showed binding to only to ME and Dsg1-transfected cells (magnifications, x200).

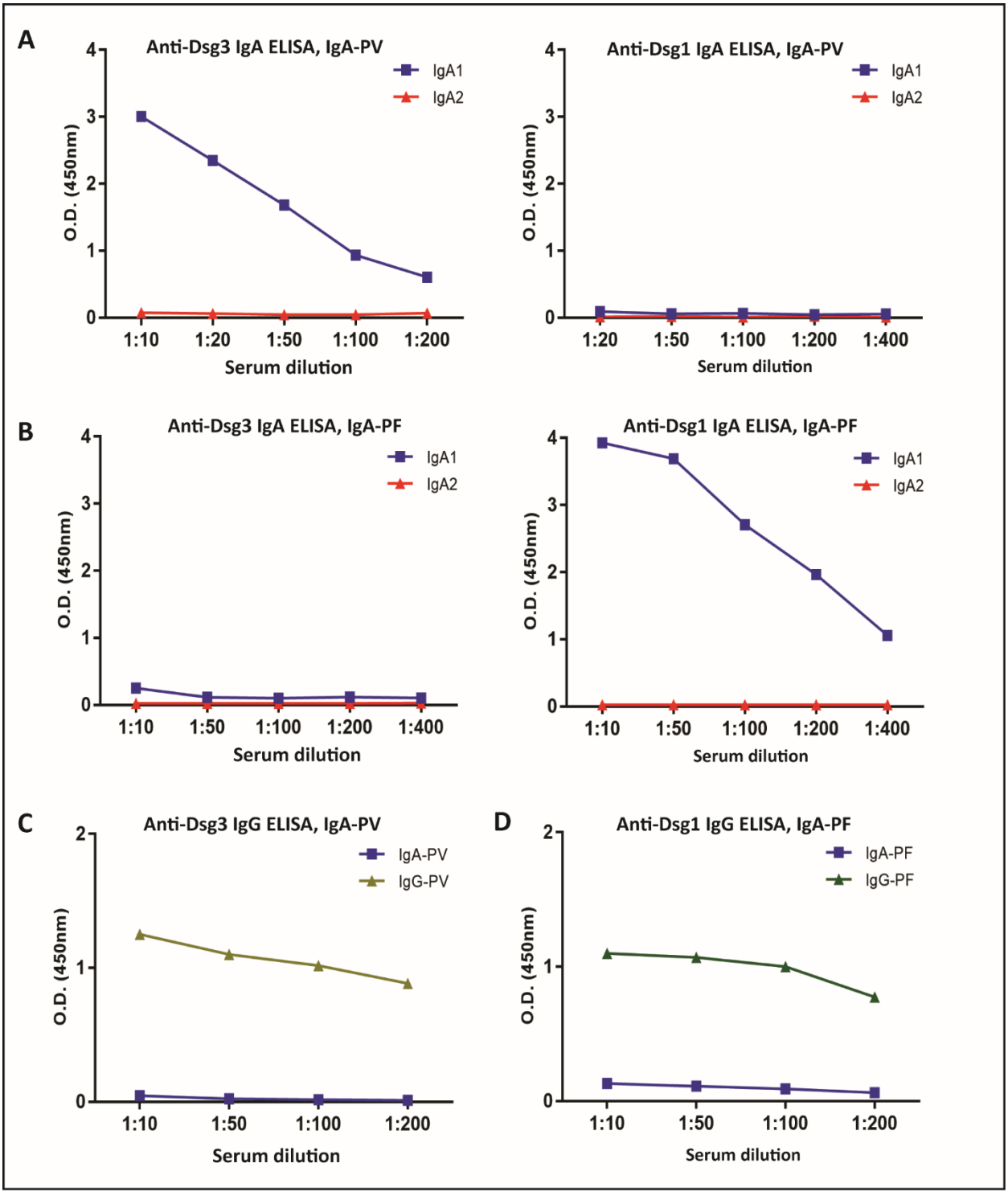

Figure 22: Dsg-ELISA testing of IgA pemphigus sera

(**A**) IgA-PV serum antibodies showed quantifiable specificity for Dsg3 but no binding to Dsg1. (**B**) In contrast, IgA-PF serum displayed reactivity against Dsg1. No IgA2 reactivity was observed for either sera tested. (**C**) IgA-PV and (**D**) IgA-PF sera had no IgG antibodies against Dsgs. IgG-PV and IgG-PF sera were used as positive controls.

3.1.4 EDTA-pretreated ELISA and immunoblotting confirmed binding of serum IgA autoAbs to calcium-sensitive conformational and linear epitopes of Dsg

EDTA inhibition ELISA and immunoblotting are useful methods for defining antigens whose epitopes are calcium-sensitive and linear, respectively. To investigate binding of serum antibodies to calcium-stabilized epitopes on Dsg, EDTA-pretreatment Dsg ELISA was conducted. Calcium depletion by EDTA led to a significant reduction of serum IgA reactivity in an EDTA dose-dependent manner (Fig. 23A-B). Additionally, IgA pemphigus sera displayed specific binding to Dsg3/1(ec)-His, co-migrated with the bands recognized by positive controls murine anti-Dsg3 and anti-Dsg1 mAbs (Fig. 23C-D). These findings confirmed binding of serum IgA to both calcium-dependent conformational and linear epitopes of Dsgs.

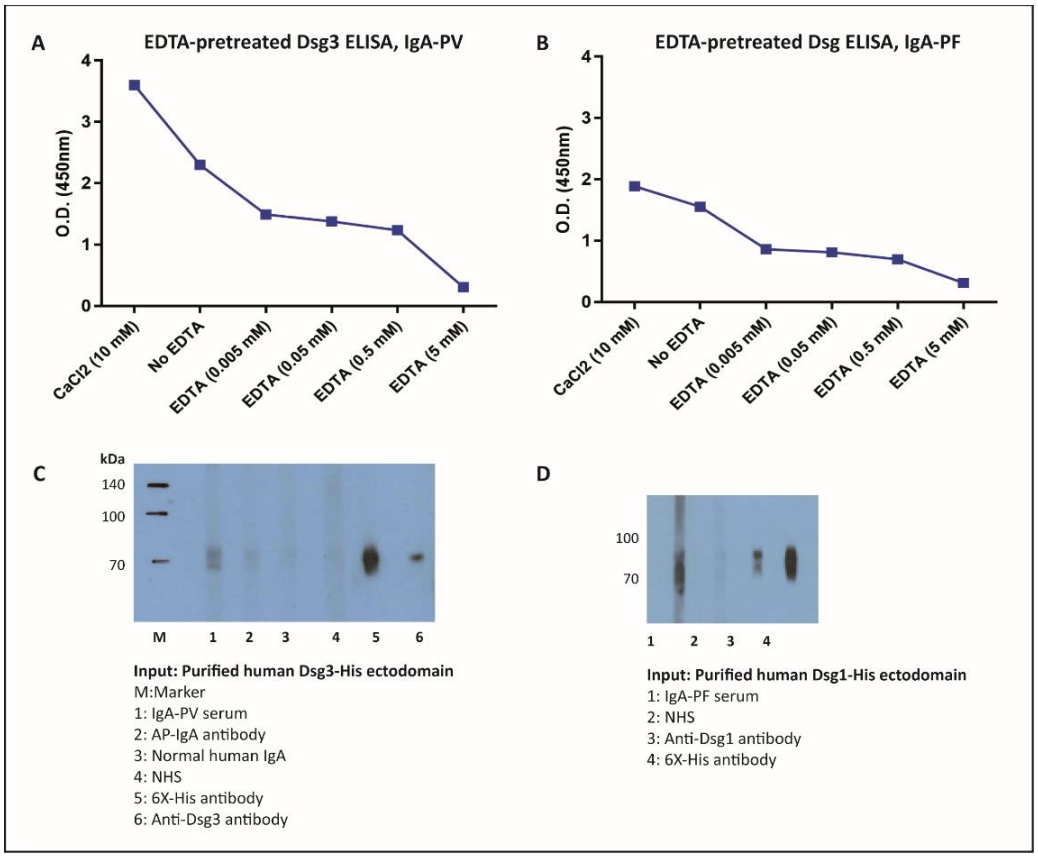

Figure 23: IgA pemphigus sera recognized conformational and linear epitopes of Dsgs

(**A-B**) EDTA-induced inhibition of antibody binding to Dsg substrates; anti-Dsg reactivity was diminished in EDTA-treated wells, though it increased in the calcium-treated well. (**C-D**) Immunoblot analysis of serum autoAbs; IgA binding was detected by HRP-conjugated anti-human IgA antibody. Commercial anti-Dsg3/1 mAbs and anti-His-tag mAb were used as controls.

3.1.5 Removal of serum IgA antibodies by Peptide M agarose did not detect any hidden anti-Dsg3 IgG antibodies in the patient's serum

To really confirm that no anti-Dsg3 IgG antibodies present in the patient's serum potentially masked by IgA autoAbs against the same epitopes of antigen, all IgA antibodies were removed from serum by Peptide M agarose. Total IgG concentration did not change after IgA removal (Fig. 24A). Interestingly, no anti-Dsg3 IgG antibody was detected in the IgA-depleted serum (Fig. 24B). Moreover, Dsg3 reactivity remained unaltered after affinity purification (Fig. 24C). Since the IgA-PV patient had no Dsg1 IgA/IgG reactivity; therefore, this patient could be used as a suitable candidate for construction of a specific IgA1 phage library against Dsg3.

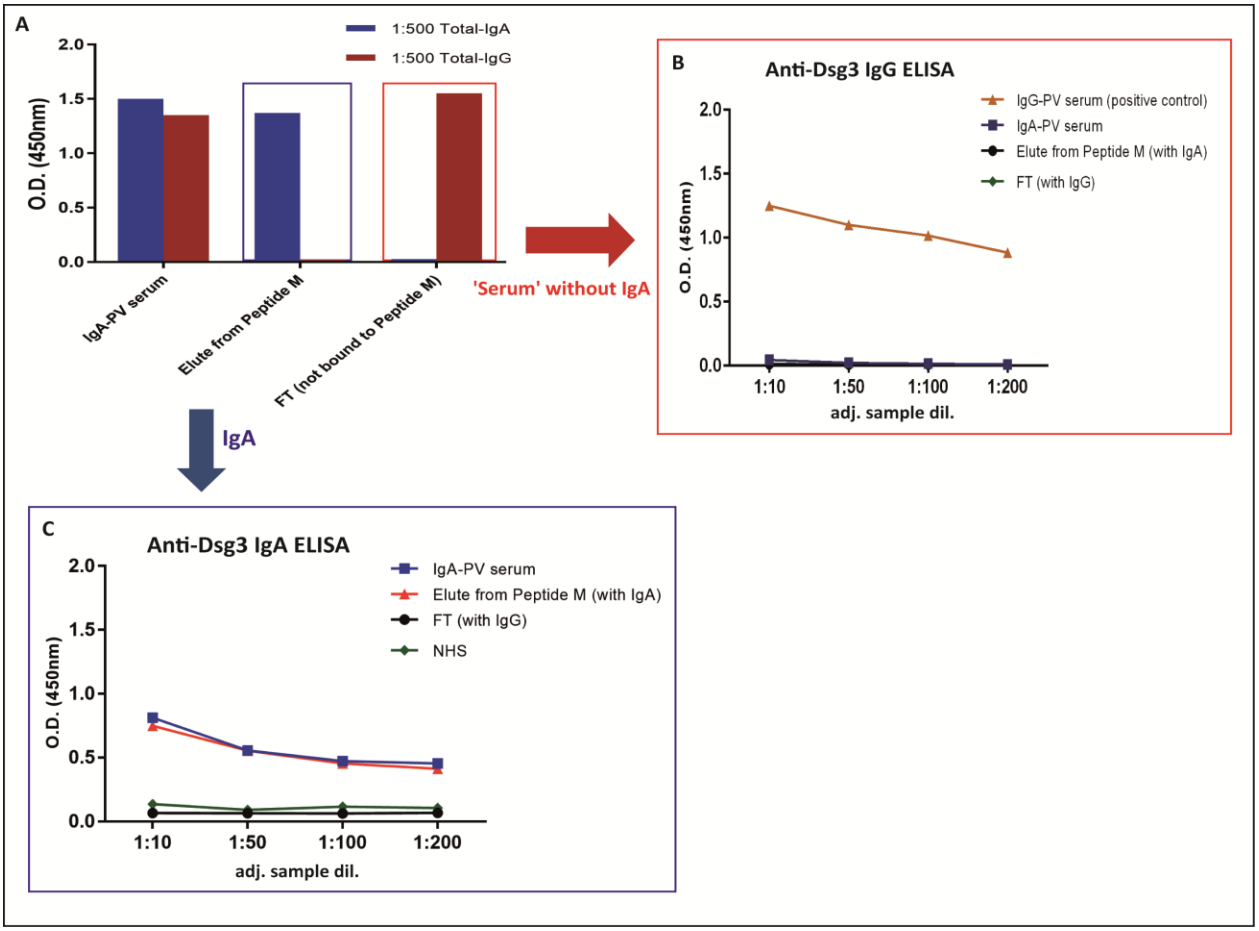

Figure 24: IgA depletion of the patient's serum by Peptide M agarose

(**A**) Affinity purification of serum IgA. (**B**) IgA-depleted serum demonstrated no Dsg3-IgG reactivity. An IgG-PV serum was used as a positive control. (**C**) Eluate from IgA affinity purification maintained its Dsg3 reactivity, showing the effectiveness of the purification procedure.

3.2 Part II: APD cloning of the IgA1 autoAb repertoire from IgA-PV patient to select and identify Dsg3-specific mAbs

3.2.1 Construction of an IgA1-specific phage display library

To construct an IgA1 phage display library, total RNA was isolated from PBMCs of our IgA-PV patient. IgA1 subclass-specific first-round PCR was used to amplify human immunoglobulin variable regions of heavy (V_H) and light (V_L) chains. The resulting products showed a band of ~350 bp corresponding to the V_L and a band of ~550 bp (first round PCR) or a band of ~450 bp (second round PCR) corresponding to the V_H on a 1% agarose gel (Fig. 25A-D). The amplified V_H and V_L fragments were purified and connected together with a $(Gly_4Ser)_3$ linker by overlap PCR. Overlap PCR displayed the expected size of about 800 bp for scFvs (Fig. 25E). Figure 24F illustrates the schematic view of the designed Dsg3-scFv.

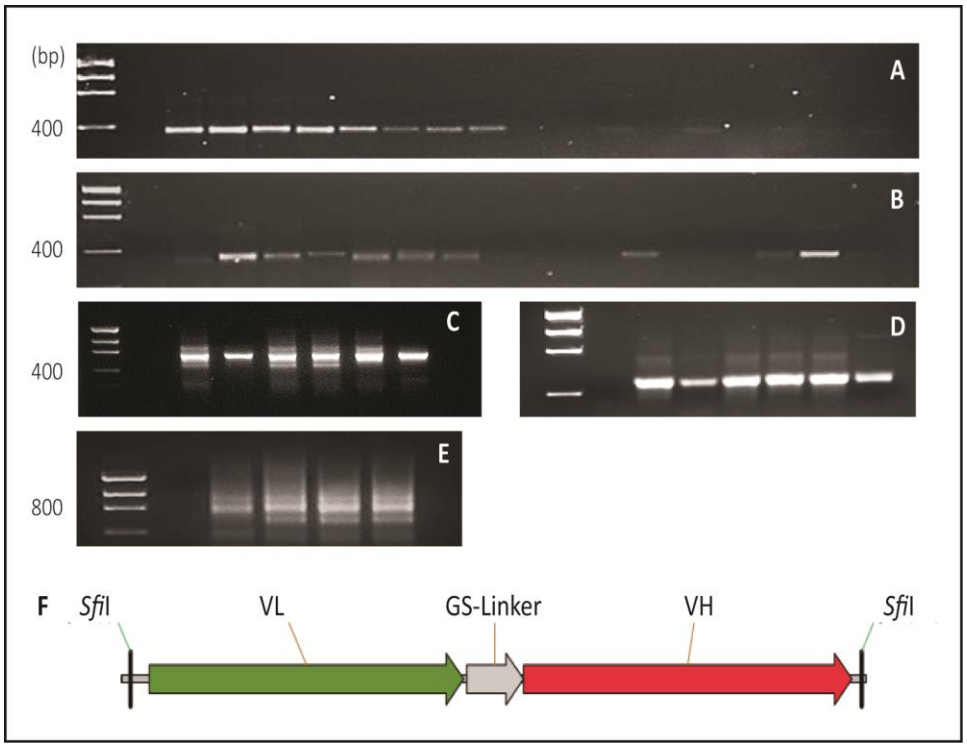

Figure 25: Construction of human IgA1 phage display library

PCR products were separated on a 1% agarose gel. Fragment sizes are indicated in bp along with a low molecular weight DNA ladder. (**A**) V_λ chain fragments, (**B**) V_κ chain fragments, (**C**) V_H chain fragments of the first and (**D**) the second rounds of PCR, and (**E**) overlap PCR products. (**F**) Schematic view of the Dsg3 single chain variable fragment (Dsg3-scFv).

Assembled fragment DNA (i.e., scFv coding DNA) was purified from the gel and digested with *Sfi*I restriction enzyme. The *Sfi*I-digested scFv fragment was cloned into the *Sfi*I-digested phage display vector, pComb3X. To prepare a phage library, the recombinant vectors were electroporated into a XL1-Blue suppressor strain of *E. coli*, followed by helper phage infection. In this system, a filamentous phage particle expresses the scFv (with a C-terminal 6x-His tag and a HA tag) fused to pIII bacteriophage coat protein. The IgA1 library comprised 2.82×10^9 independent transformants (Table 16). Each phage particle displays a particular V_H/V_L pair on its surface (folded into a single monovalent antigen-binding site) with the corresponding cDNA encoding the scFv within the particle.

Table 16: Transformants from large electroporations into *E. coli*

Library part	# Electroporations	# Transformants (output titer)
Kappa (VH/VK)	4 (5 uL DNA each)	1.56×10^9
Lambda (VH/VL)	4 (5 uL DNA each)	1.26×10^9

3.2.2 Screening of scFv phage display library and identification of Dsg3-specific phages

In order to identify the antigen-specific phages, 3-4 rounds of selection against Dsg substrates was performed. After each round, the eluted phages were reamplified in XL1-Blue *E. coli* to form the secondary libraries for subsequent panning. Polyclonal phage ELISA was used to evaluate the enrichment of libraries after screening as well as the binding specificity to immobilized substrates. Polyclonal phage ELISAs were performed with the unselected library and the libraries of all screening rounds. With the third round of selection, enrichment for Dsg3-specific phage was observed as shown by anti-M13 polyclonal phage ELISA (Fig. 26).

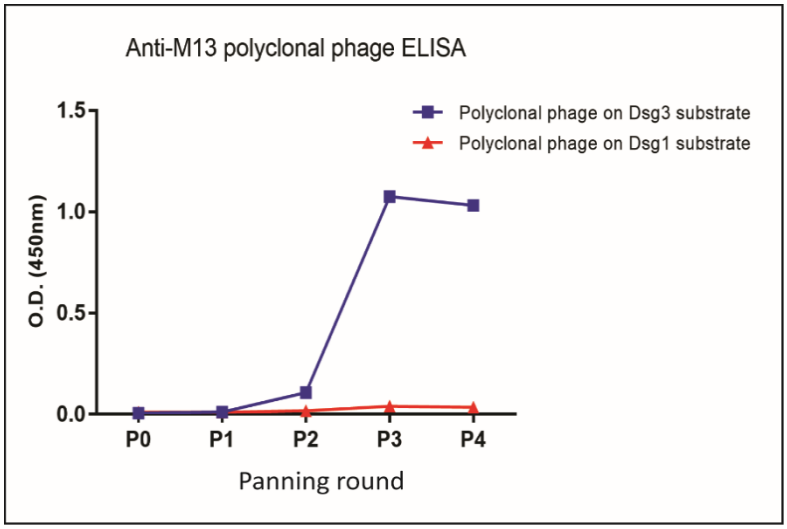

Figure 26: Selection of Dsg phage binders by anti-M13 polyclonal phage ELISA

Dsg-coated ELISA wells were incubated with bacteriophages (titer of 1:1K) from an unselected library (P0) and the first (P1), second (P2), and third (P3) rounds of panning; the reactions were developed using an HRP-conjugated anti-M13 antibody.

More than 50 individual clones were randomly selected from 3-4 rounds and screened by anti-M13 ELISA; of these, three clones ((D3)3-1, 3-6, and 4-8) displayed positive reactivity towards Dsg3 (Fig. 27). As demonstrated by anti-M13 monoclonal phage ELISA, the applied screening process could effectively remove non-functional scFvs or scFvs with weak binding to Dsg3.

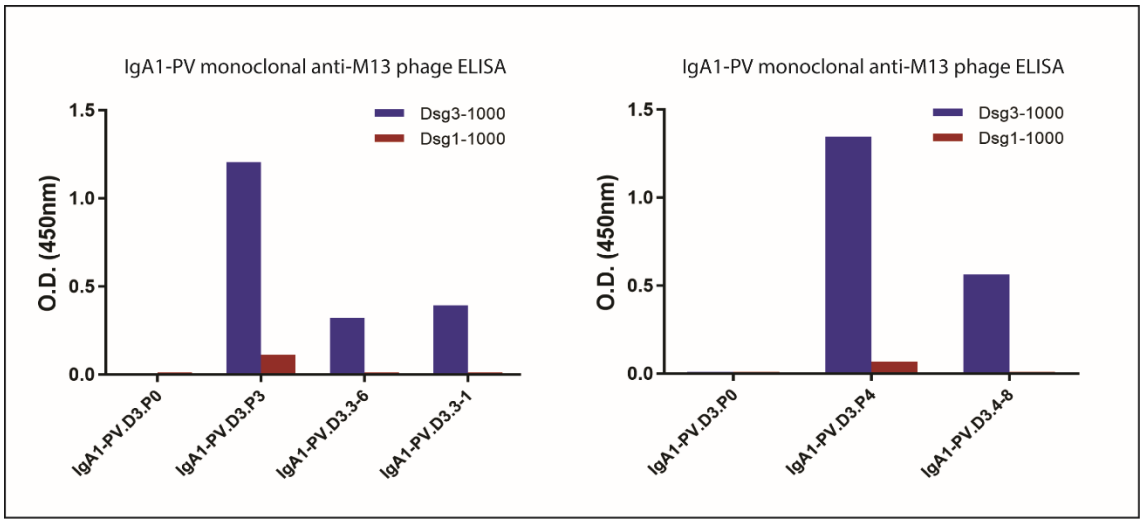

Figure 27: Selection of Dsg-specific clones by anti-M13 monoclonal phage ELISA

Dsg-coated ELISA wells were incubated with bacteriophages (titer of 1:1K) of single clones and the reactions were developed using an HRP-conjugated anti-M13 antibody.

3.2.3 Genetic and proteomic analysis of isolated Dsg3-specific mAbs

Through sequencing monoclonals, three anti-Dsg3 mAbs were identified representing 2 B-cell clonal lineages as defined by H-CDR3 sequence. Sequence alignment of clones indicated the expected sequence arrangements of human IgA1 V_H/V_L (Fig. 28). Table 17 outlines the VH/VL gene usage, H-CDR3 amino acid sequence, and mutational statues of monoclonals. Differences from germline sequences are noted as somatic mutations. Our monoclonals showed two VH gene usages (IGHV3-23*04 and IGHV3-30*04) with mutation counts ranging from 19 to 31 and two VL gene usages (IGL8-61*01 and IGK2-28*01) containing 16-38 mutations. The V_H and V_L CDR3s were 9-15 amino acids long on average. The 3-1 and 3-6 mAbs, genetically derived from the same B cell clone, shared the same CDR3 sequences in both V_H and V_L. Overall, the selected binders originated from two different IGHV and IGKV/IGLV germline genes, indicating sequence diversity with high somatic diversification.

>IgA1-PV_D3_4-8

AGGCGGCCGAGCTCGTGATGACCCAGTCTCCACTCTCCCTGCCCGTCACCCCTGGAGAGCCGGCCTCCATCTCCTGCAGGTCTAGTCAGAGCCTCCTGCATAGTAA
TGGAAACAACTATTTGGATTGGTACCTGCAGAAGCCAGGGCAGTCTCCACAGCTCCTGATCTATTTGGCTTCTACTCGGGCCTCCGGGGTCCCTGACAGGTTCAGT
GGCAATGGATCAGGCACTGATTTTACACTGAAAATCAGCAGAGTGGAGGCTGAGGATGTTGGCATTTATTATTGCATGCAAGGTCTACGACTTCCGGTCACCTTCG
GCCAAGGGACACGACTGGAGATTAAAGGTGGTTCCTCTAGATCTTCCTCCTCTGGTGGCGGTGGCTCGGGCGGTGGTGGGCAGGTGCAGCTGGTGCAGTCTGGGGG
AGGCTTGATACAGCCGGGGGGGGTCCCTAAGACTCTCCTGTGCAGCCTCTGGATTCACCTTCAGTTCCTATCCTATTCACTGGGTCCGCCAGGCTCCAGGCAAGGGA
CTGGAGTGGGTGGCAGTAATATTGAAAGATGGAAGGATTAAATATTATGCAGACTCCGTGAGGGGCCGATTCACCATCTCCAGAGACAATTCCAGGAACACAATGT
ATCTGCAAATGAAGAGCCTAAGAGTTGATGACACGGCTGTCTATTATTGTGCGAGAGATGATGTGGAAACGGATCTTGACTACTGGGGCCAGGGAACCCTGGTCAC
CGTCTCCTCAGCATCCCCGACCAGCCCCAAGGTCACTAGTGGCCAGGCCGGCCAGCACCATCACCATCA

>IgA1-PV_D3_3-6

TGATGGTGATGGTGCTGGCCGGCCTGGCCACTAGTGACCTTACCGTCCTAGACCGTCCTAGGGGGCTGGTCGGGGATGCTGAGGAGACGGTGACCGTGGTCCC
CCGGCCCCAGACATTCATACCGTAGTAGTCTACAGACGACCCTGTGCTCCTCGCACAGTAATAGACGGCCGTGTCCTCGGCTCTCAGGTTGTTCATTTGCAGAGAT
ACCGTGTTCTTGGAAAAGTCTCTGGAGATGGTGAACCGGCCCTTCACGGAATCTGCGTAGAATGTGCCAGCTCCACTACCACTGATACCCGAGACCCACTCCAGCC
CCTTCCCTGGAGCCTGGCGGACCCAGCTCATGGCATAACTGCTAAAGGTGAATCCAGAGGCTGTGCAGGAGAGTCTCAGGGACTCGCCAGGCTGTGCCAAGCCTCC
CCCAGACTCCACCAGCTGCACCTCCCCACCACCGCCCGAGCCACCGCCACCAGAGGAGGAAGATCTAGAGGAACCACCGCCTAGGACGGTCACCTTGGTCCCGCCG
CCGAACACCCAAGTGCCACCCACAAACAGAAGACAATAATAATGGGACTCATCATCTGCCTGGGCCCCCGTGACGGTGAGGGCGGCTTTGTTCGCAACAATGGAGC
CAGAGAAGCGATGAGGGACCCCAGAAGAGCGAAGGTTTGTGTCGAAGATGAGCGTGCGCGGAGCCTGGCCTGGGGTCTGCTGGTACCAGGCGGGATAGTAGTCAGC
AGAAACTGAGCCGGAACTCAAGCCACAAGAGAGAGTGATTGTCCCTCCAGGGGACACTGAGAACGATGGCTCCTGAGTCACCACGAGCTCGGCCGCCTGG

>IgA1-PV_D3_3-1

GCGCATGGTGATGGTGATGGTGCTGGCCGGCCTGGCCACTAGTGACCTTGGGGCTGGTCGGGGATGCTGAGGAGACGGTGACCGTGGTCCCCCGGCCCCAGACATT
CATACCGTAGTAGTCTACAGACGACCCTGTGCTCCTCGCACAGTAATAGACGGCCGTGTCCTCGGCTCTCAGGTTGTTCATTTGCAGAGATACCGTGTTCTTGGAA
AAGTCTCTGGAGACGGTGAACCGGCCCTTCACGGAATCTGCGTAGAATGTGCCAGCTCCACTACCACTGATACCCGAGACCCACTCCAGCCCCTTCCCTGGAGCCT
GGCGGACCCAGCTCATGGCATAACTGCTAAAGGTGAATCCAGAGGCTGCACAGGAGAGTCTCAGGGACCCCCCAGGCTGCACCGAGCCTCCCCCAGACTCCACCAG
CTGCACCTCCCCACCACCGCCCGAGCCACCGCCACCAGAGGAGGAAGATCTAGAGGAACCACCACCTAGGACGGTCACCTTGGTGCCGCCGCCGAACACCCAAGTG
CCACCCACAAACAGAAGACAATAATAATGGGACTCATCATCTGCCTGGGCCCCCGTGACGGTGAGGGCGGCTTTGTTCGCAACAATGGAGCCAGAGAAGCGATGAG
GGACCCCAGAAGAGCGAAGGTTTGTGTCGAAGATGAGCGTGCGCGGAGCCTGGCCTGGGGTCTGCTGGTACCAGGCGGGATAGTAGTCAGCAGAAACTGAGCCGGA
ACTCAAGCCACAAGAGAGAGTGATTGTCCCTCCAGGGGACACTGAGAACGATGGCTCCTGAGTCACCACGAGCTCGGCCGCCTGG

Figure 28: Sequence alignment of cloned Dsg3-scFvs

The VH (yellow box), VL (green box), and linker (in pink) sequences are illustrated. For D3_4-8 scFv, the reverse complement sequence of VH-VL is shown.

Table 17: Characteristics of heavy and light chain variable regions of cloned anti-Dsg3 mAbs

mAb designation	Dsg3	Dsg1	Ca^{2+} sens.	Linear epitopes	H-CDR3	VH gene	VH mut#	L-CDR3	VL gene	VL mut#
IgA1-PV.D3.3-1	+	-	+	+	ARSTGSSVDYYGMNV	3-23*04	19	LLFVGGTWV	L8-61*01	38
IgA1-PV.D3.3-6	+	-	+	+	ARSTGSSVDYYGMNV	3-23*04	21	LLFVGGTWV	L8-61*01	38
IgA1-PV.D3.4-8	+	-	+	+	ARDDVETDLDY	3-30*04	31	MQGLRLPVT	K2-28*01	16

Next, LC-MS/MS was performed specifically on affinity-purified anti-Dsg3 serum IgA from the same patient, according to a previously established protocol by Chen *et al.*, [101]. The purification was extremely efficient and left few, if any, detectable anti-Dsg3 antibodies in the pass-through (Fig. 29). However, the APD-detected Dsg3 antibody clones could not be reliably detected via their H-CDR3 peptides in the heavy chains of the affinity-purified IgA antibodies.

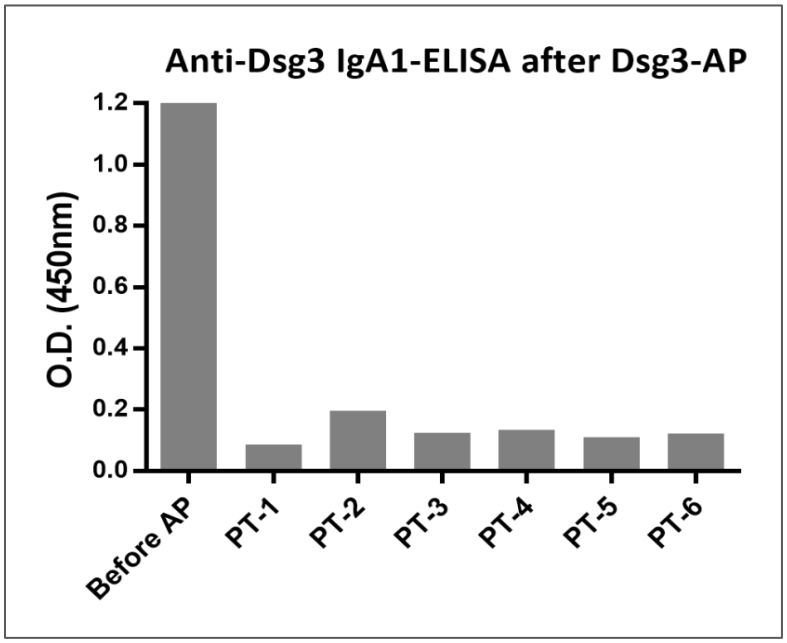

Figure 29: Dsg3-IgA1 ELISA after affinity purification

The IgA pemphigus serum was affinity purified on Dsg3. The pass-through was analyzed as the unbound fraction and the eluate from the Dsg3 was analyzed as the bound fraction, which represents the anti-Dsg3 autoAbs. Abbreviation: AP, affinity purification; PT, pass-through of AP.

3.2.4 Expression and purification of scFv mAbs

E. coli TOP10F´ was used to express the recombinant mAbs as soluble scFvs. Soluble scFvs, engineered with a C-terminal His tag, were purified by IMAC. Integrity and purity of the IPTG-induced scFv preparations were evaluated by SDS-PAGE. The results of small-scale expression and purification of 3-6 scFv are represented in Figure 30. The highest level of protein expression occurred at 10-12 hours after IPTG induction (Fig. 30A). No significant scFv secretion was detected in the supernatants of bacterial cultures (Fig. 30B). The purified scFv contained a protein band of about 37 kDa (Fig. 30C).

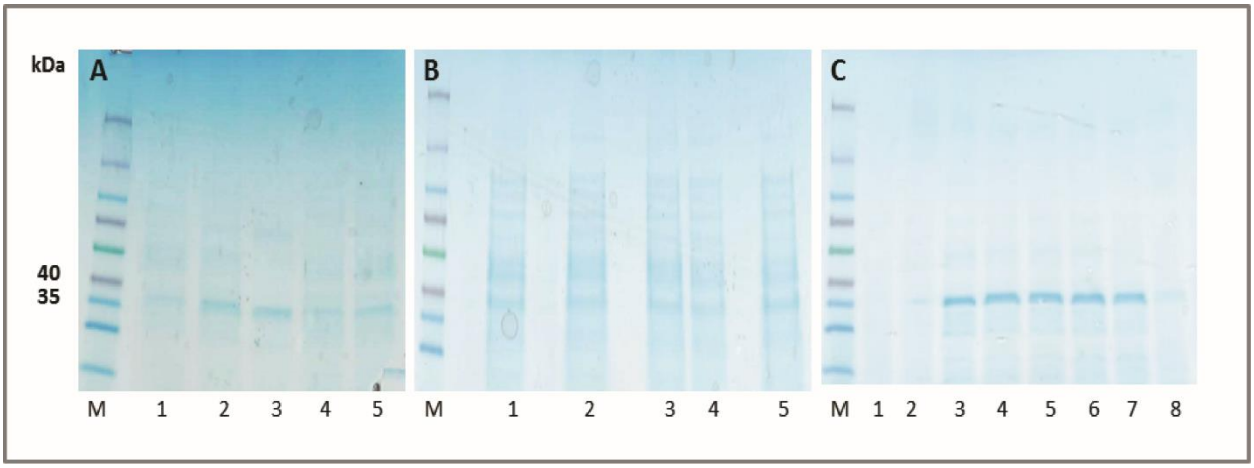

Figure 30: Analysis of 3-6 scFv expression and purification by SDS-PAGE

(**A**) Optimization of 3-6 expression using a small-scale culture: cells were harvested at different time points (8, 10, 12, 14, and 16 hours) following IPTG induction; M: size marker, lanes 1-5: the purified scFv. (**B**) Supernatants of bacterial cultures incubated at different time points (8, 10, 12, 14, and 16 hours) after IPTG induction. (**C**) Large-scale production of 3-6; M: size marker, lanes 1-8: eluates 1-8.

3.2.5 Immunochemical properties of human IgA1-PV scFv mAbs

3.2.5.1 Anti-HA ELISA

Representative soluble scFvs were tested for binding to Dsg substrates using anti-HA ELISAs. All the scFvs bound to Dsg3 in a dose-dependent manner (Fig. 31A). None of the monoclonals bound to human Dsg1.

3.2.5.2 Three anti-Dsg3 mAbs bound to the surfaces of keratinocytes in IIF microscopy

All mAbs had keratinocyte cell surface staining, as shown by IIF on ME (Fig. 31B). Monoclonals 3-1 and 3-6, genetically derived from the same clone, showed 10-fold higher IIF titers than the second mAb 4-8. The isolated anti-Dsg3 scFv mAbs reproduced the binding specificity of polyclonal serum antibodies by both ELISA and IIF assays.

3.2.5.3 Binding to calcium-sensitive conformational and linear epitopes of Dsg

Most pathogenic autoAbs from pemphigus patients recognize conformational epitopes of Dsgs [21, 22]. EDTA-pretreatment anti-HA ELISA was used to analyze binding of mAbs to the calcium-sensitive epitopes. As shown in Figure 31C, chelation of calcium cations diminished Dsg3 binding by mAbs which clearly displayed binding of monoclonals to the calcium-dependent conformational epitopes. Further characterization by immunoblotting confirmed binding of mAbs to linear epitopes of Dsg3(ec)-His ectodomain (Fig. 31D).

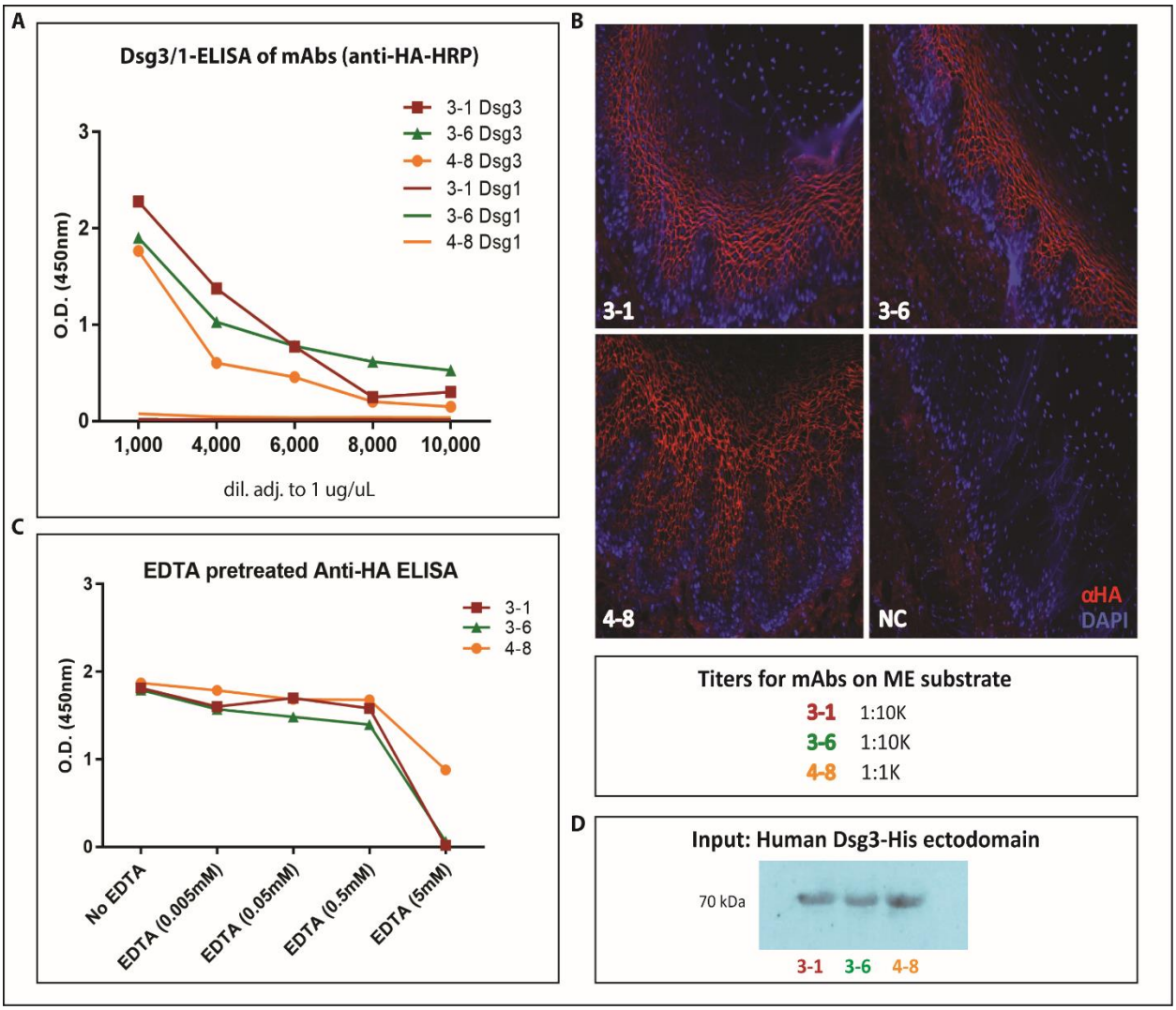

Figure 31: Isolation of human anti-Dsg3 mAbs from an IgA1 phage display library constructed from the representative IgA-PV patient

(**A**) Characterization of antigen specificity by anti-HA ELISA. As expected, all clones bound to Dsg3 substrate, whereas no Dsg1 reactivity was detected. (**B**) IIF on ME substrate; mAbs bound to keratinocyte cell surfaces throughout the epidermis (magnifications, x200). Nuclei were counterstained with DAPI (blue). (**C**) Binding of mAb to the calcium-dependent epitopes of Dsg3 was confirmed by decreased binding of scFvs in EDTA-pretreated anti-HA ELISA. (**D**) Binding of mAbs to linear epitopes of Dsg3 was deected by immunoblotting.

3.2.6 Anti-Dsg3 (VH3-23) mAbs reveal no cross-reactivity with HiB capsular polysaccharide

The mAbs 3-1 and 3-6 used VH3-23 gene segment. Interestingly, VH3-23 gene usage has been also observed in the immune response to Haemophilus influenza infection [103, 104]. As such, the cross-reactivity of the anti-Dsg3 mAbs with HiB antigen was examined. However, neither the anti-Dsg3 mAbs nor the patient's serum demonstrated cross-reactivity with HiB capsular polysaccharide by ELISA (Fig. 32).

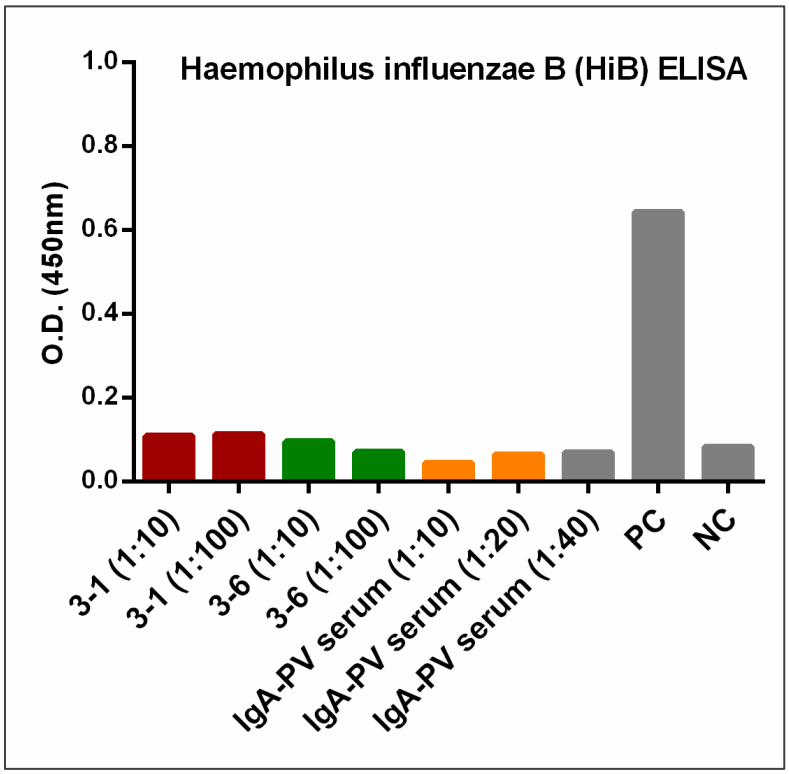

Figure 32: Haemohilus influenza B (HiB) ELISA

The anti-Dsg3 scFvs, 3-1 and 3-6, and the IgA-PV patient's serum showed no reactivity in ELISA against HiB capsular polysaccharide. Positive and negative controls of the ELISA kit were included in this assay.

3.2.7 Sera from pemphigus patients block binding of mAbs to Dsg3 in inhibition ELISA studies

The isolated mAbs were tested for their ability to inhibit binding of polyclonal serum antibodies to Dsg3. Each scFv competed with the same patient's serum on the ELISA plate. The representative IgA-PV serum led to decreased binding of the high-titer mAbs, 3-1 and 3-6. This indicates that the isolated monoclonals bound to the same or similar epitopes on Dsg3 as the polyclonal serum autoAbs (Fig. 33A). The low-titer mAb 4-8 demonstrated less inhibition by the patient's serum (Fig. 33B).

Moreover, sera from unrelated active IgA-pemphigus patients and even from active classical PV patients with Dsg3-IgG antibodies significantly blocked binding of 3-6 mAb. This finding suggested that the polyclonal serum antibodies bind at or near Dsg3 epitopes bound by cloned scFv (Fig. 33C-D). In contrast, NHS did not block binding of 3-6 to Dsg3. Consequently, these data further demonstrated the biological validity of our isolated mAb.

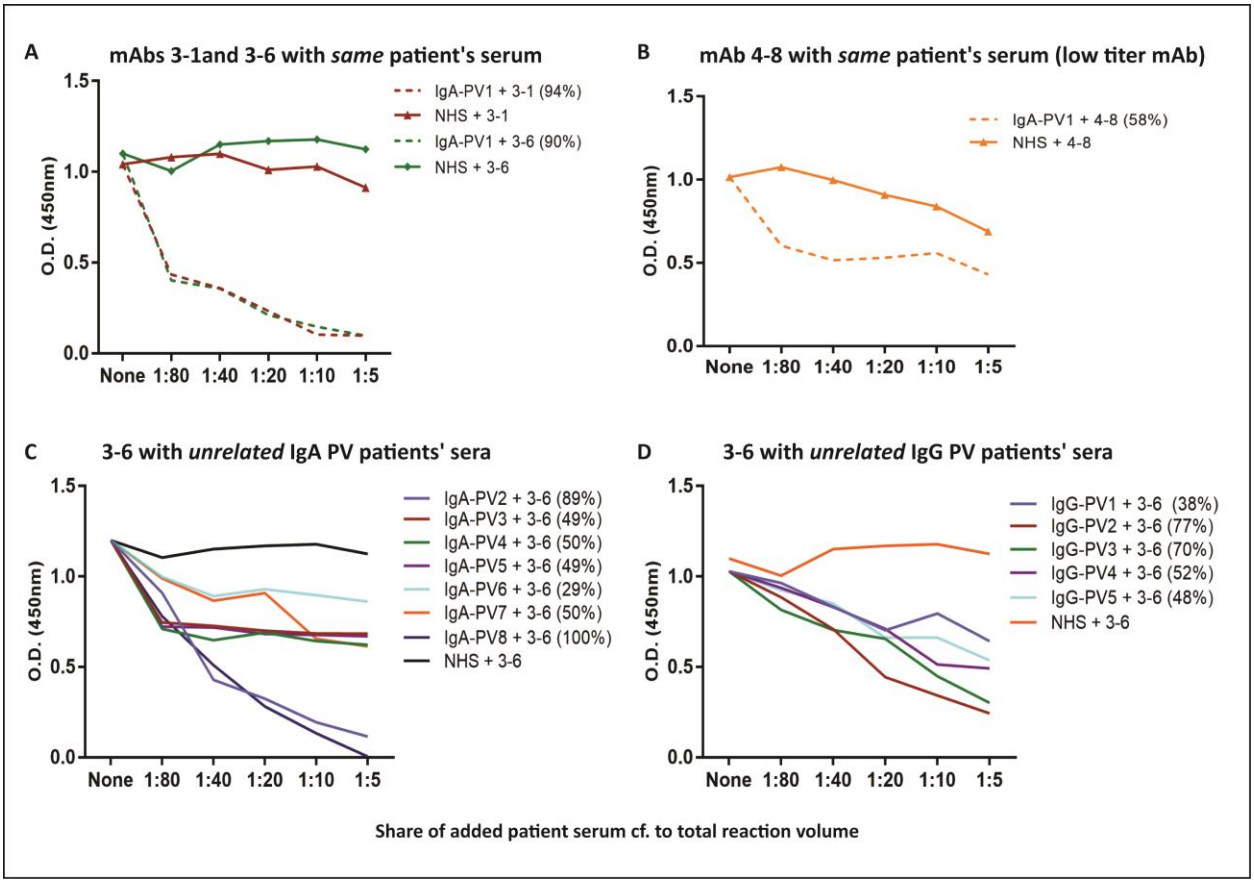

Figure 33: Multiple pemphigus sera target the same or nearby epitopes defined by anti-Dsg3 scFvs

The IgA-PV serum from which the phage library was made, eight active IgA-PV sera, five active IgG-PV sera, and one normal serum (NHS) were used in the inhibition ELISA assays. (**A**) Most strikingly, binding of high titer mAbs, 3-1 and 3-6, were inhibited by the same patient's serum. (**B**) This finding did not apply for the low-titer mAb 4-8. All unrelated IgA-PV (**C**) and IgG-PV (**D**) tested sera inhibited binding of 3-6 to Dsg3.

3.2.8 Anti-Dsg3 mAbs cause fragmentation of epidermal sheets in an *in vitro* dissociation assay

Interference with keratinocyte adhesion is considered as the pathogenic hallmark of autoAbs in pemphigus. To investigate the pathogenicity of mAbs, an *in vitro* keratinocyte dissociation assay was performed using HaCaT cells. HaCaT cells are capable of expressing Dsg1, Dsg2, and Dsg3 antigens. Confluently grown keratinocytes are incubated with antibodies and Dsg3-dominant cell-cell adhesion can be induced by specific cleavage of Dsg1 with ETA, an exotoxin produced by *Staphylococcus aureus* [15, 111-113].

Incubation of cultured keratinocytes with anti-Dsg3 scFv mAbs alone did not impair keratinocyte adhesion, as seen for the negative controls; ETA (0.5 µg/mL) and NHS (dilution, 1:10) (Fig. 34). Whereas, keratinocytes treated with mAb plus ETA showed significant monolayer fragmentation. In addition, the number of cell particles raised as the antibody concentration increased, indicating that this assay can detect the pathogenic strength in a quantitative dose-dependent manner. This finding was replicated for the same patient's serum. The IgA-PV (anti-Dsg3) serum together with ETA induced a clear weakening of keratinocyte adhesion and keratinocyte fragmentation in a serum dose-dependent fashion. Cells treated with IgA-PF (anti-Dsg1) serum plus an anti-Dsg3 mAb were dissociated into numerous smaller fragments. However, no fragment was produced when the keratinocytes were incubated with IgA-PF serum alone. In summary, the present findings demonstrated that, under the conditions used in this assay, the monoclonals and the patient's serum induced loss of keratinocyte adhesion; suggesting their direct pathogenic relevance.

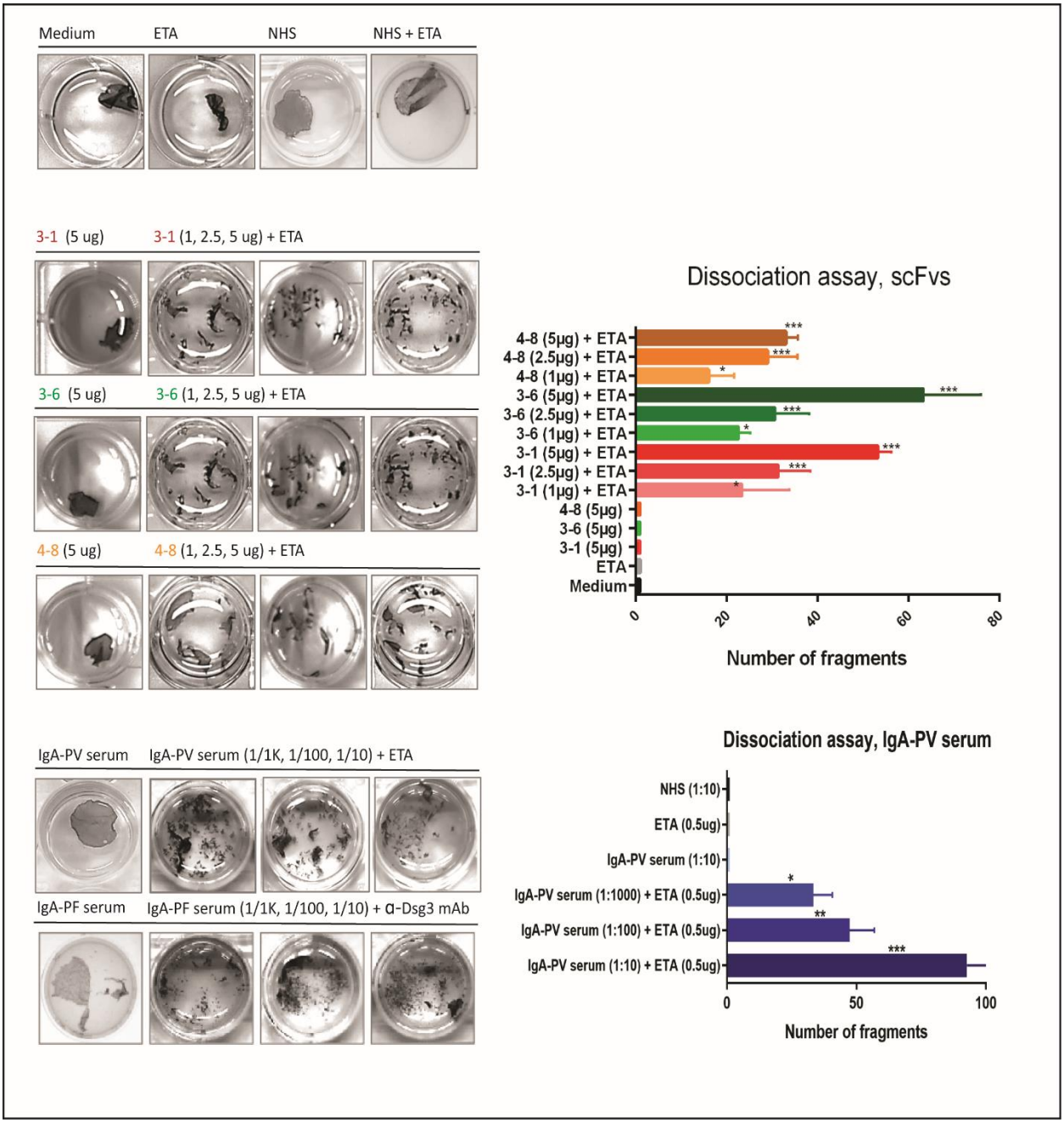

Figure 34: Anti-Dsg3 scFvs cause dissociation of cultured human epidermal keratinocytes

Cells were incubated with the anti-Dsg3 scFvs and patient's serum. ETA, NHS ± ETA, and IgA-PF were used as controls. After dispase-treatment, detached cell sheets were pipetted and fragments were counted. Left panel shows images of wells after monolayer dissociation and right panel shows the numbers of resulting fragments by histograms. The mAbs (1, 2.5, and 5 µg) and the IgA-PV serum (dilutions; 1:10, 1:100, and 1:1K) plus ETA showed pathogenic activity in a dose-dependent manner. The IgA-PF serum plus an anti-Dsg3 mAb (5 µg) caused fragmentation of keratinocyte monolayer. Each experiment was repeated three times. Kruskal Wallis test was used for multiple comparisons. $p<0.05$ was considered statistically significant. All data was analyzed using Graph-Pad Prism V6. Abbreviations: NHS, normal human serum; ETA, exfoliative toxin A.

3.2.9 Anti-Dsg3 mAbs cause acantholysis in the organ-cultured human skin

Next, the pathogenicity of mAbs was further assessed using the HSOC *in vitro* model. Histology was used to detect the pathogenicity and DIF was applied to detect the antibody binding. To exclude the possibility that the acantholysis was resulted from excessive incubation time rather than the injected antibodies, PBS-injected skin specimens were first cultured for up to 60 hours in a 5% CO_2 incubator at 37°C. At a longer incubation time of 48 hours, acantholysis was observed over all layers of the skin due to necrosis or apoptosis (Fig. 35A). As a result, the antibody-injected skin samples were harvested 24 hours after injection. In this study, anti-Dsg3 antibodies were co-injected with ETA, which inhibits Dsg1. To evaluate the optimum dose of ETA, skin specimens were injected with various amounts of ETA (100, 80, 70, and 50 ng). Based on the titration results, ETA produced a superficial epidermal blister of PF pathology at 100 ng (Fig. 35B). Therefore, for subsequent tests, 80 ng ETA was selected as the highest dose of ETA that caused no pathology (i.e., subclinical dose), but inhibited Dsg1 when co-incubated with Dsg3 mAbs.

Negative controls including PBS, subclinical dose of ETA (80 ng), and NHS caused no blisters (Fig. 36). PX4-3 mAb, isolated from a classical IgG-PV patient [68], was used as a positive control. Since PX4-3 cross-reacts with both Dsg3 and Dsg1, ETA is not required here to inactivate compensatory adhesion by Dsg1. Pathogenic PX4-3 mAb caused full-blown acantholysis, though injection of anti-Dsg3 mAbs alone led to no pathology. Mixtures of mAbs and ETA induced acantholysis over all epidermal layers, indicating that the cloned antibodies are pathogenic. This finding was replicated by the same patient's serum, inducing no split formation following individual injection. After adding ETA to the patient's serum, typical acantholysis with a visible tombstone pattern was observed. These findings indicate that binding of autoAbs to target autoantigen is necessary but not sufficient alone for blister formation in our IgA-PV patient.

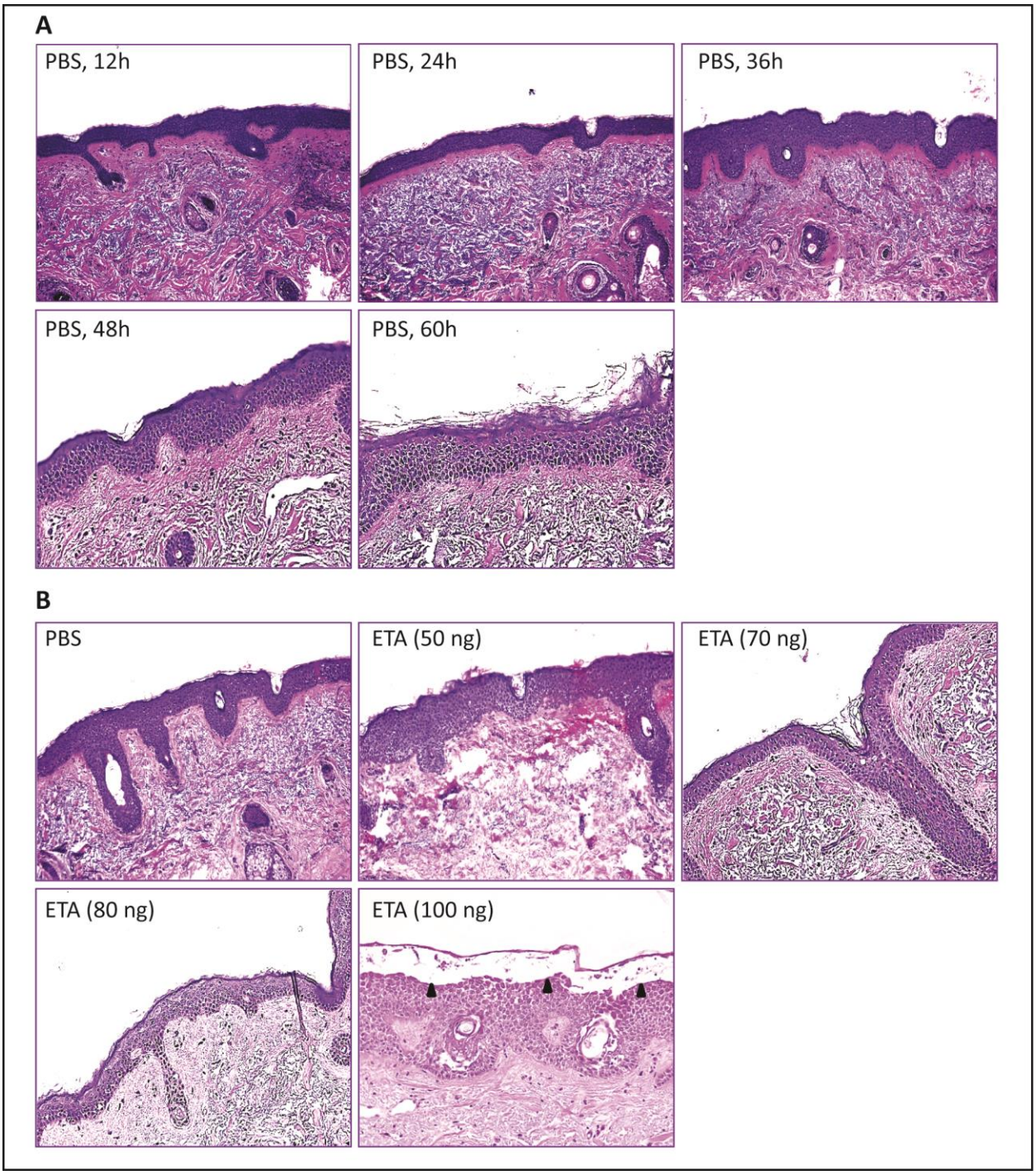

Figure 35: Optimization of the HSOC model

(**A**) Optimization of treatment time in the HSOC model. Specimens of PBS-injected human skin were incubated at different time points in a CO_2 incubator at 37°C. Skin acantholysis was observed after 48 hours of incubation. (**B**) Titration of the injected ETA. ETA caused a PF-like pathology at 100 ng (black arrow heads) but not at the lower amounts used. Each injection was repeated three times showing the same results. Base of the split is marked by black triangles. All sections were stained with hematoxylin and eosin (magnifications, x100-x200). One representative experiment out of 3 is shown.

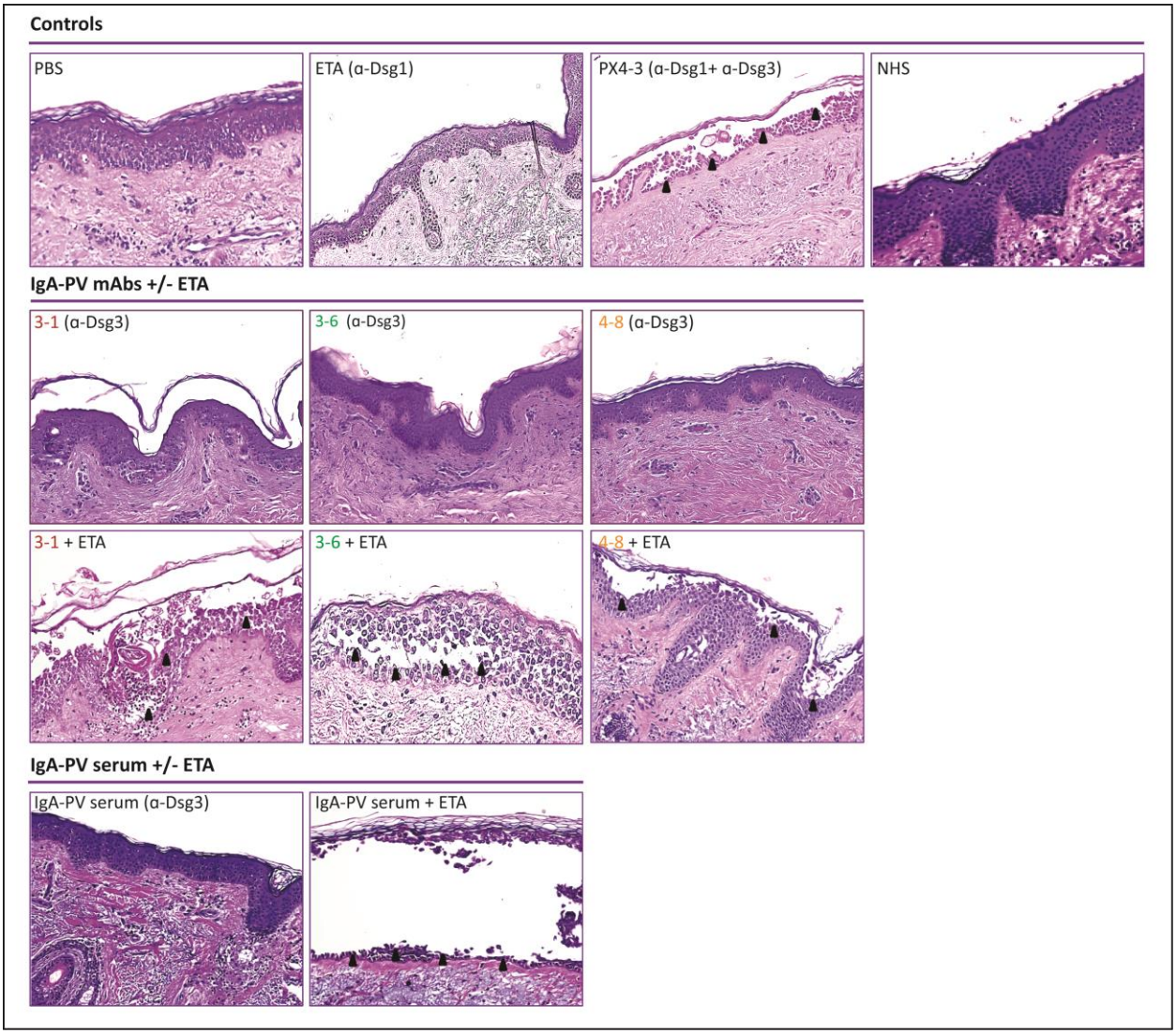

Figure 36: Human skin injection with 3 mAbs derived from the IgA-PV patient

Injection of PBS, subclinical dose of ETA, and NHS into the human skin led to no pathology. In contrast, PX4-3 mAb caused full-blown acantholysis. Injection of the anti-Dsg3 mAb together with ETA resulted in split formation, though the mAbs alone caused no pathology. The patient's serum plus ETA caused acantholysis with tombstone pattern. Each injection was repeated three times with the same results. Base of the split is marked by black triangles. All sections were stained with hematoxylin and eosin (magnifications, x100-200). One representative experiment out of 3 is presented.

To further verify the results of the HSOC model, the skin cultures were stained for IgA deposition. As Dsg3 is the autoantigen in IgA-PV, the injected skin was also stained with mouse anti-human Dsg3 mAb (Clone 5G11). DIF analysis of the injected skin showed a cell surface-staining pattern of IgA that is typical of PV (Fig. 37). Moreover, IgA deposition overlapped with Dsg3 binding.

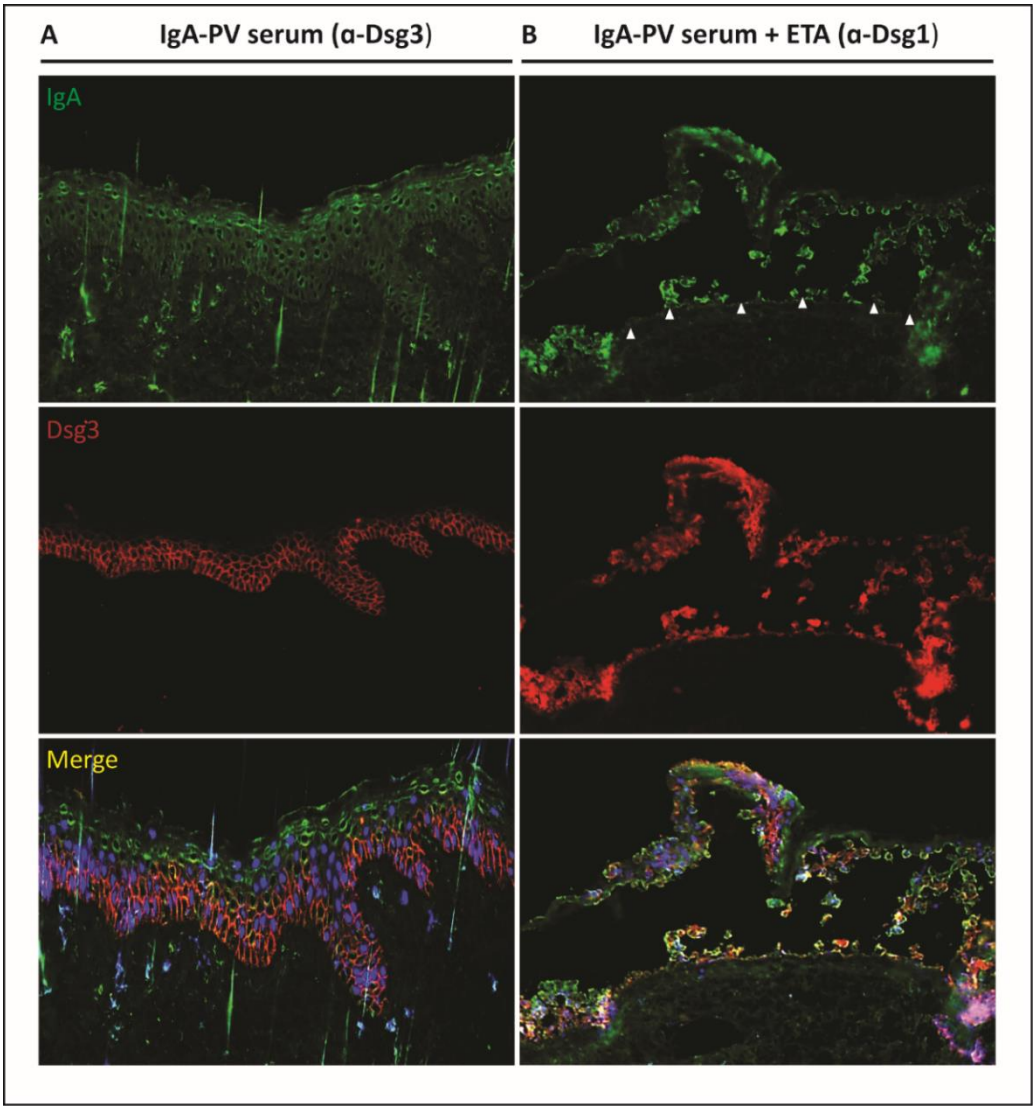

Figure 37: Direct immunofluorescence (DIF) of the HSOC model

(**A**) Injection of the patient's serum into the human skin induced no blistering. However, the corresponding DIF image revealed IgA deposition on the cell surface of epidermis. (**B**) Injection of the serum and ETA mixture caused typical pathology of pemphigus (white arrowheads). In both experiments, the deposited IgA (green) co-localized with Dsg3 (red), as shown in yellow (magnifications, x200). Optimizing some steps of the immunofluorescence protocol (e.g., IgA staining) may be needed in order to obtain the best results for the merged images (third rows). Nuclei were counterstained with DAPI (blue).

In both pathogenic models tested here, loss of cell adhesion was observed within 24 hours of the antibody-treatment. These observations were comparable to that of the positive control (PX4-3 mAb) as assessed by the number of fragments in the keratinocyte dissociation assay or the extent of acantholysis in the HSOC model. In conclusion, we suggest that our mAbs have the ability to disrupt intercellular adhesion and induce blister formation under concurrent elimination of Dsg1, meaning that they are necessary but insufficient for disease induction.

3.2.10 Cross-reactivity of human mAbs with murine keratinocytes' Dsgs

3.2.10.1 IIF on murine skin

Given the possibility that some mAbs might be specific not only for human skin; the potential cross-reactivity of scFvs with murine desmoglein (mDsg) was evaluated by IIF microscopy. Interestingly and unexpectedly, two out of three cloned mAbs (i.e., 3-1 and 3-6) bound to mDsg (Fig. 38A).

3.2.10.2 Injection of murine skin and buccal mucosa

To evaluate the *in vitro* pathogenicity, 3-6 scFv was injected into the freshly isolated murine skin and buccal mucosa. Injection of the murine skin with PBS, subclinical dose of ETA, and 3-6 alone caused no pathology. However, the concomitant injection of 3-6 with ETA resulted in blistering of skin within 24 hours (Fig. 38B). Injection of 3-6 into the buccal mucosa caused suprabasilar acantholysis characteristic of pemphigus, as presented by histology (Fig. 38C). Shown cross-reactivity of Dsg3-mAbs to murine keratinocytes may facilitate the development of a mouse model.

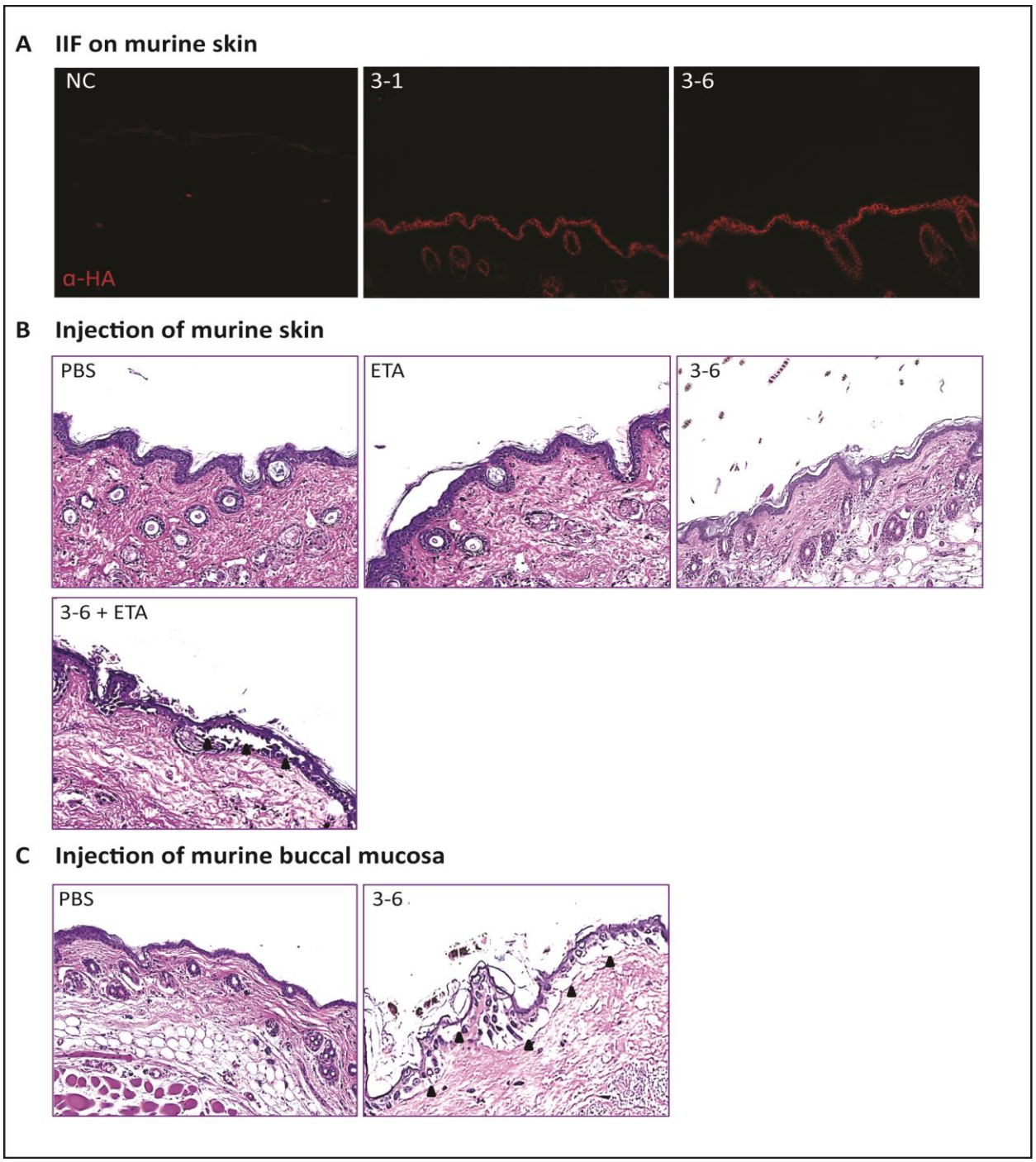

Figure 38: Binding and pathogenicity of human anti-Dsg3 mAbs as determined by injection into murine skin and buccal mucosa

(**A**) High titer mAbs, 3-1 and 3-6, demonstrated keratinocyte cell surface staining by IIF on murine skin. (**B**) As shown by histology, our mAbs caused blisters typical of pemphigus after injection into the murine skin (together with ETA) and (**C**) murine buccal mucosa. Each experiment was repeated three times with the same results. Arrowheads show the location of splits (magnifications, x200). One representative experiment out of 3 is presented.

So far, we have studied a patient with clinical, histopathological, and immunological characteristics of the IgA-PV type. Applying phage display, three anti-Dsg3 mAbs were obtained from this patient. Direct pathogenicity of the monoclonals was observed in the skin organ culture injection studies and keratinocyte dissociation assays (under elimination of Dsg1-compensation), recapitulating the effects of this patient's serum antibodies in those same assays. Further validation study by inhibition ELISA confirmed binding the mAbs and serum antibodies to the same or similar Dsg3-epitopes. Since no anti-Dsg1 IgA/IgG reactivity was detected in our patient, despite clinical affection of the skin and mucous membranes, it is assumed that additional pathophysiologic mechanisms must be involved. To address this issue, the potential contribution of FcαR-bearing cells (e.g. neutrophils) to disease will be next dissected.

3.3 Expression, purification, and characterization of recombinant anti-Dsg3 IgA1 antibodies

The scFv fragments express monovalent antigen-binding sites of native antibody molecules. To evaluate the contribution of FcαR-bearing effector cells in pathogenicity, the most promising APD-derived scFv (i.e., 3-6) was converted into a full-length IgA1 antibody. The heavy and light variable regions of scFv 3-6 were first appended with human IgA1 and lambda constant domains, respectively. Sequencing the recombinant constructs using pEE-specific primers confirmed the chemically-synthesized cassettes. HEK293 cells were then co-transfected with recombinant pEE plasmids. Supernatants of the transfected cells were harvested 48 hours after co-transfection and analyzed by total IgA and anti-Dsg3 IgA1 ELISAs, but no reactivity was detected. Thereafter, additional efforts were made to assess the integrity of the constructs. To pin down why no IgA was expressed, mispairing of 3-6 DNA constructs with heavy and light chains of an unrelated control antibody (i.e., anti-D) was conducted. Interestingly, mismatched combination of 3-6VH+αDVL resulted in high antibody expression as detected by total IgA ELISA (Fig. 39A). However, no Dsg3 reactivity was identified by anti-Dsg3 IgA1 ELISA (Fig. 39B). Obviously, heavy and light chains of 3-6 mAb are both required for the antigen-binding, but this combination could not be expressed in HEK293 cells in our hands. On the other hand, pairing of 3-6VL+αDVH was unproductive (Fig. 39A); meaning that the 3-6 antibody light chain was problematic.

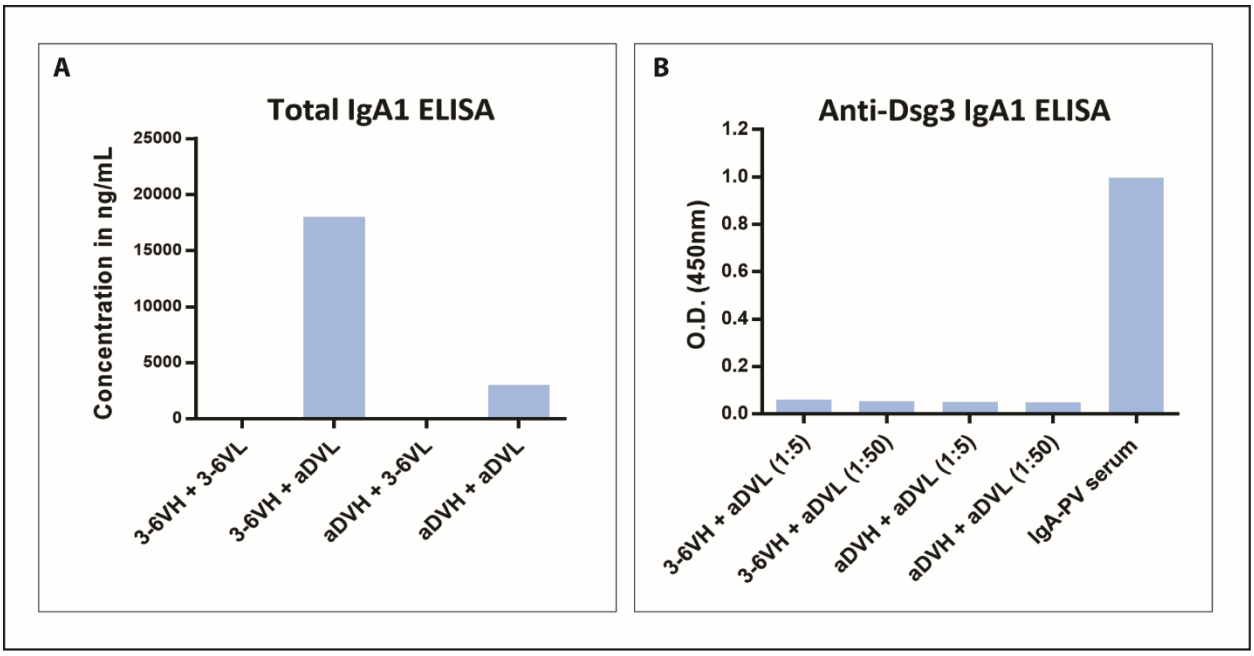

Figure 39: Testing the supernatant of transfected HEK293 cells by ELISAs

(**A**) Mixed transfection of 3-6VH+αDVL plasmids resulted in significant amount of IgA antibody, whereas that of the 3-6VH+αDVL pair failed. (**B**) Mispairing of 3-6VH+αDVL showed no specific reactivity against Dsg3. Here, αDVH+αDVL and IgA-PV serum were used as negative and positive controls, respectively.

As an alternative, yet still valid and informative strategy, the variable regions of a previously reported anti-Dgs3 IgG mAb (i.e., F779 clone) were used to generate a full-length IgA1 mAb. F779 is a well-characterized mAb cloned from a PV patient. This calcium-dependent anti-Dsg3 mAb was mapped to EC1 domain of Dsg3 and showed VH1-46 *01/03 and VLK2-24*01 gene usages (Table 18). The VH (GenBank: HQ338093.1) and VL (GenBank: HQ338094.1) of the F779 clone are presented in Figure 40 [108]. IgG1 and IgG4 variants F779, plus ETA, induced loss of cell surface Dsg3 in primary human epidermal keratinocytes and blisters in human skin [106, 108], however an IgA variant of this mAb has not been described or published so far.

Table 18: Genetic and functional characteristics of anti-Dsg3 F779 mAb

mAb designation	Dsg3	Dsg1	Ca^{2+} sens.	Linear epitopes	H-CDR3	VH gene	L-CDR3	VL gene
F779	+	-	+	+	ARSIESISGRTLGY	1-46 *03	LQATEFPYT	K2-24*01

> F779-VH

CAGGTGCAGCTGGTGCAGTCTGGGGCTGACGTGAAGAAGCCTGGAGCCTCAGTGAAGGTTTCCTGCACGGCATCTGGAA
ACACCTTCACCACCTACTCTCTACACTGGGTGCGACAGGCCCCTGGACAAGGGCTTGAGTGGATGGGAGTAATCGACCC
TAGTGGTGGTAGCACAAGCTACGCACAGAAGTTCCAGGGCAGACTCACCATGACCAGGGACACGTCCACGAGTACATTT
TACATGGAGTTGAGCAGCCTGAGATCTGAGGACACGGCCGTTTATTACTGTGCGAGGTCTATAGAGTCTATTAGTGGCC
GGACCCTTGGATACTGGGGCCAGGGAACCCTGGTCACCGTCTCCTCA

> F779-VL

GATATTGTGATGACCCAGACTCCACTCTCCTCACCTGTCACCCTTGGACAGCCGGCCTCCATCTCCTGCAGGTCTAGTG
AAACCCTCGTACACAGTGACGGAAACACCTACTTGAGTTGGCTTCAGCAGAGGCCAGGCCAGCCTCCAAGGCTCCTAAT
TTATAAGATTTCTAATCGGTTCTCTGGGGTCCCAGACAGATTCAGTGGCAGTGGGGCAGGGACAGATTTCACACTGAAA
ATCAGCAGGGTGGAAGCTGAGGATGTCGGGGTTTATTACTGCCTGCAAGCTACAGAATTTCCGTACACTTTTGGCCAGG
GGACCAAGCTGGAGATCAAA

> VH amino acid sequence

QVQLVQSGADVKKPGASVKVSCTASGNTFTTYSLHWVRQAPGQGLEWMGVIDPSGGSTSYAQKFQGRLTMTRDTSTSTF
YMELSSLRSEDTAVYYCARSIESISGRTLGYWGQGTLVTVSS

> VL amino acid sequence

DIVMTQTPLSSPVTLGQPASISCRSSETLVHSDGNTYLSWLQQRPGQPPRLLIYKISNRFSGVPDRFSGSGAGTDFTLK
ISRVEAEDVGVYYCLQATEFPYTFGQGTKLEIK

Figure 40: VH and VL sequences of F779 clone and their corresponding amino acid sequences

Culture supernatants of F779 IgA1/IgG1 transfected HEK293 cells were collected and antibody expression was assessed by SDS-PAGE analysis (Fig. 41A). F779 IgA1 mAb demonstrated Dsg3, but no Dsg1, specificity by ELISA. As expected, no IgA2 reactivity was detected (Fig. 41B). Binding to the cell surface of keratinocytes was determined by IIF microscopy on ME, Dsg3-transfceted cells, and normal human skin (Fig. 41C). Furthermore, IP experiment of F779 mAb and human Dsg3(ec)-His was performed. F779 precipitated the Dsg3-ectodomain as detected by PX4-3 mAb (Fig. 41D). Most importantly, F779 decreased binding of scFv 3-6 up to 60% in an anti-Dsg3-HA inhibition ELISA study, indicating that they share same or similar epitopes of Dsg3 (Fig. 41E). Regarding these features, F779 IgA1 could be used as a proper alternative to mAb 3-6 to establish an *in vitro* model of IgA pemphigus.

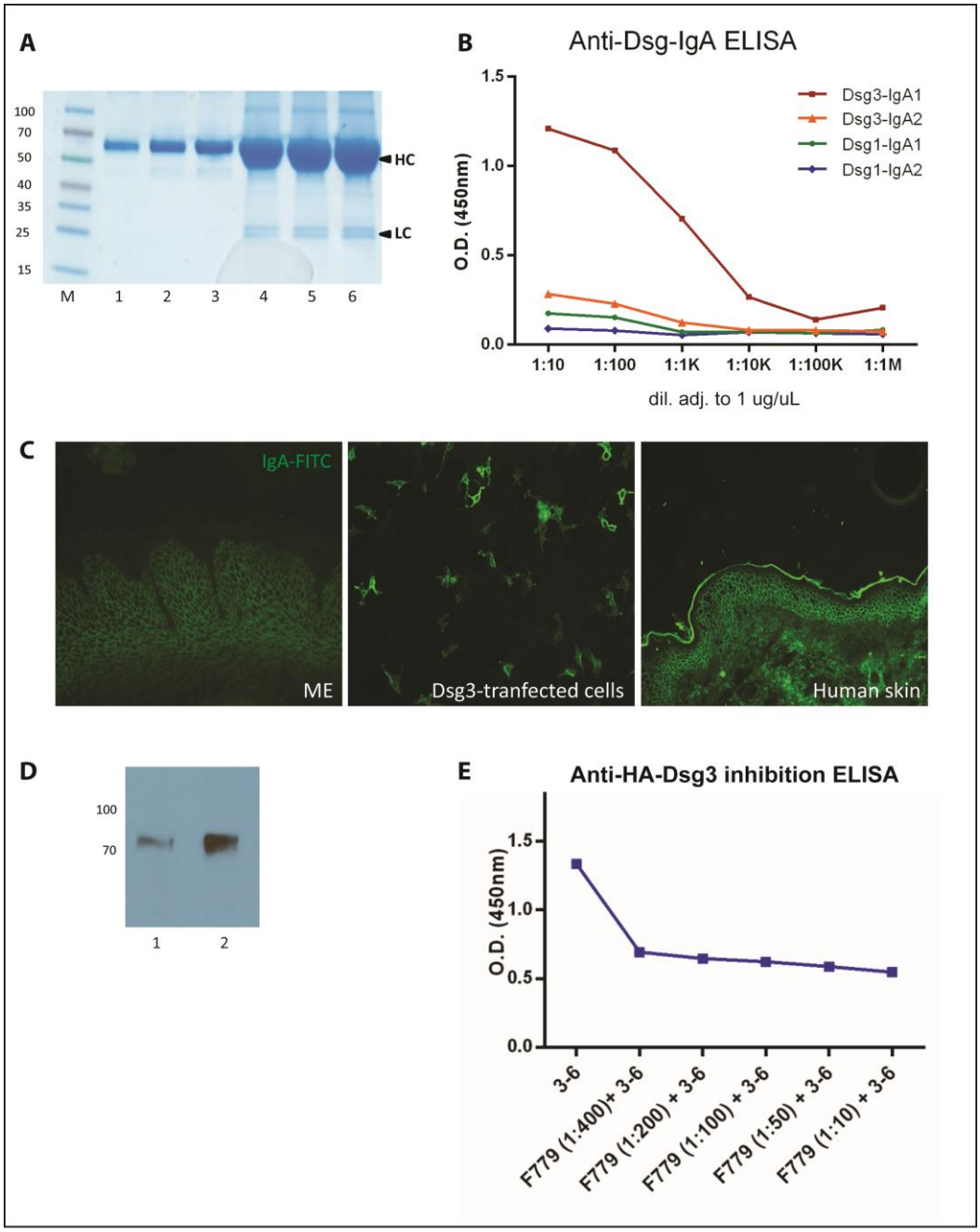

Figure 41: Characterization of F779 anti-Dsg3 IgA1

(**A**) Analysis of F779 IgA1 expression by SDS-PAGE; M: size marker, lanes 1-3: BSA standard (2, 4, and 6 µg), lanes 4-6: culture supernatant (0.5, 0.75, and 1 µL/well). (**B**) Binding curves of F779 against Dsg3/Dsg1 by ELISA. (**C**) IIF on ME, Dsg3-transfected cells, and human skin. F779 bound to the cell surface of keratinocytes (magnification x200). (**D**) Immunoblot of IP using human Dsg3(ec)-His. F779 precipitates Dsg3(ec) as detected by PX4-3 mAb; lane 1: IP eluate, lane 2: Dsg3(ec). (**E**) Inhibition ELISA study showed decreased binding of 3-6 to Dsg3 by F779 IgA1 (maximum inhibition approximately 60%). This finding is suggested to be related to the antibody-antigen binding kinetics.

The IgG1 isotype of F779 mAb was recombinantly produced in HEK293 cells, purified from the culture supernatant, and analyzed by SDS-PAGE (Fig 42A). F779 IgG1 specifically bound to Dsg3 but not Dsg1 (Fig 42B). IIF staining of normal human skin and ME demonstrated keratinocyte cell surface binding of F779 IgG1 (Fig. 42C).

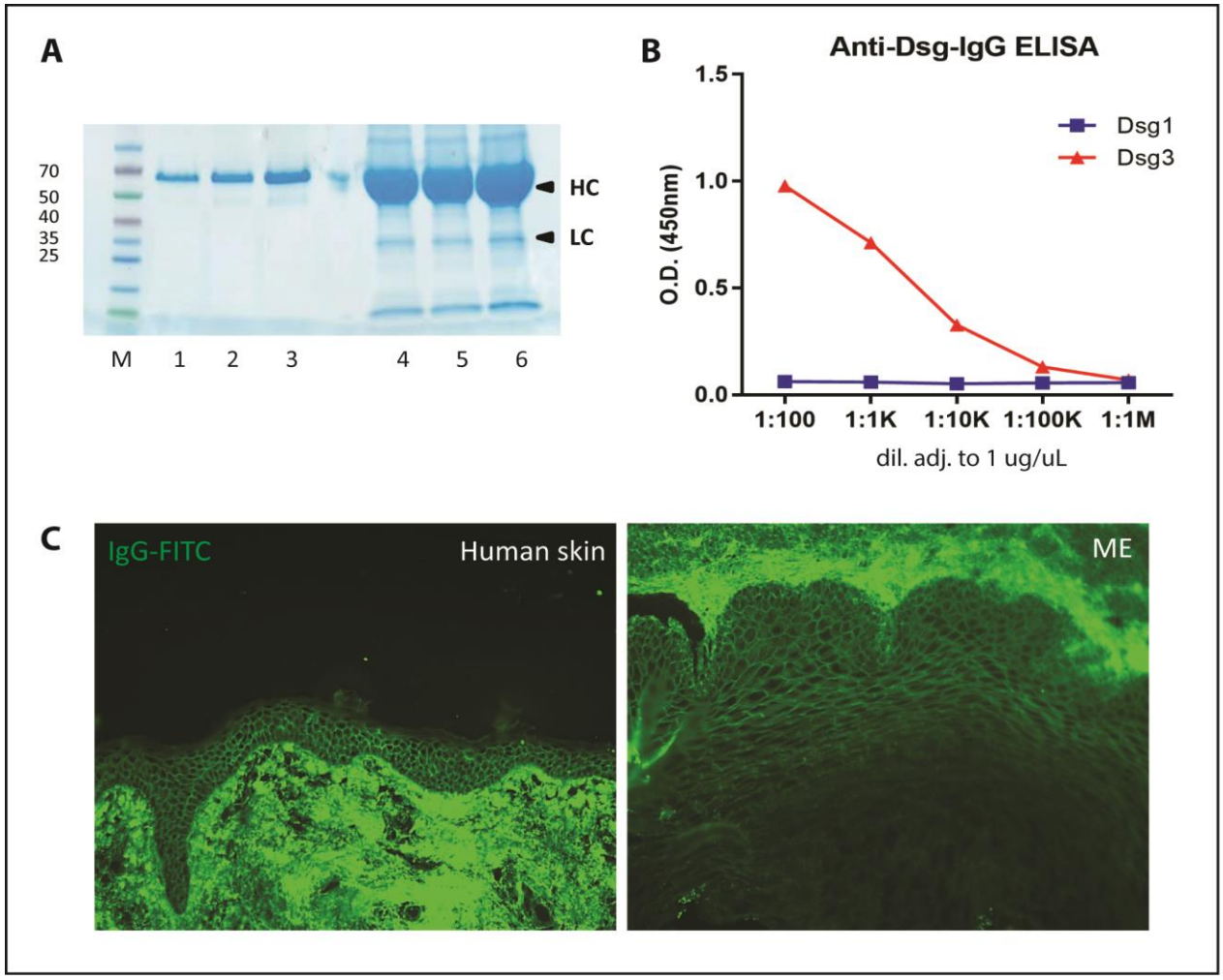

Figure 42: Characterization of F779 anti-Dsg3 IgG1

(**A**) Analysis of F779 IgG1 expression by SDS-PAGE; M: size marker, lanes 1-3: BSA standard (2, 4, and 8 µg), lanes 4-6: culture supernatant of transfected cells (0.5, 0.75, and 1 µL/well). (**B**) F779 IgG1 specifically bound to Dsg3 but not Dsg1. (**C**) IIF on human skin and ME showed IgG deposition (dilution, 1:1K) at the keratinocyte cell surface (magnification x200).

3.3.1 Cross-reactivity of anti-Dsg3 F779 IgA1 and F779 IgG1 mAbs with murine skin

Cross-reactivity of anti-Dsg3 F779 IgA1 and F779 IgG1 mAbs with murine skin was tested by IIF microscopy. As shown in Figure 43, both isotypes bound to the cell surface of murine keratinocytes' Dsgs. These mAbs could greatly facilitate the development of improved disease models and novel therapeutic strategies.

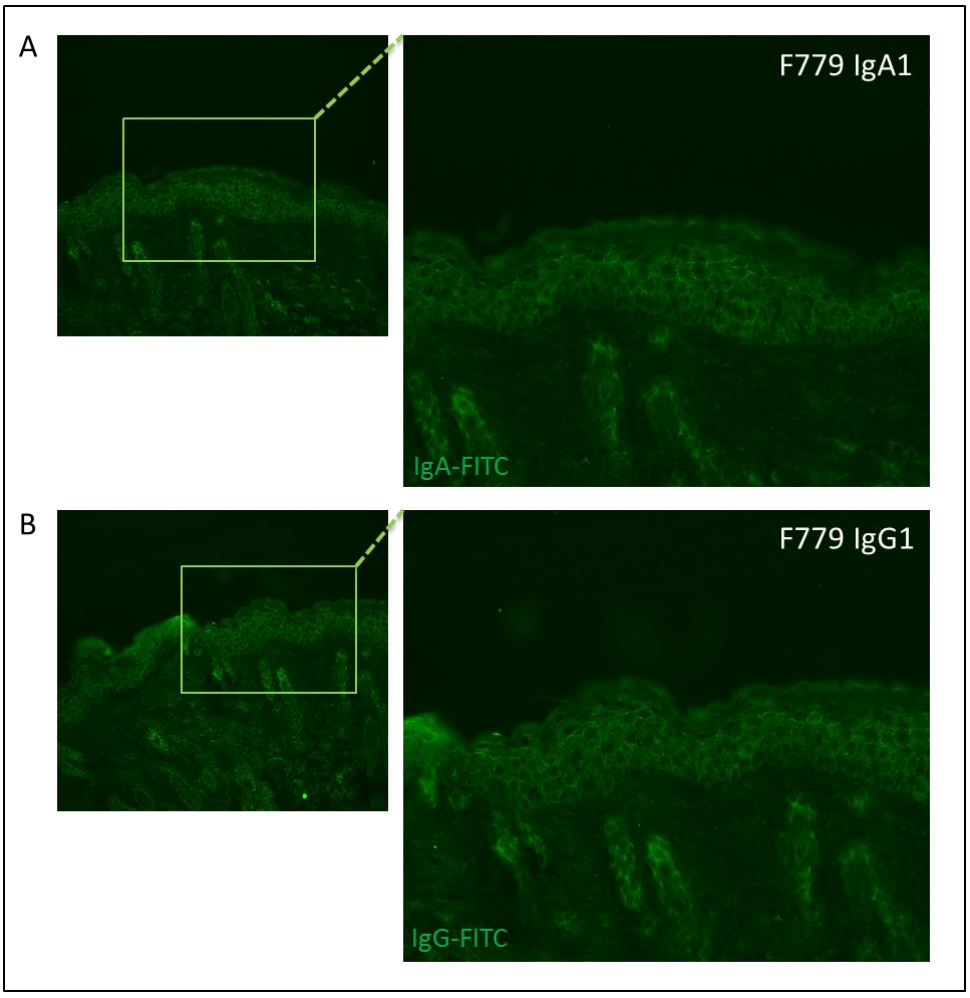

Figure 43: Cross-reactivity of two isotypes of F779 mAbs with murine skin

(**A**) Binding of anti-Dsg3 F779 IgA1 and (**B**) F779 IgG1 mAbs to murine skin was detected by anti-human IgA-FITC and IgG-FITC antibodies, respectively (magnifications, x200).

3.3.2 F779 IgA1 mAbs induce intraepidermal acantholysis in cryosections of human skin

In IgA-mediated blistering diseases, accumulation of IgA-immune complexes in the skin may result in neutrophil recruitment and activation, release of superoxide, inflammatory cytokines, and proteases, and ultimately cause tissue damage [114]. To dissect the Fc-dependent mechanisms involved in pathogenesis of IgA pemphigus, an *in vitro* cryosection assay of human skin was conducted (Fig. 44). Incubation of human skin cryosections with F779 IgA1 and human peripheral polymorphonuclear leukocytes (PMNs) led to induction of intraepidermal acantholysis and typical pemphigus pathology, without requiring Dsg1 inactivation by ETA or anti-Dsg1 mAbs. However, the same antibody in the form of IgG1 (F779 IgG1) as well as the negative controls, NH IgA and NH IgG, did not cause pathology under the same assay conditions. These *in vitro* data clearly demonstrate that the interaction of anti-Dsg3-IgA-Fc:FcαR mediates pathogenicity in IgA pemphigus.

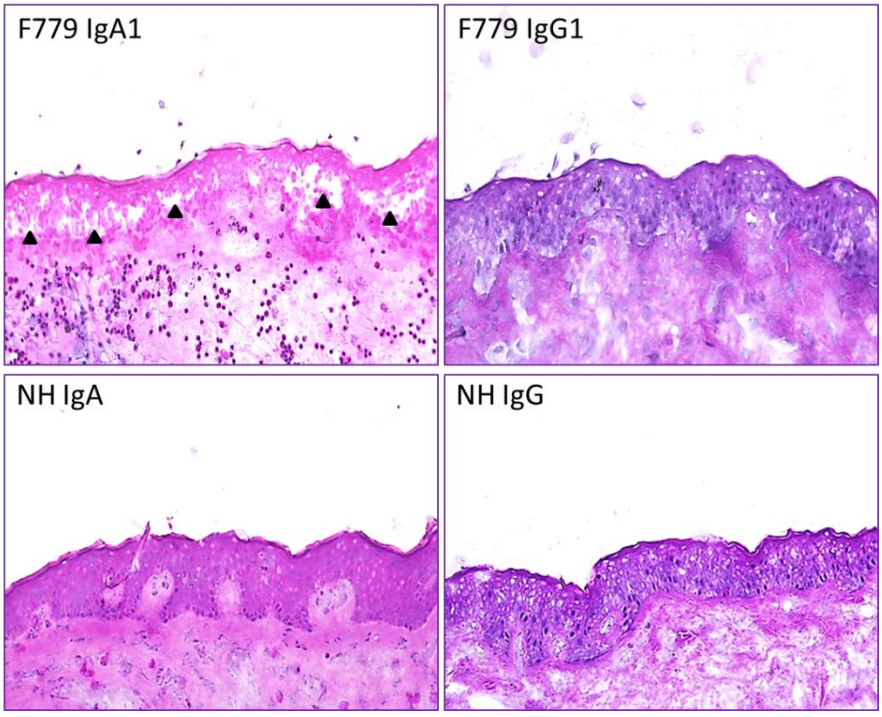

Figure 44: Anti-Dsg3 IgA1 mAbs induce leukocyte-dependent blistering in human skin cryosections

Incubation of human skin cryosections with F779 IgA1 and human PMNs resulted in intraepidermal acantholysis. Though, F779 IgG1, NH IgA, and NH IgG were ineffective under the same conditions. Base of the split is marked by black triangles. All sections were stained with hematoxylin and eosin (magnifications, x200). Three repetitions for each antibody were performed.

3.3.3 F779 IgA1 mAbs specifically bind to human PMNs

To confirm binding of F779 IgA1 to FcαR on human PMNs, FACS analysis was conducted. The F779 IgA1 mAb and human PMNs were incubated for 60 min at 37ºC to form soluble complexes. Cells were next stained with FVS450, FITC-conjugated anti-human IgA antibody, and APC-conjugated anti-human CD66b antibody. Figure 45 presents the gating strategy. The first step in gating often distinguishes cell populations based on their forward and side scatter properties. Forward versus side scatter (FSC vs SSC) gives an estimation of the size and the granularity of cells, respectively. The light scatter patterns of granulocytes, monocytes, and lymphocytes allow them to be distinguished from cellular debris and dead cells, which are often found at the bottom left corner of the density plot. First, FSC vs SSC gating was applied to identify granulocyte population and remove debris (Fig. 45A). A side scatter area (SSC-A) vs. side scatter height (SSC-H) gating was then used to exclude doublets (Fig. 45B). After excluding the dead cells (Fig. 45C), a two-parameter density plot was created by plotting CD66b-APC vs IgA-FITC. About 88% of the cells were double positive for these two markers ($IgA^{+}CD66b^{+}$), as shown by the purple box in Figure 45D.

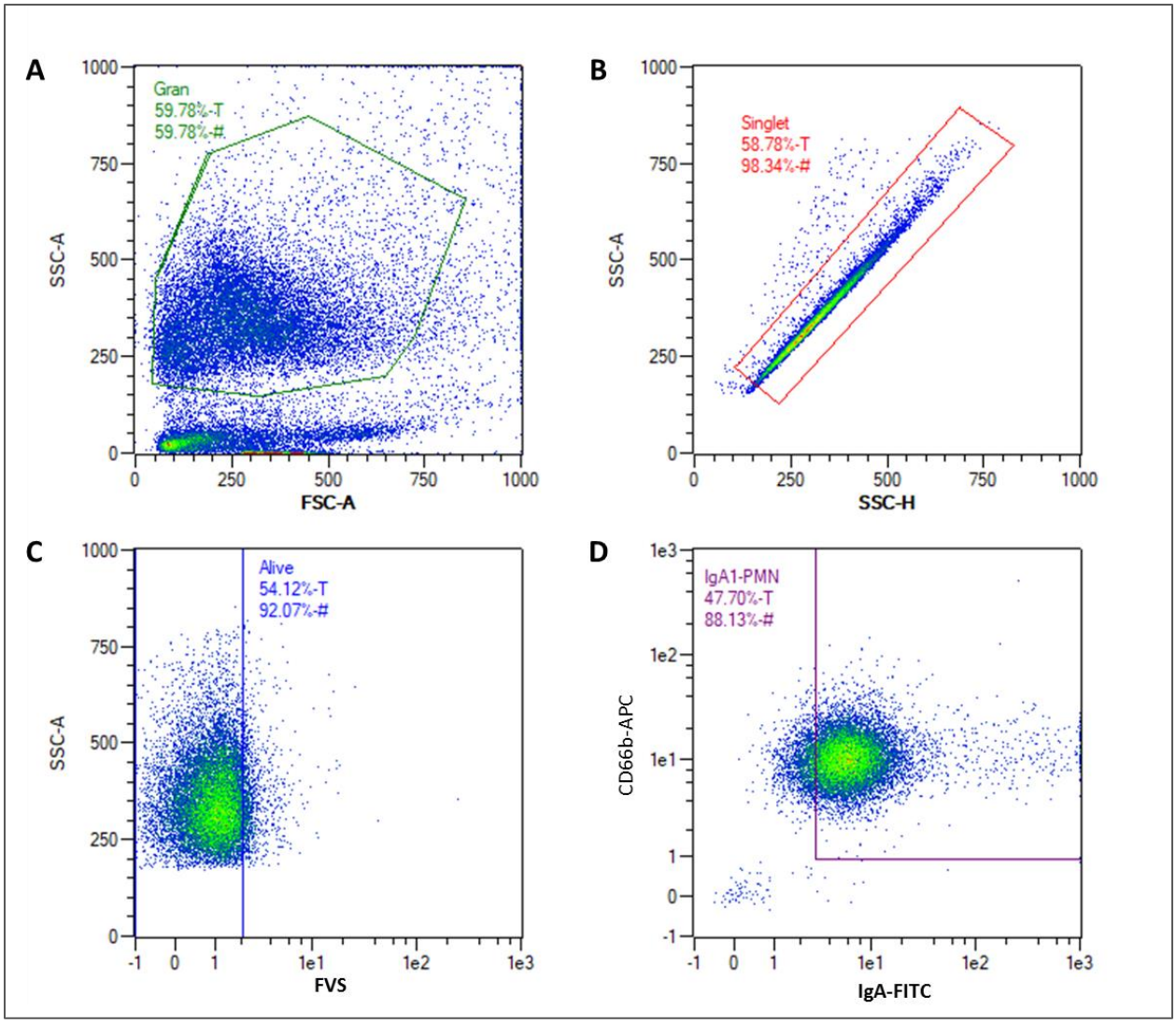

Figure 45: Sequential gating to identify specific IgA-bound PMN population

(**A**) SSC vs FCS density plot. Each dot or point on the plot represents an individual particle that has passed through the laser. A gate has been applied to identify the granulocyte population. (**B**) SSC-A vs SSC-H plot for excluding the doublets. (**C**) Single parameter histogram to exclude the dead cells. (**D**) A two-parameter density plot for granulocytes stained with CD66b-APC and IgA-FITC antibodies. Double positive cells ($IgA^{+}CD66b^{+}$) are shown in the purple box. One representative experiment out of 3 is displayed here.

4 DISCUSSION

4.1 Selection and characterization of a clinically active IgA-PV patient suitable for isolation of mAbs

Intercellular IgA dermatosis (IAD) is a heterogeneous disease entity characterized clinically by vesiculopustular eruptions and histopathologically by *in vivo* bound and/or circulating IgA, but no or much less so, IgG autoAbs [115]. Little is known about the pathomechanisms leading to tissue pathology; however, histopathological studies have shown dense neutrophilic infiltrates suggesting a possible pathophysiological role for neutrophils. Furthermore, no disease model or monoclonal IgA antibody has been described so far, replicating the findings seen in any of the IAD spectrum diseases. Accordingly, current therapies for IgA-mediated skin diseases are nonspecific, variable, often refractory, and dependent on general suppression of the immune system by glucocorticoids [114]. Characterization of individual autoAbs is highly required to better understand the pathophysiology of diseases and to develop more specifically targeted therapies. Though, serum-derived polyclonal antibodies have limitations to address these questions. Additionally, the autoAb profiles vary among patients and even within the same patient over time and using clinical procedures such as plasmapheresis to obtain large volumes of patient sera is declining [21]. To address this issue, the antibody phage display (APD) technique was used to selectively clone and characterize circulating IgA^+ B-cell clones. Phage display is a very sensitive screening method for finding antigen-specific antibodies because it has the capacity for screening up to 10^8 independent mAbs in large phage libraries that are identified by multiple rounds of affinity selection, followed by amplification. APD libraries "immortalize" the *in vivo* autoimmune response of the subject studied, significantly facilitating structural and functional analyses of monoclonal, recombinant autoAbs and assessing their role in disease pathology [116]. Indeed, this methodology gives the possibility to clone, select, and characterize human immune libraries, thereby facilitates the study of autoimmune disease pathophysiology, clinical diagnosis, and development of potential therapeutic agents. To date, many autoimmune disorders have been investigated by phage display such as autoimmune thrombocytopenia (AITP), Wegener's granulomatosis, autoimmune thyroid disease, and autoimmune diabetes [83]. Moreover, therapeutic mAbs generated by phage display are increasingly introduced to the

market. For instance, phage display technology has enabled the development of new drugs for rheumatoid arthritis, multiple sclerosis (MS), and an inflammatory bowel disease [117-119].

Besides, phage display proved to be an important technique in investigating autoimmune skin blistering diseases. APD has been successfully used to clone antigen-specific mAbs (e.g., anti-Dsg) as a single-chain variable fragment (scFv) format from PV, PF, and PNP patients [21-23, 93, 120]. Applying the APD method, pathogenic and nonpathogenic antibodies of IgG subclasses have been previously isolated from these patients. Characterizations of the isolated mAbs revealed that the scFv format of anti-Dsg antibody can reproduce the Dsg-binding specificities of anti-Dsg IgG. However, detailed characterization of polyclonal IgA autoAbs or isolation of IgA monoclonals has not been reported yet for IAD diseases. Therefore, we sought out to address this issue, for the first time, as the main aim of the present study. To this end, first a cohort of sera with IgA pemphigus was screened to detect an active patient with high titer of circulating IgA antibody against Dsg using ELISA and IF microscopy. Thereafter, a clinically active female patient was selected as a suitable candidate for phage library preparation. The IEN-subtype of IAD is clinically characterized by vesiculopustular skin eruptions and intercellular IgA deposition throughout the entire epidermis. The histological features of our case were identical to those of the IEN-subtype. Though, Dsg3, the most commonly seen antigen in the IgA-PV subtype, was detected as the target autoantigen of IgA autoantibodies in this patient. According to the preclinical studies, this particular patient was diagnosed as IEN-subtype by histology with features of IgA-PV subtype by serology. The presence of intercellular complement component C3 on DIF is another feature seen in the majority of classical pemphigus patients but often absent in most cases of IgA pemphigus, as in our IgA-PV patient [51]. This may imply that the acantholysis in IgA pemphigus lesions is complement-independent.

Next, the patient's serum was completely depleted from IgA antibodies by Peptide M agarose; however no Dsg-IgG reactivity was detected that could be potentially masked by specific IgA binding to the same epitopes of Dsg. Further analysis of patients' serum showed that the Dsg3-reactivity was abrogated following EDTA pretreatment, suggesting that the autoAbs bound to calcium-dependent conformational epitopes of Dsg3. Generally, participation of Dsg3 conformational epitopes in PV has received great attention. Aoyama *et al.*, reported that the

presumptive depletion of Dsg3 from desmosomes is dependent on the pathogenicity of anti-Dsg3 IgG against conformational epitopes of Dsg3 [27]. A previous study by Futei *et al.* has established that the dominant autoimmune epitopes in PV are found in the N-terminal adhesive surfaces of Dsg3. By using domain-swapping approach, they have shown that the majority of autoimmune IgG in PV sera reacted with epitopes formed by amino terminal residues 1-161 of Dsg3 [121]. Further data corresponding to these findings obtained from an observation performed by Kamiya *et al.*, who demonstrated that the conformational Dsg3 ELISA reflected the pathogenicity of anti-Dsg3 antibodies more accurately than the conventional Dsg3 ELISA [122]. Therefore, using both conventional and EDTA-pretreatment ELISAs would be useful in monitoring the disease activity of PV, especially in inactive phase of disease. By using immunoblotting, an additional reactivity of the IgA-PV patient's serum autoAbs to linear epitopes was confirmed. Interestingly, it has also been shown that IgG titers against a small stretch of the NH2-terminus of Dsg3 are associated with active PV [123]. In line with this observation, another group reported that PV IgG could also detect non-conformational epitopes of Dsg3 [124]. However, the pathophysiological significance of anti-Dsg3 antibodies against linear epitopes in pemphigus remains largely unknown and needs to be clarified.

4.2 Construction of an IgA1 antibody repertoire and isolation of mAbs to human Dsg3

Here, an APD library was constructed, for the first time, from PBMCs of a clinically active IgA-PV patient. PCR was used to clone the V_H and V_L of the peripheral B cells into a vector that creates a phage particle with the antibody expressed on its surface and the cDNA encoding that antibody inside. The antibody was expressed as a single chain variable fragment (scFv) that contains only the V_H and V_L folded into the proper antigen-binding configuration. The specific-IgA1 phage library produced from our IgA-PV patient was panned on Dsg3 and Dsg1 ELISA wells to isolate the antigen-specific clones. By panning this library, three Dsg3-reactive monoclonal phage clones were isolated, in the form of scFv. Next, the V_H repertoire of the selected monoclonals was sequenced and the clonal relatedness of heavy chains was determined based on the shared CDR3 nucleotide (or their deduced amino acid) sequences [125]. The results indicated that the isolated clones were genetically derived from two distinct B cell populations (by VH gene usage and H-CDR3 amino acid sequence). Our APD-derived clonotypes could not

be detected reliably by proteomic analysis of circulating antigen-specific antibodies affinity-purified from the same patient's serum. This could be explained by several possibilities. First, the strict selection criteria for analysis of mass spectrometry data have been used to define circulating anti-Dsg3 antibodies that might have filtered out some APD-clonotypes [101]. Second, the APD approach may isolate pemphigus B cell receptors (BCRs) which were not secreted as antibodies into the serum. Third, memory B cells that encode autoAbs might have been present without secreting detectable antibodies at the particular time point studied, therefore not contributing significantly to the serologic response at that time point, but potentially at a later point of time [102]. Last, the anti-Dsg3 antibodies may be bound too strongly to the resin, therefore not eluted even after boiling the Dsg3 beads in Laemmli sample buffer for subsequent SDS-PAGE.

The soluble scFv mAbs were recombinantly produced in *E. coli* and purified on a metal affinity column because they contain a His tag. As expected, all these scFvs bound to Dsg3, as detected by ELISA and IFT on Dsg-transfected cells. Moreover, they showed high-titer binding to ME by IIF, as did the serum polyclonal IgA from the same patient. Monkey esophagus (ME) is an excellent substrate for detecting anti-desmoglein antibodies. The fluorescence pattern created by circulating autoAbs (or anti-Dsg3 scFvs) demonstrates the same pattern as would a perilesional skin biopsy with DIF [126]. Further observations showed that the mAbs can target both calcium-stabilized conformational and linear epitopes of Dsg3. Previous studies have indicated that the immunologic properties of mAbs cloned from pemphigus patients are mainly dependent on their V_H region; with light chain usage being promiscuous [21, 22, 127]. More exactly, the same heavy chain with different light chains show similar antigen-binding characteristics and pathogenicity [120]. Two of the mAbs shared VH3-23 locus and one mAb had VH3-30 gene usage. Previously it has been shown that the APD-derived mAbs cloned from PV and PF patients displayed the same VH gene usages [128, 129]. In another study, pathogenic anti-Dsg3 mAbs (e.g., clone PF1-8-15) isolated from PF patients used VH3-30 heavy chain gene [21, 120]. The biological validity of our mAbs was exemplified by an inhibition ELISA study. All three mAbs were tested for their ability to inhibit binding of serum-derived polyclonal IgA/IgG antibodies to human Dsg3 ELISA. Sera from the same patient, from unrelated active IgA-PV patients, and from active IgG-PV patients decreased binding of scFvs in inhibition ELISAs,

indicating that they bind to similar or identical Dsg3 epitopes. Consequently, these data further confirmed that our cloned mAbs recapitulate the *in vitro* antigen-binding properties of the patient's serum autoAbs.

4.3 Human anti-Dsg3 mAbs are pathogenic and reproduce the pemphigus phenotype

To investigate the pathogenicity of mAbs, I used *in vitro* dissociation assay of cultured human keratinocytes and the HSOC model which have not been earlier described for any of the IAD diseases. Keratinocyte cultures (e.g., NHEK cells, HaCaT cells, and DJM-1 cells), mostly used as monolayers, could serve as an *in vitro* model to study the pathomechanisms in pemphigus. Keratinocytes grown in a low-calcium medium will proliferate until confluent and then become growth arrested. In a high-calcium medium (e.g., 1.2 mM or higher), cells will differentiate, form desmosomes, and stratify [130]. Thus, Dsg expression is highly dependent on the cell line or the medium used. HaCaT cells, a non-tumorigenic human keratinocyte cell line, are capable of expressing Dsgs in monolayers, therefore considered as an appropriate experimental model for pemphigus [131]. Dissociation assay detects the pathogenic strength of autoAbs as disruption of intercellular adhesion in a quantitative fashion [132]. All three mAbs plus ETA, which allows inactivation of Dsg1-dependent compensatory adhesion, led to dose-dependent cell-sheet dissociation of cultured human keratinocytes. This finding was replicated by the same patient's serum autoAbs. Accordingly, it was shown that anti-Dsg3 mAbs isolated from a PNP patient cause fragmentation of epidermal sheets in an *in vitro* dissociation assay, following Dsg1 elimination by ETA [93]. Cloning of pathogenic human PV mAbs by phage display was also reported by Payne *et al.*, [22].

Cultured keratinocyte monolayer is a convenient model, but its desmosomal make-up in terms of adhesion molecules does not exactly reflect the *in vivo* situation. However, in the HSOC model the architecture of the human skin is still intact, especially in regard to Dsc and Dsg expression [131]. Hence, this *in vitro* model closely mimics the epidermal architecture of human skin. The injected skin can be easily processed and evaluated with immunofluorescence microscopy or H&E staining. Furthermore, because the antibody is injected intradermally into the skin, it reaches all the cell layers almost simultaneously in contrast to slowly diffusing in to the epidermis when just subjected into the well. This method has been formerly used as a well-

established model to study the mechanisms of acantholysis and to screen the therapeutic drugs in pemphigus, for instance, hydrocortisone, dapsone, methylprednisolone, and protease inhibitors [131]. Here, the soluble scFv could be used to test for pathogenicity by injecting it into the human skin. If the antibodies are pathogenic, they will cause typical pemphigus pathology. Michel and Ko were among the first who successfully induced *in vitro* acantholysis using the HSOC model [133], based on the work of Sarkany *et al.* [134]. Van der Wier *et al.* [131] performed a HSOC model with air-liquid interface in which a biopsy of normal human skin is not floated on lens paper but is instead placed on a trans-well culture plate with the epidermal side up and the bottom side in contact with the solution. Biopsies can be easily harvested at any time and processed for microscopy. A recent study has shown that polyclonal PV and PF IgGs are pathogenic in the HSOC [135]. In addition, the Fab′ fragment and scFv of pemphigus IgG, both of which lack the effector constant region, can also induce typical PF or PV blisters in skin organ culture [23]. In 1993, Supapannachart and Mutasim were able to induce intraepidermal acantholysis with two IgA pemphigus sera (SPD-subtype) using skin explant cultures. IF microscopy showed that the antibody was fixed to the cell surface antigens before the onset of acantholysis, suggesting a possible role for circulating antibody in disease induction [136]. To further examine the pathogenicity of our cloned mAbs, we applied the HSOC, being an *ex vivo* model of human skin, that has proved to be a well-established and informative method in our laboratory. Here, the scFvs were co-injected with low-dose ETA into the dermis of normal human skin. Histology displayed blister formation and epidermal acantholysis. When injected intradermally into the skin, the patient's serum autoAbs showed cell surface-staining pattern by DIF microscopy. However, these autoAbs alone did not result in skin blistering, unless Dsg1 compensation was impaired by ETA, as replicated by our mAbs. Collectively, these data indicate that our mAbs reproduce similar immunohistological and functional characteristics of patient's serum IgA autoAbs. In line with our observations, Lo *et al.*, showed that the pathogenicity of anti-Dsg3 IgG mAbs in skin assays require inactivation of Dsg1, for example by co-injection of ETA [108]. In a previous study, anti-Dsg3 mAbs isolated from a PNP patient caused acantholysis in organ-cultured human skin, when injected with a minimal amount of ETA [93]. Co *et al.*, have demonstrated that VH1-46 anti-Dsg3 mAbs cloned from PV patients induced suprabasal blisters in the human skin explants in the presence of ETA [106]. To our knowledge, the present study provided the first evidence for the *in vitro* pathogenicity of IgA-PV autoAbs.

Most importantly, our modified *in vitro* HSOC model can be also used to evaluate the *in vitro* effect of a pharmacological substance on human skin injected by scFvs or serum autoAbs by comparing the percentage of epidermal split formation over the total length of the epidermis in the positive control versus the section in which the test substance was also applied.

In classical IgG types of PV, the clinical phenotype of pemphigus is defined by the autoAb profile. In mucosal-dominant PV, anti-Dsg3 antibodies play a critical role in acantholysis. AutoAbs against Dsg3 merely result in mucosal blistering because Dsg1 partially compensates for the function of Dsg3. The possible hypotheses that have been described for the pathogenesis of IgG-mediated PV are as follows: the desmoglein compensation theory, the antibody-induced apoptosis theory, and the basal-cell shrinkage hypothesis [137]. Accordingly, acantholysis in PV is not Fc-dependent. By contrast, in the human skin, Dsg1 can provide compensatory adhesion if Dsg3 is inactivated. Consequently, to determine the pathogenicity of anti-Dsg3 mAbs in the human skin assays, inactivation of Dsg1 is required for instance by co-injection of ETA which specifically cleaves Dsg1. These assays were conducted under concurrent elimination of Dsg1 by ETA, because anti-Dsg1 IgA/IgG reactivity was absent in our IgA-PV patient despite clinical manifestations of the skin and mucous membranes. Our findings clearly indicated that anti-Dsg3 mAbs alone are necessary but insufficient for disease induction in IgA-PV. We therefore assumed that additional pathophysiologic mechanisms (e.g., Fc-dependent mechanisms) must be involved, actually leading to the observed tissue pathology of the skin and mucous membranes.

4.4 Human anti-Dsg3 mAbs showed no cross-reactivity to bacterial HiB antigen

The concept of shared VH gene usage as a basis for triggering autoimmunity (e.g., pemphigus) has been firstly described by Cho *et al.,* [106]. They have suggested that a shared VH gene usage is considered to be a determinant of antibody cross-reactivity to self and foreign antigens. By testing the VH1-46 IgG mAbs from PV patients and rotavirus-exposed individuals, they demonstrated a rare cross-reactivity to Dsg3 and rotavirus antigen VP6. The abovementioned concept explains why only a small percentage of individuals exposed to a particular foreign agent develop autoimmunity and why cross-reactive antibodies are not detected in all individuals. The shared VH gene usage model indicates that two antigens initially stimulate similar B cell responses due to differences in VH genes. However, as the immune reaction

proceeds, divergent evolution of the B cell lineages to foreign and self-antigens likely occur. Secondary autoantigen-specific B cell responses can be also stimulated. Therefore, at the time of the autoimmune disease diagnosis, the vast majority of autoAbs are likely only autoantigen-reactive and no longer cross-reactive [138].

Shared VH3-23 gene usage was observed in B cells reacting to Dsgs in pemphigus patients and also in response to infection with *Haemophilus influenzae*, *M. tuberculosis*, HIV-1 envelope gp120, and *staphylococcal* protein A [103, 139-141]. In protective immune response to HiB polysaccharide (PS), most individuals utilized an A2 light chain paired with a VH3-23 heavy chain to form HiB PS-specific Fab [104]. The intriguing connection between an autoimmune response to a self-antigen (i.e., Dsg3 in IgA-PV) and an immune response to a foreign antigen (e.g., HiB-PS) prompted us to investigate whether VH3-23 B cells may be predisposed to Dsg3-HiB cross-reactivity. To address this question, the anti-HiB-HA ELISA was performed using our VH3-23 mAbs, 3-1 and 3-6. However, none of the VH3-23 anti-Dsg3 mAbs demonstrated cross-reactivity to HiB antigen. This hypothesis could be further investigated with other cross-reactive antigens mentioned above.

4.5 Conversion of the APD-derived monovalent scFv into a full-length IgA1 antibody

Phage display libraries are rich resources for discovery of potential therapeutic antibodies. Monoclonal antibodies (mAbs) provide additional insights into the biology of autoimmune diseases, which is difficult to discern with studies of polyclonal patients' sera [22]. Furthermore, the use of specific mAbs as therapeutic tools to treat autoimmune diseases has increased dramatically in the last decade [114]. The scFv libraries are the most common APD libraries due to the efficient display of antibody by phage particles and the ease by which soluble antibodies can be expressed for high-throughput screening [87]. However, Fab fragment and full-length immunoglobulin are the preferred antibody formats in many final applications. Full-length antibodies offer several advantages over scFvs including the bivalent binding, longer half-life, and Fc-mediated effector functions [142]. To study the possible contribution of Fc-dependent mechanisms in the pathology of IgA pemphigus, the most promising anti-Dsg3 mAb, 3-6, was subcloned into a full-length IgA1 antibody via attachment of IgA1/λ constant domains to the scFv-derived variable regions. Testing the supernatant of HEK293 cells co-transfected with

3-6VL/λ and 3-6VH/IgA1 plasmids did not show any Dsg3-IgA1 reactivity by ELISA and IFT. Mixed cloning of 3-6 heavy and light chains with those of an irrelevant control antibody (anti-D) implied that the heavy chain construct has been correctly expressed. Accordingly, the observed failure to clone the full-length (3-6) IgA1 mAb is probably due to its light chain (3-6VL/λ) construct since the 3-6VL+αDVH pair was not expressed in HEK293 cells. One approach to address this issue would be to further modify the DNA sequence of 3-6 light chain, for instance by codon-optimization or swapping from lambda to kappa light chain. Besides, full-length antibody expression in mammalian cells (e.g., HEK293 cells) does not exactly reflect the scFv expression in *E. coli*, as observed for 3-6 mAb. Therefore, we chose a pragmatic yet similarly informative strategy to alternatively switch from the APD-derived 3-6 mAb to a previously isolated anti-Dsg3 clone (i.e., F779). F779 IgA1 and IgG1 mAbs were recombinantly produced in HEK293 cells and then characterized by ELISA and IF microscopy before being used in downstream experiments. By inhibition ELISA study, F779 IgA1 led to decreased binding of the 3-6 scFv mAb, indicating that they recognize similar, if not identical, epitopes of Dsg3. Since the antigen binding and epitope specificity of these two mAbs were very similar, F779 was selected as a highly suited substitute for studying the pathophysiological mechanisms in IgA-PV.

4.6 Pathogenicity of anti-Dsg3 IgA1 autoAbs is Fc-dependent in IgA pemphigus

Several chronic inflammatory diseases are considered to be mediated by neutrophils. Linear IgA dermatosis (LAD) is an autoimmune bullous skin disease which is characterized by aberrant IgA deposition, dense neutrophilic inflammatory infiltrates, and epidermal blisters. van der Steen *et al.*, demonstrated that cross-linking of FcαRI by IgA autoimmune complexes induced neutrophil recruitment and tissue damage in LAD patients [63]. In an inflammatory bowel disease, exacerbations of ulcerative colitis (UC) are dominated by massive neutrophil influx in the lamina propria and IgA is the prevalent antibody in this area. Therefore, deranged IgA-induced neutrophil recruitment may contribute to the pathogenesis of UC [143]. We assume that the same mechanism may play a role in the pathology of IgA pemphigus since on histopathology neutrophils figure prominently, as in our IgA-PV patient [51].

To unravel the possible role of FcαRI-bearing cells in pathogenesis of IgA pemphigus, an *in vitro* cryosection model of human skin was applied. Incubation of human skin cryosections with

F779 IgA1 mAb and human PMNs led to intraepidermal acantholysis and typical pathology without requirement of Dsg1 inactivation. In contrast, the IgG1 variant of F779 mAb led to no pathology under the same conditions. Our *in vitro* results clearly demonstrate that the observed tissue pathology caused by Dsg3-IgA1 mAbs is Fc-dependent. Previously, IgG autoAbs to type VII collagen were shown to trigger an Fcγ-dependent neutrophil activation and blister formation in cryosections of human skin [144]. Moreover, IgG4 autoAbs, purified from bullous pemphigoid (BP) patients, induced dermal-epidermal separation in skin cryosections when co-incubated with leukocytes from healthy volunteers [145]. Further work by Recke *et al.,* demonstrated the capability of rIgA1 and rIgA2 mAbs to type VII collagen to induce leukocyte-dependent dermal-epidermal separation in cryosections of human skin [105].

Shown cross-reactivity to murine keratinocytes' Dsgs by IIF microscopy, these anti-Dsg3 F779 mAbs may facilitate the development of *in vivo* disease models and further investigation of the involved pathophysiologic mechanisms.

4.7 Therapeutic implications

Currently, treatment of IgA-mediated blistering skin diseases is based on general suppression of the immune responses using dapsone in combination with systemic corticosteroids [51]. Besides suffering from severe side effects, some patients may relapse under therapy confirming the recalcitrant nature of diseases in response to therapies [146]. Removing autoAbs by immunoapheresis is a commonly used alternative strategy, however this is an intensive treatment since the patient's plasma needs to be filtered multiple times [147]. Due to the frequently observed refractory reactions, potentially safer and more effective therapies are highly required. A recent study by Heineke *et al.,* demonstrated that IgA autoAbs can activate FcαRI via their Fc-tail, resulting in neutrophil migration and activation [114]. The interaction of IgA and FcαRI has not been studied in IgA pemphigus so far. We here present *in vitro* data showing, for the first time, that the Dsg3-IgA1-Fc:FcαRI interaction mediates tissue pathogenicity in IgA-PV. Therefore, blocking the interaction of IgA-Fc portion and FcαRI-bearing cells may be very effective future treatment for the difficult-to-treat disorders of skin. Since inflammation in autoimmune blistering diseases occurs within the skin, a topical applied therapy might also be desirable. Successful delivery of therapeutic peptides through the epidermis has been already

demonstrated. Spindler *et al.*, showed that when a peptide targeting desmoglein was applied topically in an ointment, IgG autoAb-mediated blistering skin in a pemphigus mouse model was abrogated [148].

Peptides that interfere with IgA-FcαRI interaction and are small enough to pass the epidermis may represent as prospective therapeutic candidates. Surface proteins that bind human IgA-Fc have been identified in *Staphylococcus* group A (*S. pyogenes*) and group B bacteria. The *staphylococcal* M proteins, M22, Arp4, or Sir22, bind to the monomeric and dimeric forms of IgA1 and IgA2 [149]. These proteins recognize the Cα2-Cα3 interdomain region of IgA-Fc and inhibit binding of IgA to human CD89 (FcαRI) [150]. Peptide M is a 50-residue synthetic peptide that corresponds to amino acids 35-83 of *staphylococcal* protein Sir22 (M22) (Fig. 46). Peptide M must form a coiled-coil dimer to bind IgA; therefore, a C-terminal cysteine residue is included to initiate dimerization via a disulfide bond [151]. This additional cysteine residue is not present in the intact M protein. Peptide M binds human IgA with high specificity and is commonly used for single-step affinity purification of IgA and for specific detection of IgA-bound to antigen [152]. This IgA-binding synthetic peptide is suggested as a valuable inhibitory model system to study the interaction of human IgA-FcαRI. The inhibitory function of dimeric Peptide M should be first evaluated by *in vitro* cryosection assay.

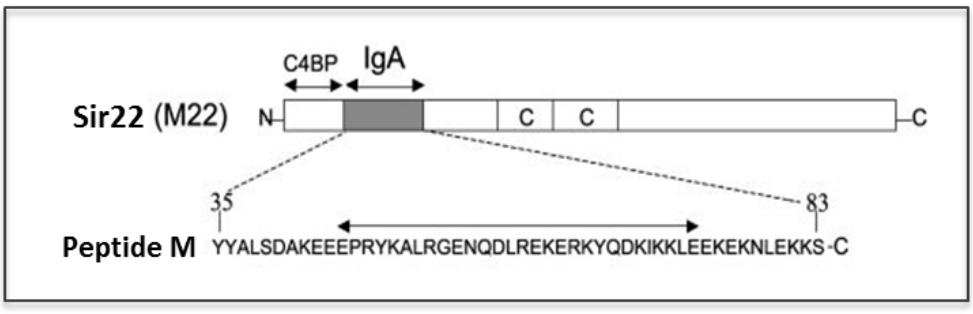

Figure 46: Schematic representation of *streptococcal* Sir22 (M22) protein and Peptide M sequence

Peptide M includes a 29-residue IgA-binding region (horizontal arrow) and 10 amino acids on either side of this region. In addition, it includes a C-terminal cysteine residue, not present in Sir22, to promote dimerization. The most N-terminal part of Sir22 is the hypervariable domain that binds the human complement regulator C4BP. The C-terminal end of Sir22 is covalently bound to peptidoglycan in the bacterial cell wall. Adopted and modified from [152].

On the basis of my aforementioned observations, we propose the following hypothetical model for the sequence of events possibly involved in the pathology of IgA-PV (Fig. 47):

One can suggest that the primary event leading to disease initiates with binding of IgA autoAbs to their target autoantigen in the epidermis (i.e., Dsg3). Abnormal accumulation of Dsg3-IgA complexes leads to excessive cross-linking of FcαRI on PMNs (mainly neutrophils). Tissue damage is secondary due to release of reactive oxygen species (ROS) and proteolytic enzymes from activated PMNs. However, still this model is not complete and some questions remain unresolved. Besides, we suggest that blocking of IgA-FcαRI interactions by dimeric disulfide-linked Peptide M compound may exerts an inhibitory action on these activities; therefore interfere with and reduce tissue damage. This compound could contribute to the development of novel therapeutic strategies not only for IgA pemphigus but also for other IgA-mediated skin diseases, such as linear IgA dermatosis (LAD), IgA-EBA, or mucous membrane pemphigoid (MMP), which may decrease severe morbidity and improve quality of life for these patients.

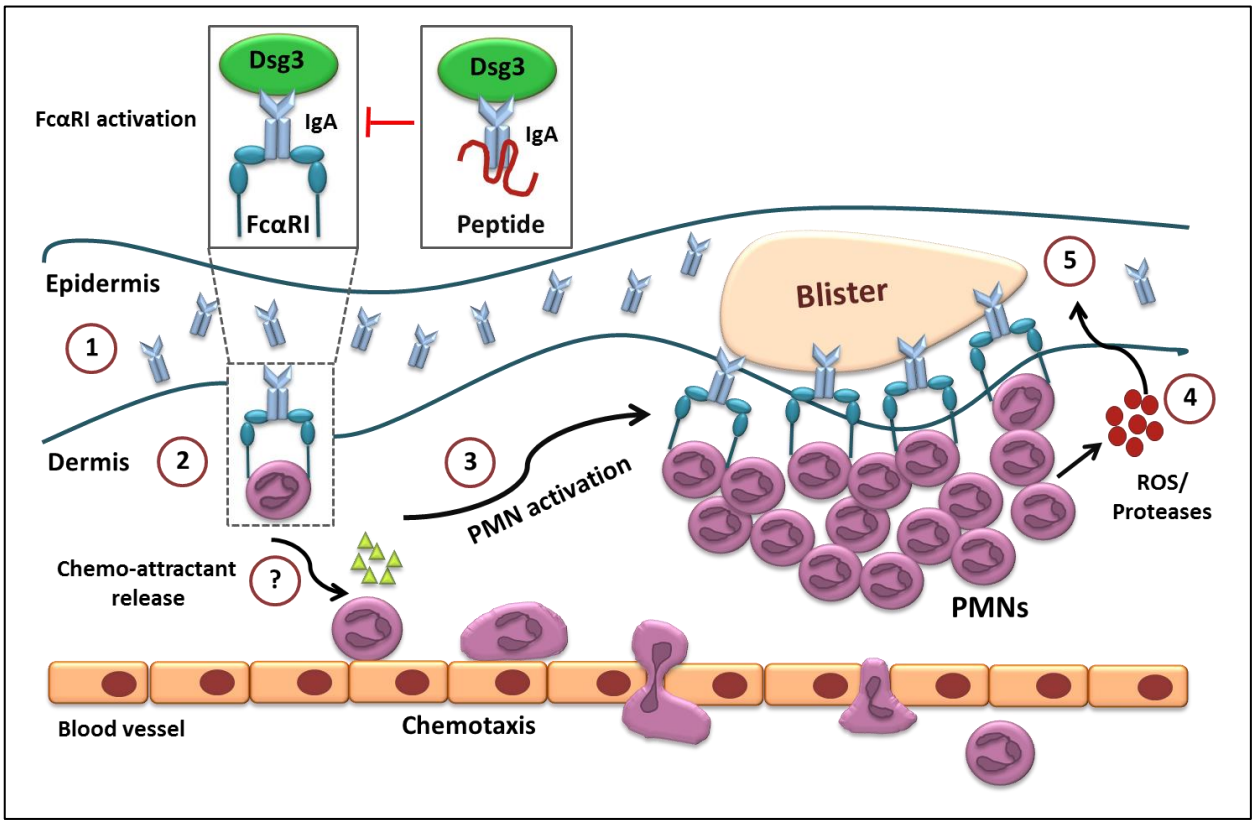

Figure 47: Hypothetical model for disease induction through anti-Dsg3-IgA:FcαRI interaction

(**1**) Deposition of IgA autoAbs into the skin. (**2**) Activation of FcαRI on PMNs by immune complexes. (**3**) Release of chemoattractants, induction of chemotaxis, and activation of newly recruited PMNs. (**4**) Production of ROS and proteases from activated PMNs. (**5**) Blister formation. Blocking of IgA-Fc:FcαRI interaction by dimeric disulfide-linked Peptide M compound inhibits tissue damage at early stage of disease (adopted from [153]).

5 CONCLUSION

Taken together, this study describes the first successful cloning and characterization of IgA mAbs from a clinically active IgA-PV patient using an antibody phage display. Our mAbs confirmed the compensation model of Dsg3 and Dsg1 molecules formerly described in classical, IgG-mediated pemphigus diseases. The results of the *in vitro* keratinocyte dissociation assay and the human skin organ culture injection assay showed that three mAbs are pathogenic, under concurrent elimination of Dsg1 by ETA. These findings indicated that the anti-Dsg3-IgA mAbs are necessary but insufficient for disease induction alone. Therefore, additional Fc-dependent cellular mechanisms were likely to be involved in disease induction. For the first time, we established the cryosection assay as an *in vitro* model of disease. Our conclusive experimental data show that Dsg3-IgA1-Fc:FcαRI interaction is triggering skin pathogenicity in IgA pemphigus, without requiring concurrent inactivation of Dsg1 by ETA or anti-Dsg1 mAbs. Blocking the interaction of anti-Dsg3-IgA-Fc portion and FcαR-bearing cells may be a very effective future treatment for this difficult-to-treat disorder of the skin.

6 REFERENCES

1. Kolarsick, P.A., M.A. Kolarsick, and C. Goodwin, *Anatomy and physiology of the skin.* Journal of the Dermatology Nurses' Association, 2011. **3**(4): p. 203-213.
2. Khavkin, J. and D.A. Ellis, *Aging skin: histology, physiology, and pathology.* Facial Plastic Surgery Clinics, 2011. **19**(2): p. 229-234.
3. James, W.D., D. Elston, and T. Berger, *Andrew's Diseases of the Skin E-Book: Clinical Dermatology*. 2011: Elsevier Health Sciences.
4. Elbe-Bürger, A., *Skin architecture and function*, in *Handbook of Burns*. 2012, Springer. p. 29-46.
5. Getsios, S., A.C. Huen, and K.J. Green, *Working out the strength and flexibility of desmosomes.* Nature reviews Molecular cell biology, 2004. **5**(4): p. 271.
6. Delva, E., D.K. Tucker, and A.P. Kowalczyk, *The desmosome.* Cold Spring Harbor perspectives in biology, 2009. **1**(2): p. a002543.
7. Kowalczyk, A.P. and K.J. Green, *Structure, function, and regulation of desmosomes*, in *Progress in molecular biology and translational science*. 2013, Elsevier. p. 95-118.
8. Baum, S., et al., *Diagnosis and classification of autoimmune blistering diseases.* Autoimmunity reviews, 2014. **13**(4-5): p. 482-489.
9. Culton, D.A., Z. Liu, and L.A. Diaz, *Autoimmune Bullous Skin Diseases—Pemphigus and Pemphigoid*, in *The Autoimmune Diseases (Fifth Edition)*. 2014, Elsevier. p. 955-970.
10. Kneisel, A. and M. Hertl, *Autoimmune bullous skin diseases. Part 2: diagnosis and therapy.* JDDG: Journal der Deutschen Dermatologischen Gesellschaft, 2011. **9**(11): p. 927-947.
11. Kasperkiewicz, M., et al., *Pemphigus.* Nature Reviews Disease Primers, 2017. **3**: p. 17026.
12. Amagai, M., V. Klaus-Kovtun, and J.R. Stanley, *Autoantibodies against a novel epithelial cadherin in pemphigus vulgaris, a disease of cell adhesion.* Cell, 1991. **67**(5): p. 869-877.
13. Hammers, C.M. and J.R. Stanley, *Mechanisms of disease: pemphigus and bullous pemphigoid.* Annual Review of Pathology: Mechanisms of Disease, 2016. **11**: p. 175-197.
14. Mahoney, M.G., et al., *Explanations for the clinical and microscopic localization of lesions in pemphigus foliaceus and vulgaris.* The Journal of clinical investigation, 1999. **103**(4): p. 461-468.
15. Amagai, M., et al., *Toxin in bullous impetigo and staphylococcal scalded-skin syndrome targets desmoglein 1.* Nature medicine, 2000. **6**(11): p. 1275.
16. Stahley, S.N. and A.P. Kowalczyk, *Desmosomes in acquired disease.* Cell and tissue research, 2015. **360**(3): p. 439-456.
17. Anhalt, G.J., et al., *Induction of pemphigus in neonatal mice by passive transfer of IgG from patients with the disease.* New England Journal of Medicine, 1982. **306**(20): p. 1189-1196.
18. Sekiguchi, M., et al., *Dominant autoimmune epitopes recognized by pemphigus antibodies map to the N-terminal adhesive region of desmogleins.* The Journal of Immunology, 2001. **167**(9): p. 5439-5448.
19. Tsunoda, K., et al., *Induction of pemphigus phenotype by a mouse monoclonal antibody against the amino-terminal adhesive interface of desmoglein 3.* The Journal of Immunology, 2003. **170**(4): p. 2170-2178.
20. Rock, B., R.S. Labib, and L.A. Diaz, *Monovalent Fab'immunoglobulin fragments from endemic pemphigus foliaceus autoantibodies reproduce the human disease in neonatal Balb/c mice.* The Journal of clinical investigation, 1990. **85**(1): p. 296-299.
21. Ishii, K., et al., *Isolation of pathogenic monoclonal anti-desmoglein 1 human antibodies by phage display of pemphigus foliaceus autoantibodies.* Journal of Investigative Dermatology, 2008. **128**(4): p. 939-948.
22. Payne, A.S., et al., *Genetic and functional characterization of human pemphigus vulgaris monoclonal autoantibodies isolated by phage display.* The Journal of clinical investigation, 2005. **115**(4): p. 888-899.

23. Yamagami, J., et al., *Homologous regions of autoantibody heavy chain complementarity-determining region 3 (H-CDR3) in patients with pemphigus cause pathogenicity.* The Journal of clinical investigation, 2010. **120**(11): p. 4111-4117.
24. Ludwig, R.J., et al., *Mechanisms of autoantibody-induced pathology.* Frontiers in immunology, 2017. **8**: p. 603.
25. Calkins, C.C., et al., *Desmoglein endocytosis and desmosome disassembly are coordinated responses to pemphigus autoantibodies.* Journal of Biological Chemistry, 2006. **281**(11): p. 7623-7634.
26. Oktarina, D., et al., *IgG-induced clustering of desmogleins 1 and 3 in skin of patients with pemphigus fits with the desmoglein nonassembly depletion hypothesis.* British Journal of Dermatology, 2011. **165**(3): p. 552-562.
27. Aoyama, Y. and Y. Kitajima, *Pemphigus vulgaris-IgG causes a rapid depletion of desmoglein 3 (Dsg3) from the Triton X-100 soluble pools, leading to the formation of Dsg3-depleted desmosomes in a human squamous carcinoma cell line, DJM-1 cells.* Journal of Investigative Dermatology, 1999. **112**(1): p. 67-71.
28. Yamamoto, Y., et al., *Anti-desmoglein 3 (Dsg3) monoclonal antibodies deplete desmosomes of Dsg3 and differ in their Dsg3-depleting activities related to pathogenicity.* Journal of Biological Chemistry, 2007. **282**(24): p. 17866-17876.
29. Schulze, K., et al., *An adult passive transfer mouse model to study desmoglein 3 signaling in pemphigus vulgaris.* Journal of Investigative Dermatology, 2012. **132**(2): p. 346-355.
30. Cipolla, G.A., et al., *crosstalk between signaling Pathways in Pemphigus: A role for endoplasmic reticulum stress in p38 Mitogen-Activated Protein Kinase Activation?* Frontiers in Immunology, 2017. **8**: p. 1022.
31. Bektas, M., et al., *A pathophysiologic role for epidermal growth factor receptor in pemphigus acantholysis.* Journal of Biological Chemistry, 2013: p. jbc. M112. 438010.
32. Pretel, M., et al., *An imbalance in Akt/mTOR is involved in the apoptotic and acantholytic processes in a mouse model of pemphigus vulgaris.* Experimental dermatology, 2009. **18**(9): p. 771-780.
33. Berkowitz, P., et al., *Induction of p38MAPK and HSP27 phosphorylation in pemphigus patient skin.* The Journal of investigative dermatology, 2008. **128**(3): p. 738-740.
34. Spindler, V., et al., *Protective endogenous cyclic adenosine 5'-monophosphate signaling triggered by pemphigus autoantibodies.* The Journal of Immunology, 2010: p. 1002675.
35. Sajda, T. and A.A. Sinha, *Autoantibody signaling in Pemphigus vulgaris: development of an integrated model.* Frontiers in immunology, 2018. **9**.
36. Sharma, P., X. Mao, and A.S. Payne, *Beyond steric hindrance: the role of adhesion signaling pathways in the pathogenesis of pemphigus.* Journal of dermatological science, 2007. **48**(1): p. 1-14.
37. Varigos, G.A., *Subcorneal pustulosis with IgA abnormalities in serum and small bowel mucosa: case report.* Australasian Journal of Dermatology, 1979. **20**(2): p. 75-77.
38. Wallach, D., *Intraepidermal IgA pustulosis.* Journal of the American Academy of Dermatology, 1992. **27**(6): p. 993-1000.
39. Sneddon, I., *Subcorneal pustular dermatosis.* International journal of dermatology, 1977. **16**(8): p. 640-644.
40. Kuan, Y.-Z., et al., *Intraepidermal neutrophilic IgA dermatosis.* Journal of the American Academy of Dermatology, 1990. **22**(5): p. 917-919.
41. Beutner, E.H., et al., *IgA pemphigus foliaceus: report of two cases and a review of the literature.* Journal of the American Academy of Dermatology, 1989. **20**(1): p. 89-97.
42. Chorzelski, T.P., S. Jabłońska, and E. Maciejowska, *Linear IgA bullous dermatosis of adults.* Clinics in dermatology, 1991. **9**(3): p. 383-392.

43. Hashimoto, T., K. Teye, and N. Ishii, *Clinical and immunological studies of 49 cases of various types of intercellular IgA dermatosis and 13 cases of classical subcorneal pustular dermatosis examined at Kurume University.* British Journal of Dermatology, 2017. **176**(1): p. 168-175.
44. Hashimoto, T., et al., *Human desmocollin 1 (Dsc1) is an autoantigen for the subcorneal pustular dermatosis type of IgA pemphigus.* Journal of investigative dermatology, 1997. **109**(2): p. 127-131.
45. Duker, I., et al., *Subcorneal pustular dermatosis-type IgA pemphigus with autoantibodies to desmocollins 1, 2, and 3.* Arch Dermatol, 2009. **145**(10): p. 1159-62.
46. Arai, R., et al., *IgA pemphigus with non-pustular erythematous lesions and IgA antibodies to desmocollins 1 and 2.* European Journal of Dermatology, 2013. **23**(3): p. 362-365.
47. Asahina, A., et al., *IgA pemphigus associated with diffuse large B-cell lymphoma showing unique reactivity with desmocollins: unusual clinical and histopathological features.* British Journal of Dermatology, 2013. **168**(1): p. 224-226.
48. Ishii, N., A. Ishida-Yamamoto, and T. Hashimoto, *Immunolocalization of target autoantigens in IgA pemphigus.* Clinical and experimental dermatology, 2004. **29**(1): p. 62-66.
49. Kneisel, A. and M. Hertl, *Autoimmune bullous skin diseases. Part 1: clinical manifestations.* JDDG: Journal der Deutschen Dermatologischen Gesellschaft, 2011. **9**(10): p. 844-857.
50. Teraki, Y., et al., *Intercellular IgA dermatosis of childhood: selective deposition of monomer IgA1 in the intercellular space of the epidermis.* Archives of dermatology, 1991. **127**(2): p. 221-224.
51. Tsuruta, D., et al., *IgA pemphigus.* Clinics in dermatology, 2011. **29**(4): p. 437-442.
52. Męcińska-Jundziłł, K., et al., *Discrepancies among clinical, histological and immunological findings in IgA pemphigus: a case report and literature survey.* Advances in Dermatology and Allergology/Postępy Dermatologii i Alergologii, 2016. **33**(6): p. 480.
53. Hegazy, S., et al., *IgA pemphigus showing IgA antibodies to desmoglein 1 and 3.* Dermatology practical & conceptual, 2016. **6**(4): p. 31.
54. Adam, Z., et al., *IgA pemphigus associated with monoclonal gammopathy completely resolved after achievement of complete remission of multiple myeloma with bortezomib, cyclophosphamide and dexamethasone regimen.* Wiener klinische Wochenschrift, 2010. **122**(9-10): p. 311-314.
55. Lamberts, A., et al., *effectiveness and safety of rituximab in recalcitrant Pemphigoid Diseases.* Frontiers in Immunology, 2018. **9**: p. 248.
56. He, Y., et al., *Persistence of autoreactive IgA-secreting B cells despite multiple immunosuppressive medications including rituximab.* JAMA dermatology, 2015. **151**(6): p. 646-650.
57. Nakamura, K. and T. Nishikawa, *Intercellular IgA dermatosis with clinical features of subcorneal pustular dermatosis.* Arch Dermatol, 1987. **123**: p. 1062-1065.
58. Bond, M., et al., *A mouse T cell product that preferentially enhances IgA production. II. Physicochemical characterization.* The Journal of Immunology, 1987. **139**(11): p. 3691-3696.
59. Fujihashi, K., et al., *gamma/delta T cell-deficient mice have impaired mucosal immunoglobulin A responses.* Journal of Experimental Medicine, 1996. **183**(4): p. 1929-1935.
60. Feng, S.y., et al., *A case of IgA/IgG pustular pemphigus.* International journal of dermatology, 2012. **51**(3): p. 321-324.
61. Aleyd, E., M.H. Heineke, and M. van Egmond, *The era of the immunoglobulin A Fc receptor Fcα RI; its function and potential as target in disease.* Immunological reviews, 2015. **268**(1): p. 123-138.
62. Carayannopoulos, L., J.M. Hexham, and J.D. Capra, *Localization of the binding site for the monocyte immunoglobulin (Ig) A-Fc receptor (CD89) to the domain boundary between Calpha2 and Calpha3 in human IgA1.* Journal of Experimental Medicine, 1996. **183**(4): p. 1579-1586.
63. van der Steen, L.P., et al., *Blocking Fcα receptor I on granulocytes prevents tissue damage induced by IgA autoantibodies.* The Journal of Immunology, 2012: p. 1101763.

64. Boyd, S.D. and S.A. Joshi, *High-throughput DNA sequencing analysis of antibody repertoires*, in *Antibodies for Infectious Diseases*. 2015, American Society of Microbiology. p. 345-362.
65. Murphy, K. and C. Weaver, *Janeway's immunobiology*. 2016: Garland Science.
66. Schroeder, H.W. and L. Cavacini, *Structure and function of immunoglobulins.* Journal of Allergy and Clinical Immunology, 2010. **125**(2): p. S41-S52.
67. Czajkowsky, D.M. and Z. Shao, *The human IgM pentamer is a mushroom-shaped molecule with a flexural bias.* Proceedings of the National academy of Sciences, 2009. **106**(35): p. 14960-14965.
68. Stone, K.D., C. Prussin, and D.D. Metcalfe, *IgE, mast cells, basophils, and eosinophils.* Journal of Allergy and Clinical Immunology, 2010. **125**(2): p. S73-S80.
69. Chen, K., et al., *Immunoglobulin D enhances immune surveillance by activating antimicrobial, proinflammatory and B cell–stimulating programs in basophils.* Nature immunology, 2009. **10**(8): p. 889.
70. Woof, J.M., *Immunoglobulin A: molecular mechanisms of function and role in immune defence*, in *Molecular and Cellular Mechanisms of Antibody Activity*. 2013, Springer. p. 31-60.
71. Woof, J.M. and M.A. Kerr, *The function of immunoglobulin A in immunity.* The Journal of pathology, 2006. **208**(2): p. 270-282.
72. Bonner, A., et al., *Location of secretory component on the Fc edge of dimeric IgA1 reveals insight into the role of secretory IgA1 in mucosal immunity.* Mucosal immunology, 2009. **2**(1): p. 74.
73. Monteiro, R.C. and J.G. Van De Winkel, *IgA Fc receptors.* Annual review of immunology, 2003. **21**(1): p. 177-204.
74. Maliszewski, C.R., et al., *Expression cloning of a human Fc receptor for IgA.* Journal of Experimental Medicine, 1990. **172**(6): p. 1665-1672.
75. Monteiro, R.C., H. Kubagawa, and M. Cooper, *Cellular distribution, regulation, and biochemical nature of an Fc alpha receptor in humans.* Journal of Experimental Medicine, 1990. **171**(3): p. 597-613.
76. Kremer, E., et al., *The gene for the human IgA Fc receptor maps to 19q13. 4.* Human genetics, 1992. **89**(1): p. 107-108.
77. Van Egmond, M., et al., *IgA and the IgA Fc receptor.* Trends in immunology, 2001. **22**(4): p. 205-211.
78. Bakema, J. and M. Van Egmond, *The human immunoglobulin A Fc receptor FcαRI: a multifaceted regulator of mucosal immunity.* Mucosal immunology, 2011. **4**(6): p. 612.
79. Morton, H.C., et al., *Functional Association between the Human Myeloid Immunoglobulin A Fc Receptor (CD89) and FcR γChain MOLECULAR BASIS FOR CD89/FcR γCHAIN ASSOCIATION.* Journal of Biological Chemistry, 1995. **270**(50): p. 29781-29787.
80. Smith, G.P., *Filamentous fusion phage: novel expression vectors that display cloned antigens on the virion surface.* Science, 1985. **228**(4705): p. 1315-1317.
81. McCafferty, J., et al., *Phage antibodies: filamentous phage displaying antibody variable domains.* nature, 1990. **348**(6301): p. 552.
82. Lowman, H.B., et al., *Selecting high-affinity binding proteins by monovalent phage display.* Biochemistry, 1991. **30**(45): p. 10832-10838.
83. Bazan, J., I. Całkosiński, and A. Gamian, *Phage display—A powerful technique for immunotherapy: 1. Introduction and potential of therapeutic applications.* Human vaccines & immunotherapeutics, 2012. **8**(12): p. 1817-1828.
84. Hamzeh-Mivehroud, M., et al., *Phage display as a technology delivering on the promise of peptide drug discovery.* Drug discovery today, 2013. **18**(23-24): p. 1144-1157.
85. Doerner, A., et al., *Therapeutic antibody engineering by high efficiency cell screening.* FEBS letters, 2014. **588**(2): p. 278-287.
86. Saeed, A.F., et al., *Antibody engineering for pursuing a healthier future.* Frontiers in microbiology, 2017. **8**: p. 495.

87. Chan, C.E., et al., *The role of phage display in therapeutic antibody discovery*. International immunology, 2014. **26**(12): p. 649-657.
88. Sommavilla, R., *Antibody engineering: advances in phage display technology and in the production of therapeutic immunocytokines*. 2010, ETH Zurich.
89. Huang, J.X., S.L. Bishop-Hurley, and M.A. Cooper, *Development of anti-infectives using phage display: biological agents against bacteria, viruses, and parasites.* Antimicrobial agents and chemotherapy, 2012. **56**(9): p. 4569-4582.
90. Hammers, C.M. and J.R. Stanley, *Antibody phage display: technique and applications.* The Journal of investigative dermatology, 2014. **134**(2): p. e17.
91. Arbache, S.T., et al., *Immunofluorescence testing in the diagnosis of autoimmune blistering diseases: overview of 10-year experience.* Anais brasileiros de dermatologia, 2014. **89**(6): p. 885-889.
92. Ishii, K., et al., *Characterization of autoantibodies in pemphigus using antigen-specific enzyme-linked immunosorbent assays with baculovirus-expressed recombinant desmogleins.* The Journal of Immunology, 1997. **159**(4): p. 2010-2017.
93. Saleh, M.A., et al., *Pathogenic anti-desmoglein 3 mAbs cloned from a paraneoplastic pemphigus patient by phage display.* Journal of Investigative Dermatology, 2012. **132**(4): p. 1141-1148.
94. Ishii, K. and M. Amagai, *In vitro pathogenicity assay for anti-desmoglein autoantibodies in pemphigus*, in *Molecular Dermatology*. 2013, Springer. p. 219-225.
95. Lin, Z., et al., *In vivo antigen-driven plasmablast enrichment in combination with antigen-specific cell sorting to facilitate the isolation of rare monoclonal antibodies from human B cells.* Nature protocols, 2014. **9**(7): p. 1563.
96. Jackson, M.V. and A.D. Krasnodembskaya, *Analysis of Mitochondrial Transfer in Direct Co-cultures of Human Monocyte-derived Macrophages (MDM) and Mesenchymal Stem Cells (MSC).* Bio-protocol, 2016. **7**(9).
97. Andris-Widhopf, J., et al., *Methods for the generation of chicken monoclonal antibody fragments by phage display.* Journal of immunological methods, 2000. **242**(1-2): p. 159-181.
98. Barbas III, C., et al., *Phage Display: A Laboratory Manual Cold Spring Harbor Laboratory Press Cold Spring Harbor.* New York, 2001.
99. Ahmad, Z.A., et al., *scFv antibody: principles and clinical application.* Clinical and developmental immunology, 2012. **2012**.
100. Wine, Y., et al., *Molecular deconvolution of the monoclonal antibodies that comprise the polyclonal serum response.* Proceedings of the National Academy of Sciences, 2013. **110**(8): p. 2993-2998.
101. Chen, J., et al., *Proteomic analysis of pemphigus autoantibodies indicates a larger, more diverse, and more dynamic repertoire than determined by B cell genetics.* Cell reports, 2017. **18**(1): p. 237-247.
102. Wine, Y., et al., *Serology in the 21st century: the molecular-level analysis of the serum antibody repertoire.* Current opinion in immunology, 2015. **35**: p. 89-97.
103. Osei, A., et al., *Restricted VH3 gene usage in phage-displayed Fab that are selected by intravenous immunoglobulin.* Arthritis & Rheumatology, 2000. **43**(12): p. 2722-2732.
104. Lucas, A.H. and D.C. Reason, *Polysaccharide vaccines as probes of antibody repertoires in man.* Immunological reviews, 1999. **171**(1): p. 89-104.
105. Recke, A., et al., *Recombinant human IgA1 and IgA2 autoantibodies to type VII collagen induce subepidermal blistering ex vivo.* The Journal of Immunology, 2014: p. 1400160.
106. Cho, M.J., et al., *Shared VH1-46 gene usage by pemphigus vulgaris autoantibodies indicates common humoral immune responses among patients.* Nature communications, 2014. **5**: p. 4167.
107. Yeh, S.-W., et al., *Pathogenic human monoclonal antibody against desmoglein 3.* Clinical Immunology, 2006. **120**(1): p. 68-75.

108. Lo, A.S., et al., *Pathogenicity and epitope characteristics do not differ in IgG subclass-switched anti-desmoglein 3 IgG1 and IgG4 autoantibodies in pemphigus vulgaris.* PloS one, 2016. **11**(6): p. e0156800.
109. Gammon, W.R., et al., *An in vitro model of immune complex-mediated basement membrane zone separation caused by pemphigoid antibodies, leukocytes, and complement.* Journal of Investigative Dermatology, 1982. **78**(4): p. 285-290.
110. Sitaru, C., et al., *Autoantibodies to bullous pemphigoid antigen 180 induce dermal–epidermal separation in cryosections of human skin.* Journal of Investigative Dermatology, 2002. **118**(4): p. 664-671.
111. Mao, X., et al., *Autoimmunity to desmocollin 3 in pemphigus vulgaris.* The American journal of pathology, 2010. **177**(6): p. 2724-2730.
112. Hanakawa, Y., et al., *Enzymatic and molecular characteristics of the efficiency and specificity of exfoliative toxin cleavage of desmoglein 1.* Journal of Biological Chemistry, 2004. **279**(7): p. 5268-5277.
113. Nishifuji, K., et al., *Removal of amino-terminal extracellular domains of desmoglein 1 by staphylococcal exfoliative toxin is sufficient to initiate epidermal blister formation.* Journal of dermatological science, 2010. **59**(3): p. 184-191.
114. Heineke, M.H., et al., *Peptide mimetics of immunoglobulin A (IgA) and FcαRI block IgA-induced human neutrophil activation and migration.* European journal of immunology, 2017. **47**(10): p. 1835-1845.
115. Ebihara, T., et al., *Autoantigens for IgA anti-intercellular antibodies of intercellular IgA vesiculopustular dermatosis.* Journal of investigative dermatology, 1991. **97**(4): p. 742-745.
116. Žager, U., M. Lunder, and B. Božič, *Using phage display in autoimmunity research.* Acta Chimica Slovenica, 2011. **58**(4).
117. Rau, R., *Adalimumab (a fully human anti-tumour necrosis factor α monoclonal antibody) in the treatment of active rheumatoid arthritis: the initial results of five trials.* Annals of the rheumatic diseases, 2002. **61**(suppl 2): p. ii70-ii73.
118. Coles, A.J., et al., *The window of therapeutic opportunity in multiple sclerosis.* Journal of neurology, 2006. **253**(1): p. 98-108.
119. Colombel, J.F., et al., *Early mucosal healing with infliximab is associated with improved long-term clinical outcomes in ulcerative colitis.* Gastroenterology, 2011. **141**(4): p. 1194-1201.
120. Yamagami, J., et al., *Antibodies to the desmoglein 1 precursor proprotein but not to the mature cell surface protein cloned from individuals without pemphigus.* The Journal of Immunology, 2009. **183**(9): p. 5615-5621.
121. Futei, Y., et al., *Use of domain-swapped molecules for conformational epitope mapping of desmoglein 3 in pemphigus vulgaris.* Journal of investigative dermatology, 2000. **115**(5): p. 829-834.
122. Kamiya, K., et al., *A higher correlation of the antibody activities against the calcium-dependent epitopes of desmoglein 3 quantified by ethylenediaminetetraacetic acid-treated enzyme-linked immunosorbent assay with clinical disease activities of pemphigus vulgaris.* Journal of dermatological science, 2013. **70**(3): p. 190-195.
123. Müller, R., et al., *IgG reactivity against non-conformational NH2-terminal epitopes of the desmoglein 3 ectodomain relates to clinical activity and phenotype of pemphigus vulgaris.* Experimental dermatology, 2006. **15**(8): p. 606-614.
124. Müller, R., et al., *IgG against extracellular subdomains of desmoglein 3 relates to clinical phenotype of pemphigus vulgaris.* Experimental dermatology, 2008. **17**(1): p. 35-43.
125. Hammers, C.M., et al., *Persistence of anti-desmoglein 3 IgG+ B-cell clones in pemphigus patients over years.* Journal of Investigative Dermatology, 2015. **135**(3): p. 742-749.
126. Odell, I.D. and D. Cook, *Immunofluorescence techniques.* The Journal of investigative dermatology, 2013. **133**(1): p. e4.

127. Payne, A.S., D.L. Siegel, and J.R. Stanley, *Targeting pemphigus autoantibodies through their heavy-chain variable region genes.* Journal of Investigative Dermatology, 2007. **127**(7): p. 1681-1691.
128. Qian, Y., et al., *Antigen selection of anti-DSG1 autoantibodies during and before the onset of endemic pemphigus foliaceus.* Journal of Investigative Dermatology, 2009. **129**(12): p. 2823-2834.
129. Qian, Y., et al., *Dissecting the anti-desmoglein autoreactive B cell repertoire in pemphigus vulgaris patients.* The Journal of Immunology, 2007. **178**(9): p. 5982-5990.
130. Watt, F.M., D.L. Mattey, and D.R. Garrod, *Calcium-induced reorganization of desmosomal components in cultured human keratinocytes.* The Journal of cell biology, 1984. **99**(6): p. 2211-2215.
131. van der Wier, G., H.H. Pas, and M.F. Jonkman, *Experimental human cell and tissue models of pemphigus.* Dermatology research and practice, 2010. **2010**.
132. Kawasaki, H., et al., *Synergistic pathogenic effects of combined mouse monoclonal anti-desmoglein 3 IgG antibodies on pemphigus vulgaris blister formation.* Journal of investigative dermatology, 2006. **126**(12): p. 2621-2630.
133. MICHEL, B. and C.S. KO, *An organ culture model for the study of pemphigus acantholysis.* British Journal of Dermatology, 1977. **96**(3): p. 295-302.
134. Sarkany, I. and G. Caron, *Phytohaemagglutinin induced mitotic stimulation of epithelial cells in organ culture of adult human skin.* British Journal of Dermatology, 1965. **77**(8-9): p. 439-442.
135. Spindler, V., et al., *Pemphigus IgG causes skin splitting in the presence of both desmoglein 1 and desmoglein 3.* The American journal of pathology, 2007. **171**(3): p. 906-916.
136. Supapannachart, N. and D.F. Mutasim, *of Intraepidermal Acantholysis.* Arch Dermatol, 1993. **129**: p. 605-608.
137. Pan, M., X. Liu, and J. Zheng, *The pathogenic role of autoantibodies in pemphigus vulgaris.* Clinical and Experimental Dermatology: Clinical dermatology, 2011. **36**(7): p. 703-707.
138. Cho, M.J., et al., *Determinants of VH1-46 cross-reactivity to pemphigus vulgaris autoantigen desmoglein 3 and rotavirus antigen VP6.* The Journal of Immunology, 2016: p. 1600567.
139. Chin, S.T., et al., *Comparative study of IgA VH 3 gene usage in healthy TST− and TST+ population exposed to tuberculosis: deep sequencing analysis.* Immunology, 2015. **144**(2): p. 302-311.
140. Berberian, L., et al., *Immunoglobulin VH3 gene products: natural ligands for HIV gp120.* Science, 1993. **261**(5128): p. 1588-1591.
141. Domiati-Saad, R. and P.E. Lipsky, *Staphylococcal enterotoxin A induces survival of VH3-expressing human B cells by binding to the VH region with low affinity.* The Journal of Immunology, 1998. **161**(3): p. 1257-1266.
142. Bujak, E., et al., *Reformatting of scFv antibodies into the scFv-Fc format and their downstream purification*, in *Monoclonal Antibodies*. 2014, Springer. p. 315-334.
143. van der Steen, L., et al., *Immunoglobulin A: FcαRI interactions induce neutrophil migration through release of leukotriene B4.* Gastroenterology, 2009. **137**(6): p. 2018-2029. e3.
144. Sitaru, C., et al., *Autoantibodies to type VII collagen mediate Fcγ-dependent neutrophil activation and induce dermal-epidermal separation in cryosections of human skin.* The American journal of pathology, 2002. **161**(1): p. 301-311.
145. Mihai, S., et al., *IgG4 autoantibodies induce dermal–epidermal separation.* Journal of cellular and molecular medicine, 2007. **11**(5): p. 1117-1128.
146. Wozel, G. and C. Blasum, *Dapsone in dermatology and beyond.* Archives of dermatological research, 2014. **306**(2): p. 103-124.
147. Schmidt, E. and D. Zillikens, *Immunoadsorption in dermatology.* Archives of dermatological research, 2010. **302**(4): p. 241-253.
148. Spindler, V., et al., *Peptide-mediated desmoglein 3 crosslinking prevents pemphigus vulgaris autoantibody-induced skin blistering.* The Journal of clinical investigation, 2013. **123**(2).

149. Hatanaka, T., et al., *Human IgA-binding Peptides Selected from Random Peptide Libraries AFFINITY MATURATION AND APPLICATION IN IGA PURIFICATION.* Journal of Biological Chemistry, 2012. **287**(51): p. 43126-43136.
150. Pleass, R.J., et al., *Streptococcal IgA-binding proteins bind in the Cα2-Cα3 interdomain region and inhibit binding of IgA to human CD89.* Journal of Biological Chemistry, 2001. **276**(11): p. 8197-8204.
151. Johnsson, E., et al., *An IgA-binding peptide derived from a streptococcal surface protein.* Journal of Biological Chemistry, 1999. **274**(21): p. 14521-14524.
152. Sandin, C., et al., *Isolation and detection of human IgA using a streptococcal IgA-binding peptide.* The Journal of Immunology, 2002. **169**(3): p. 1357-1364.
153. Heineke, M.H. and M. van Egmond, *Immunoglobulin A: magic bullet or Trojan horse?* European journal of clinical investigation, 2017. **47**(2): p. 184-192.

7 APPENDIX

7.1 Materials

7.1.1 Chemicals

Name	Cat. no.	Source
ABTS™ Solution	11684302001	Sigma-Aldrich, Darmstadt, Germany
Acetone	5025.1	Carl Roth GmbH & Co. KG, Karlsruhe, Germany
Advantage® 2 PCR Kit - 30 Rxns	639207	Takara Bio Europe/SAS, Saint-Germain-en-Laye, France
BD Difco™ Dehydrated Culture Media: LB Agar, Miller	DF0445-07-6	Thermo Fisher scientific, Dreieich, Germany
BD Difco™ LB Broth, Lennox	DF0402-07-0	Thermo Fisher scientific, Dreieich, Germany
β-mercaptoethanol	M6250	Sigma-Aldrich, Darmstadt, Germany
Blotting-Grade Blocker	170-6404	Bio-Rad Laboratories GmbH, Munich, Germany
Bovine Serum Albumin (BSA)	A7906	Sigma-Aldrich, Darmstadt, Germany
Carbenicillin	C1389	Sigma-Aldrich, Darmstadt, Germany
Citric acid	251275	Sigma-Aldrich, Darmstadt, Germany
Crystal violet	C0775-25G	Sigma-Aldrich, Darmstadt, Germany
Defined keratinocyte-SFM (1X)	10744019	Thermo Fisher scientific, Dreieich, Germany
Deoxynucleotide (dNTP) Mix	N0447S	New England Biolabs, Frankfurt, Germany
Dextran 500	9219.2	Carl Roth GmbH & Co. KG, Karlsruhe, Germany
Dispase II	D4693	Sigma-Aldrich, Darmstadt, Germany
DNA Gel Loading Dye (6X)	R0611	Thermo Fisher scientific, Dreieich, Germany
DNA Ladder (1 kb)	N3232	New England Biolabs, Frankfurt, Germany
DNA ladder (100 bp)	N3231	New England Biolabs, Frankfurt, Germany
Dulbecco's Modified Eagle's Medium (DMEM)	D5796	Sigma-Aldrich, Darmstadt, Germany
ECL Western Blotting detection Reagent	RPN2106	Amersham Biosciences Corp., Munich, Germany
*EcoR*I	R0101S	New England Biolabs, Frankfurt, Germany
Eosin Y-solution alcoholic	102439	Merck KGaA, Darmstadt, Germany
Ethanol 70%	T913.3	Carl Roth GmbH & Co. KG, Karlsruhe, Germany
Ethanol 96%	T171.4	Carl Roth GmbH & Co. KG, Karlsruhe, Germany
Ethanol, Absolute (200 Proof), Molecular Biology Grade	BP2818-100	Thermo Fisher scientific, Dreieich, Germany
Exfoliative Toxin A	ST101	Toxin Technology, Inc., Sarasota, FL, USA
FastBreak cell lysis reagent, 10X	V857C	Promega GmbH, Mannheim, Germany
FBS Gold Plus	FCS.GP.0500	Bio&Sell GmbH, Feucht, Germany
Ficoll-Hypaque™ Plus	17-1440-02	GE Healthcare Europe GmbH, Freiburg, Germany

Formalin solution, neutral buffered, 10%	HT501128	Sigma-Aldrich, Darmstadt, Germany
FuGENE® HD Transfection Reagent	E2311	Promega GmbH, Mannheim, Germany
Fuji medical x-ray film	4741019289	Fujifilm Global, Tokyo, Japan
Glycerol for molecular biology	G5516	Sigma-Aldrich, Darmstadt, Germany
Glycine-HCl	G7403-250G	Sigma-Aldrich, Darmstadt, Germany
Glycogen, molecular biology grade	R0561	Thermo Fisher scientific, Dreieich, Germany
GoTaq® DNA Polymerase	M3001	Promega GmbH, Mannheim, Germany
Haematoxylin	104302	Merck KGaA, Darmstadt, Germany
*Hind*III	R0104S	New England Biolabs, Frankfurt, Germany
Hydrochloric acid (25%)	6331.1	Carl Roth GmbH & Co. KG, Karlsruhe, Germany
Imidazole	1/0012/48	Thermo Fisher scientific, Dreieich, Germany
IPTG	BP1620-10	Thermo Fisher scientific, Dreieich, Germany
Kanamycin Sulfate	11815032	Thermo Fisher scientific, Dreieich, Germany
LB agar	BP1425-500	Thermo Fisher scientific, Dreieich, Germany
Magnesium chloride	BP214-500	Thermo Fisher scientific, Dreieich, Germany
Mini-PROTEAN® TGX™ Precast Gel	456-1093	Bio-Rad Laboratories GmbH, Munich, Germany
MOPS	6979.2	Carl Roth GmbH & Co. KG, Karlsruhe, Germany
Nitrocellulose membranes (0.45 µm)	1620115	Bio-Rad Laboratories GmbH, Munich, Germany
PEG 8000	BP233-1	Thermo Fisher scientific, Dreieich, Germany
Penicillin-streptomycin	15140122	Thermo Fisher scientific, Dreieich, Germany
Peptide M/Agarose	GEL-PDM-2	InvivoGen Europe, Toulouse, France
Polymorphprep™	AXS-1114683	Axis-Shield, Heidelberg, Germany
Polyoxyethylene sorbitan monolaurate (Tween 20)	P1379	Sigma-Aldrich, Darmstadt, Germany
Ponceau S solution	P7170-1L	Sigma Aldrich, Darmstadt, Germany
Q5® High-Fidelity DNA polymerase	M0491	New England Biolabs, Frankfurt, Germany
Roti-Histofix (4% solution)	P087.2	Carl Roth GmbH & Co. KG, Karlsruhe, Germany
RPMI 1640 with L-glutamine	BE12-702F	Lonza Cologne GmbH, Koeln, Germany
RPMI 1640 with L-glutamine w/o glucose w/o phenol red	C4116.0500	Genaxxon bioscience GmbH, Ulm, Germany
*Sfi*I	R0123S	New England Biolabs, Frankfurt, Germany
SimplyBlue SafeStain	LC6060	Invitrogen, Carlsbad, CA, USA
SMARTer™ PCR cDNA Synthesis Kit- 10 Rxns	634925	Takara Bio Europe/SAS, Saint-Germain-en-Laye, France
S.O.C. Medium	15544-034	Thermo Fisher scientific, Dreieich, Germany
Sodium Acetate (3 M), pH 5.5	AM9740	Thermo Fisher scientific, Dreieich, Germany
Sodium dihydrogen phosphate monohydrate	1.06346.0500	Merck Millipore, Darmstadt, Germany
Sodium chloride	A317188	Merck KGaA, Darmstadt, Germany
Spectra Multicolor Broad Range Protein Ladder	26634	Thermo Fisher scientific, Dreieich, Germany
SuRE/Cut™ Buffer M	11417983001	Sigma-Aldrich, Darmstadt, Germany

3% TAE Mini ReadyAgarose™ Precast Gel	1613018	Bio-Rad Laboratories GmbH, Munich, Germany
TALON Superflow	28-9574-99	GE Healthcare Europe GmbH, Freiburg, Germany
TC-Plate 12 well Standard.F	83.3921	Sarstedt AG&Co., Nuembrecht, Germany
Tetracycline	BP92-100	Thermo Fisher scientific, Dreieich, Germany
T4 DNA Ligase	M0202S	New England Biolabs, Frankfurt, Germany
Tissue-Tek O.C.T compound	4583	Sakura Finetek Germany GmbH, Staufen, Germany
Tris Base	BP152-500	Thermo Fisher scientific, Dreieich, Germany
Tris-HCl	9090.2	Carl Roth GmbH & Co. KG, Karlsruhe, Germany
Triton X-100	3051.2	Carl Roth GmbH & Co. KG, Karlsruhe, Germany
Trypan blue	T8154	Sigma-Aldrich, Darmstadt, Germany
Tryptone	BP9726-2	Thermo Fisher scientific, Dreieich, Germany
UltraPure™ Agarose	16500-100	Thermo Fisher scientific, Dreieich, Germany
UltraPure™ DNase/RNase-Free Distilled Water	AM9937	Thermo Fisher scientific, Dreieich, Germany
UltraPure™ Phenol: Chloroform: Isoamyl Alcohol	15593031	Thermo Fisher scientific, Dreieich, Germany
Universal-Agarose, peqGOLD	732-2789	VWR International GmbH, Darmstadt, Germany
Yeast extract	BP1422-2	Thermo Fisher scientific, Dreieich, Germany
Xylene	534056	Sigma-Aldrich, Darmstadt, Germany

7.1.2 Antibodies

Antibodies	**Cat. no.**	**Source**
Alexa Fluor ®594 goat anti-rat IgG (H+L)	A11007	Invitrogen Corp., Carlsbad, CA, USA
Anti-HA High Affinity from rat IgG1	11867423001	Sigma-Aldrich, Darmstadt, Germany
Anti-His (C-Term)-HRP Antibody	MA1-135	Invitrogen Corp., Carlsbad, CA, USA
Anti-M13, HRP Conjugate, Monoclonal	27-9421-01	GE Healthcare Europe GmbH, Freiburg, Germany
APC anti-human CD66b Antibody	305118	BioLegend GmbH, Fell, Germany
DAPI Fluoromount-G®	0100-20	SouthernBiotech, Birmingham, USA
F(ab)2 anti-human IgG FITC	30242	Bio-Rad Laboratories GmbH, Munich, Germany
FITC-labeled anti-human IgA (goat)	AF101-0115	EUROIMMUN, Luebeck, Germany
Fixable Viability Stain 450 (FVS450)	562247	BD Bioscience, NJ, USA
Goat anti-Human IgA Antibody HRP Conjugated	A80-102P	Bethyl Laboratories, Inc, Montgomery, T, USA
Goat anti-Human IgA-FITC	2050-02	SouthernBiotech, Birmingham, USA
Goat anti-Human IgG-Fc Fragment Antibody HRP Conjugated	A80-104P	Bethyl Laboratories, Inc, Montgomery, TX, USA
Anti-HA-Peroxidase, High Affinity from rat IgG1	12013819001	Sigma-Aldrich, Darmstadt, Germany
Mouse anti-Human Desmoglein 3	MCA2273	Bio-Rad Laboratories GmbH, Munich,

(Clone 5G11)		Germany
Mouse anti-Human Desmoglein 1 (Clone DSG1/1733)	MCA2271T	Bio-Rad Laboratories GmbH, Munich, Germany
Mouse Anti-Human IgA1-HRP	9130-05	SouthernBiotech, Birmingham, USA
Mouse Anti-Human IgA2-HRP	9140-05	SouthernBiotech, Birmingham, USA
Polyclonal Rabbit anti-human IgA/HRP	P0216	Dako Deutschland GmbH, Hamburg, Germany
Polyclonal rabbit anti-mouse Immunoglobulins, HRP	P0161	Dako Deutschland GmbH, Hamburg, Germany

7.1.3 Kits

Name	**Cat. no.**	**Source**
Anti-Desmoglein 3 ELISA (IgG) Test instruction	EA1496 G	EUROIMMUN, Luebeck, Germany
Anti-Desmoglein 1 ELISA (IgG) Test instruction	EA1495 G	EUROIMMUN, Luebeck, Germany
Haemophilus influenzae B (HiB) IgG ELISA	RE56351	IBL International GmbH, Hamburg, Germany
Human IgA ELISA Quantitation Set	E80-102	Bethyl Laboratories, Inc, Montgomery, TX, USA
Human IgG ELISA Quantitation Set	E80-104	Bethyl Laboratories, Inc, Montgomery, TX, USA
IIFT-Mosaic: Desmoglein 1 /Desmoglein 3	FA1495-1005-1	EUROIMMUN, Luebeck, Germany
Mesacup-2 Desmogl.DSG3 ELISA Kit 48wells	7885E	MBL, Nagoya, Japan
Mesacup-2 Desmogl.DSG1 ELISA Kit 48wells	7880E	MBL, Nagoya, Japan
Monkey Oesophagus BIOCHIP	FB1501-1005	EUROIMMUN, Luebeck, Germany
PureLink™ PCR Purification Kit	K3100-01	Invitrogen Corp., Carlsbad, CA, USA
QIAEX II Gel Extraction Kit	20021	QIAGEN GmbH, Hilden, Germany
QIAprep Spin Miniprep Kit	27104	QIAGEN GmbH, Hilden, Germany
RNeasy Midi Kit	75142	QIAGEN GmbH, Hilden, Germany

7.1.4 Disposable materials

Type of article	**Source**
Amicon Ultra-15 centrifugal filter (30 KDa)	Merck, Darmstadt, Germany
Amicon Ultra-15 centrifugal filter (3 KDa)	Merck, Darmstadt, Germany
Calibrated Plastic Inoculation Loops	COPAN innovation, Brescia, Italy
Corning® Disposable Erlenmeyer Flask (125 mL, 250 mL, 500 mL, 1 L)	STEMCELL Technologies, Köln, Germany
Cover glass slides (24x60)	Paul Marienfeld GmbH, Lauda-Königshofen, Germany
Dako-pen	Dako Deutschland GmbH, Hamburg, Germany
DNA LoBind Tubes (1.5 mL; 2 mL)	Eppendorf AG, Hamburg, Germany
EDTA-coated blood collection tube	Sarstedt AG&Co., Nuembrecht, Germany
Falcon tubes (15 mL; 50 mL)	Sarstedt AG&Co., Nuembrecht, Germany

Ministart 0.2 µm	Sartorius Stedim Biotech GmbH, Göttingen, Germany
Nunc MaxiSorp C bottom wells	Bethyl Laboratories, Inc, Montgomery, TX, USA
Parafilm	Th. Geyer GmbH & Co. KG, Renningen, Germany
Pipette tips (10 µL; 100 µL; 1000 µL)	Sarstedt AG&Co., Nuembrecht, Germany
Protein LoBind Tubes (1.5 mL; 2 mL)	Eppendorf AG, Hamburg, Germany
Razor blade	PLANO, Wetzlar, Germany
Reaction tubes (1.5 mL; 2 mL)	Sarstedt AG&Co., Nuembrecht, Germany
Serological pipettes (5 mL; 10 mL; 25 mL)	Sarstedt AG&Co., Nuembrecht, Germany
Syringe, 1 mL	Becton Dickinson GmbH, Heidelberg, Germany
Transwell culture plate inserts	Corning, Corning, USA

7.1.5 Bacterial strains and plasmids

Name	**Source**
HaCaT cell line	ATCC, VA, USA
HEK293T cell line	ATCC, VA, USA
pAdVAntage vector	Promega GmbH, Mannheim, Germany
pComb3X phage display vector	Agilent Technologies, CA, USA
pEE 14.4 expression vector	Lonza Group, Basel, Switzerland
pEE 6.4 expression vector	Lonza Group, Basel, Switzerland
TOP10F' *E. coli* strain	Invitrogen Corp., Carlsbad, CA , USA
VCSM13 Interference Resistant Helper	Agilent Technologies, CA, USA
XL1-Blue *E. coli* strain	Agilent Technologies, CA, USA

7.1.6 Commercial buffers and solutions

Name	**Cat. no.**	**Source**
DPBS	14190094	Thermo Fisher scientific, Dreieich, Germany
EDTA solution 0.5M, pH 8	A3145.0500	AppliChem GmbH, Darmstadt, Germany
HBSS, calcium, magnesium, no phenol red	14025050	Thermo Fisher scientific, Dreieich, Germany
Laemmli Sample Buffer, 4x	1610747	Bio-Rad Laboratories GmbH, Munich, Germany
Tris Buffered Saline (TBS), 10x	1706435	Bio-Rad Laboratories GmbH, Munich, Germany
Tris/Glycine/SDS, 10x	1610732	Bio-Rad Laboratories GmbH, Munich, Germany
UltraPure ™ TAE Buffer, 10x	15558026	Thermo Fisher scientific, Dreieich, Germany

7.1.7 Self-made buffers and solutions

Name	**Chemical composition**
Blocking buffer	5 mL 10x TBS from Bio-Rad 0.5 gr BSA 25 µL 2 M $CaCl_2$ Add 45 mL DDW. Sterile filter and stored at 4°C.
76 mM citric acid buffer, pH 2.0	14.6 gr of citric acid Dissolved in 1 L DDW. Adjusted pH to 2.0.

CL medium	RPMI-1640 without phenol red, stabilized with L-glutamine, 25mM HEPES, and 1% FCS
Dextran-NaCl solution	3% Dextran 500 and 0.9% NaCl in DDW. Sterile filter and stored at 4°C.
FACS buffer	1% BSA in DPBS, pH 7.2
Fixation buffer	1% Paraformaldehyde (PFA) in DPBS, pH 7.2
0.1 M glycine buffer, pH 2.5	7.50 gr of glycine Dissolved in 1 L DDW. Adjusted pH to 2.5.
LB Agar	40 gr LB Agar Dissolved in 1 L DDW. Autoclaved, cooled down (60°C), and supplemented with Carbenicillin. Poured into sterile 10 cm petri dishes and allowed to solidify.
LB broth	25 gr LB Agar Dissolved in 1 L DDW. Autoclaved and supplemented with Carbenicillin before use.
50P/300N buffer	3.9 gr NaH_2PO_4 4.45 gr Na_2HPO_4 8.7 gr NaCl Dissolved in 500 mL DDW. Adjusted pH to 7.0.
Imidazole buffer	10.21 gr imidazole Dissolved in 500 mL 50P/300 N buffer.
SB medium	30 gr trypton 20 gr yeast extract 10 gr MOPS Dissolved in 1 L DDW. Adjusted pH to 7.0.
TBS-T buffer	50 mL 10x TBS 0.01% v/v Tween-20 Add 450 mL DDW. Adjusted pH to 7.6.
Top agar	875 mg Difco Agar 3.125 g Difco LB broth Filled up to 125 mL with DDW and autoclaved.
Transfer buffer (Blotting)	15 mM Tris, 66 mM glycine, and 20 % ice cold methanol
1 M Tris-HCl buffer, pH 8.0	121.10 gr Tris Dissolved in 1 L DDW. Adjusted pH to 9.0.
Washing buffer	50 mL 10x TBS 250 µL 2 M $CaCl_2$ 500 µL Tween 20 (0.1%) Add 450 mL DDW. Sterile filter and stored at RT.

7.1.8 Laboratory equipment

Equipment	**Supplier**
Accu-jet pro pipette	BRAND GmbH, Wertheim, Germany
Analytical scale ABS/ABJ-BA-def-1019	Kern & Sohn GmbH, Balingen, Germany
Benchtop microentrifuge	Eppendorf AG, Hamburg, Germany
Bio-photometer plus 8.5 mm	Eppendorf AG, Hamburg, Germany
Centrifuge 5810R	Eppendorf AG, Hamburg, Germany
CFI Plan Apo λ 10x lense	Keyence Deutschland GmbH, Neu-Isenburg, Germany
Cryostat CM3050 S	Leica Mikrosysteme Vertrieb GmbH, Wetzlar, Germany
Erlenmeyer Flasks, Polycarbonate, Sterile	VWR International GmbH, Darmstadt, Germany

Freezer -20˚	Liebherr Hausgeräte GmbH, Ochsenhausen, Germany
Freezer -80˚	Thermo Fisher Scientific GmbH, Dreieich, Germany
Gel Documentation Systems	Bio-Rad Laboratories GmbH, Munich, Germany
HERAcell incubator	Heraeus Instruments GmbH, Hanau, Germany
High-Speed centrifuge	Beckman Coulter GmbH, Krefeld, Germany
Horizontal Electrophoresis Systems	Bio-Rad Laboratories GmbH, Munich, Germany
Incubator	VWR International GmbH, Darmstadt, Germany
Infinite M200 PRO ELISA reader	Thermo Fisher Scientific GmbH, Dreieich, Germany
Keyence microscope BZ-9000E	Keyence Deutschland GmbH, Neu-Isenburg, Germany
Laminar hood	NuAire, Plymouth, Minnesota, USA
Magnetic hotplate stirrer VMS-C4	VWR International GmbH, Darmstadt, Germany
Micro-Pulser	Bio-Rad Laboratories GmbH, Munich, Germany
MACSQuant Analyzer 10	Miltenyi Biotec GmbH, Germany
Microtome	Leica Mikrosysteme Vertrieb GmbH, Wetzlar, Germany
Microwave: 700 & Grill	Severin
Mini-PROTEAN® Tetra Vertical Electrophoresis Cell	Bio-Rad Laboratories GmbH, Munich, Germany
NanoDrop 2000c spectrophotometer	Thermo Fisher Scientific GmbH, Dreieich, Germany
Neubauer cell counting chamber	Laboroptik GmbH, Friedrichsdorf, Germany
pH meter HI208	HANNA instruments, Vöhringen, Germany
Power Pac basic	Bio-Rad Laboratories GmbH, Munich, Germany
Refrigerator	Siemens, Munich, Germany
Shaker incubator	VWR International GmbH, Darmstadt, Germany
T100 thermal cycler	Bio-Rad Laboratories GmbH, Munich, Germany
Thermomixer comfort	Eppendorf AG, Hamburg, Germany
Transferpette S (10 µL, 100 µL, 1000 µL)	BRAND GmbH, Wertheim, Germany
UVP UV PCR Workstation	Thermo Fisher Scientific GmbH, Dreieich, Germany
Vortex	Vortex-Genie® 2-Scientific Industries Inc., Bohemia, New-York, USA

7.1.9 Primer sequences

Primer Name	Sequence
HSCVH1-FS	TCGTCGGCAGCGTCAGATGTGTATTAAGAGACAGCAGGTGCAGCTGGTGCAGTC
HSCVH2- FS	TCGTCGGCAGCGTCAGATGTATAAGAGACAGCAGATCACCTTGAAGGAGTC
HSCVH35- FS	TCGTCGGCAGCGTCAGATGTGTATAAGAGACAGGAGGTGCAGCTGGTGSAGTC
HSCVH3a- FS	TCGTCGGCAGCGTCAGATGTGTATAAGAGACAGGAGGAGGTGCAGCTGKTGGAGTC
HSCVH4- FS	TCGTCGGCAGCGTCAGATGTGTATAAGAGACAGGTGCAGCTGCAGGAGTC
HSCVH4a- FS	TCGTCGGCAGCGTCAGATGTGTATAAGAGACAGCAGCAGGTGCAGCTACAGCAGTG
IgA1_hinge_rev	AGTTGAGGGAGATGGGGTAGGTGGAG
HSCVH1-FL	GGTGGTTCCTCTAGATCTTCCTCCTCTGGTGGCGGTGGCTCGGGCGGTGGTGGGCAGTGCAGCTGGTGCAGTCTGG
HSCVH2-FL	GGTGGTTCCTCTAGATCTTCCTCCTCTGGTGGCGGTGGCTCGGGCGGTGGTGGGCAGATCACCTTGAAGGAGTCTGG
HSCVH35-FL	GGTGGTTCCTCTAGATCTTCCTCCTCTGGTGGCGGTGGCTCGGGCGGTGGTGGGCAGGTGCAGCTGGTGSAGTCTGG
HSCVH3a-FL	GGTGGTTCCTCTAGATCTTCCTCCTCTGGTGGCGGTGGCTCGGGCGGTGGTGGGCAGGTGCAGCTGGTGKTGGAGTCTG
HSCVH4-FL	GGTGGTTCCTCTAGATCTTCCTCCTCTGGTGGCGGTGGCTCGGGCGGTGGTGGGCAGGTGCAGCTGCAGGAGTCGGG
HSCVH4a-FL	GGTGGTTCCTCTAGATCTTCCTCCTCTGGTGGCGGTGGCTCGGGCGGTGGTGGGCAGGTGCAGCTACAGCAGTGGGG
HSCA-B_rev	CCTGGCCGGCCTGGCCACTAGTGACCTTGGGGCTGGTCGGGGATGC
RSC-B_rev	GAGGAGGAGGAGGAGGAGCCTGGCCGGCCTGGCCACTAGTG
RSC-F_sense	GAGGAGGAGGAGGAGGAGGCGGGGCCCAGGCGGCCGAGGCTC
HSCK1-F	GGGCCCAGGCGGCCGAGCTCCAGATGACCCAGTCTCC
HSCK24-F	GGGCCCAGGCGGCCGAGCTCGTGATGACYCAGTCTCC
HSCK3-F	GGGCCCAGGCGGCCGAGCTCGTGWTGACRCAGTCTCC
HSCK5-F	GGGCCCAGGCGGCCGAGCTCACACTCACGCAGTCTCC
HSCJK140-B	GGAAGATCTAGAGGAACCACCTTTGATYTCCACCTTGGTCCC
HSCJK20- B	GGAAGATCTAGAGGAACCACCTTTGATCTCCAGCTTGGTCCC
HSCJK30-B	GGAAGATCTAGAGGAACCACCTTTGATATCCACTTTGGTCCC
HSCJK50-B	GGAAGATCTAGAGGAACCACCTTTAATCTCCAGTCGTCTCCC
HSCLamla	GGGCCCAGGCGGCCGAGCTCGTGBTGACGCAGCCGCCCTC
HSCLam1b	GGGCCCAGGCGGCCGAGCTCGTGCTGACTCAGCCACCCTC
HSCLam2	GGGCCCAGGCGGCCGAGCTCGCCCTGACTCAGCCTCCCTCCGT
HSCLam3	GGGCCCAGGCGGCCGAGCTCGAGCTGACTCAGCCACCCTCAGTGTC
HSCLam4	GGGCCCAGGCGGCCGAGCTCGTGCTGACTCAATCGCCCT C
HSCLam6	GGGCCCAGGCGGCCGAGCTCATGCTGACTCAGCCCCACTC
HSCLam78	GGGCCCAGGCGGCCGAGCTCGTGGTGACYCAGGAGCCMTC
HSCLam9	GGGCCCAGGCGGCCGAGCTCGTGCTGACTCAGCCACCTTC
HSCLam10	GGGCCCAGGCGGCCGAGCTCGGGCAGACTCAGCAGCTCTC
HSCJLam1236	GGAAGATCTAGAGGAACCACCGCCTAGGACGGTCASCTTGGTSCC

7.2 Acknowledgements

Firstly, I would like to express my sincere gratitude to my supervisor Prof. Dr. Ralf J. Ludwig for giving me the opportunity to conduct my doctoral research at the Lübeck Institute of Experimental Dermatology (LIED) and for providing all the resources and necessary support.

I would especially like to thank my first mentor Dr. Christoph M. Hammers for the continuous support of my PhD study and related research, for his patience, motivation, and immense knowledge. His guidance helped me in all the time of research and writing of this thesis.

Besides, I want to acknowledge my second mentor Prof. Dr. Detlef Zillikens and also Prof. Dr. Jennifer Hundt for accepting me as an associate member in the RTG1727 and for providing the academic side to my PhD. Thanks to Prof. Dr. Enno Schmidt for his critical comments.

I would also like to thank all the colleagues at the Department of Dermatology for their profound help and support. Thank you my dear friends Tanya Sezin, Saeedeh Ghorbanalipoor, Lenche Chakievska, Yask Gupta, and Anne Braun for being constantly there for me.

A special thanks to Sadegh Mousavi and Nadine Merg for their excellent technical assistance.

Last but not least, I would like to thank my family, particularly my twin sister Shamsi, for their unconditional love, encouragement, and support throughout my PhD study and my life in general.

7.3 Declaration

I declare that I prepared the present dissertation without any assistance of third parties and have not used outside sources without declaration in the text. Any concepts or quotations applicable to these sources are clearly attributed to them.

This dissertation has not been submitted in the same or similar version to any other authority for grading.

Shirin Emtenani